



KUNGL
TEKNISKA
HÖGSKOLAN

Mekanik KTH
MSc Thesis
2003:08

Finite Element Modelling of Composite Bridge Stability

Martin Ålenius

MSc Thesis
Stockholm, 2003

Royal Institute of Technology
Department of Mechanics

Finite Element Modelling of Composite Bridge Stability

by

Martin Ålenius

August 2003

Technical Reports from
Royal Institute of Technology
Department of Mechanics
SE-100 44 Stockholm, Sweden

Preface

The work presented in this thesis was initiated by the structural engineering company Tyréns AB and the Department of Mechanics at the Royal Institute of Technology in Stockholm, where it was carried out between January 2003 and July 2003.

I would like to thank Adjunct Prof. Dr. Per-Olof Thomasson for introducing and letting me take part in this field of research, and also for his valuable advice and guidance throughout the course of this thesis.

I also express my deepest gratitude and admiration to Prof. Anders Eriksson for his encouragement during his courses at KTH and particularly the courses in the finite element methods that paved the way for this thesis. I also would like to thank him for his shrewd scientific guidance throughout the course of this thesis.

Furthermore, I thank Johan Kölfors at Scanscot Technology for helping me solve modelling problems in BRIGADE/Plus.

A special thank goes to the staff at the Department of Mechanics, particularly to Dr. Gunnar Tibert for his helpfulness and interesting discussions on finite element analysis.

Finally, I would like to thank my family and friends for their love, patience and support in accomplishment of this thesis.

Stockholm, August 2003

Martin Ålenius

Abstract

This thesis deals with stability problems for a thin-walled box girder steel-concrete composite bridge. A case study of bridge Y288 over river Ljungan was performed. The study was based on finite element modelling made in BRIGADE/Plus.

Initially, the background to this thesis is presented together with a description of the studied bridge. An introduction to the used theories, such as buckling of thin plates and torsion of thin-walled open sections is given. An extensive description of the modelling procedures in BRIGADE/Plus is presented alongside a comparison with ABAQUS.

Three different finite element models were analysed: (i) a simply supported rectangular plate uniformly compressed in one direction, (ii) profiled sheeting subjected to shear forces and (iii) the lateral torsional stability of the bridge.

The first analysis aimed to use a simple model for which analytical results were available and compare them with finite element modelling results. The finite element analysis provided results well in accordance with the analytical results for the critical buckling load by Timoshenko.

The analysis of the profiled sheeting in shear aimed to study the importance of the attachment techniques of the profiled sheeting. This analysis clearly illustrated that a substantial reduction of the stresses in the profiled sheeting is obtained with an all around attachment between the profiled sheeting and box girder, compared to a two-sided attachment. Furthermore, it distinctly demonstrated that the large axial forces that arose at the free edge of the profiled sheeting, when it is attached along two sides, were considerably diminished when an all around attachment is used.

The main aim of the lateral torsional stability analysis was to study the overall behaviour of the bridge and how it is influenced by initial imperfections and different attachment of the profiled sheeting. The profiled sheeting creates a closed cross-section, providing a structure that is more rigid than an open cross-section. In order to obtain a closed cross-section, the profiled sheeting must be given an all around attachment and also be strong enough to withstand arisen stresses, mainly at the connections between the profiled sheeting and the box girder. If the profiled sheeting fails to do this, the cross-section of the bridge behaves like an open, thin-walled cross-section.

Keywords: buckling mode, connection, finite element analysis, initial imperfections, profiled sheeting, thin-walled structure, lateral torsional stability.

Contents

Preface	iii
Abstract	v
1 Introduction	1
1.1 Aims of the Study	2
1.2 Structure of the Thesis	2
1.3 Composite Bridges	3
1.4 Finite Element Method	5
2 Studied Bridge and Used Computational Tools	9
2.1 Bridge Y288 over Ljungan	9
2.2 Computational Tools	10
2.2.1 BRIGADE/Plus	10
2.2.2 Comparison of BRIGADE/Plus and ABAQUS	11
3 Loads and Engineering Analysis	13
3.1 Loads Acting on the Bridge	13
3.1.1 Dead Loads	13
3.1.2 Live Loads	15
3.2 Engineer Calculations of Stability	16
4 Thin-Walled Structures	19
4.1 Brief Literature Review	20
4.2 Bending of Thin Plates	21

4.3	Buckling of Thin Plates	22
4.4	Plate and Box Girder Analysis	24
4.5	Torsion of Thin-Walled Open Sections	24
4.5.1	Uniform Torsion of Thin-Walled Open Sections	25
4.5.2	Non-Uniform Torsion of Thin-Walled, Open Sections	26
4.6	Buckling of Simply Supported Rectangular Plate	28
4.6.1	Comparison of Theory and BRIGADE/Plus	31
5	Creating Models in BRIGADE/Plus	35
5.1	Modelling Procedures in BRIGADE/Plus	35
5.2	Buckling in General	36
5.3	General Static Analysis	38
5.4	Linear Eigenvalue Buckling Prediction	38
5.4.1	The BUCKLE Command	39
5.4.2	The IMPERFECTION Command	39
5.5	Elements	40
5.6	Improving Convergence	40
5.7	Assumptions	41
6	Profiled Sheeting in Shear	43
6.1	Profiled Sheet Attachment	43
6.2	Profiled Sheet Thickness	45
6.3	Results	45
7	Lateral Torsional Stability	51
7.1	Implementation of Geometric Imperfections	53
7.1.1	Linear Eigenvalue Prediction	53
7.2	Postbuckling Analysis	55
7.3	Results	56
7.3.1	Box Girder with Open Cross-Section	56
7.3.2	Box Girder with Closed Cross-Section	70

7.3.3	Box Girder with Partly Closed Cross-Section	75
7.3.4	Comparison of Results	80
8	Conclusions	83
8.1	Finite Element Calculations	83
8.2	Suggested Direction for Further Research	85
	Bibliography	87
A	ABAQUS Template	89
A.1	Template	89
B	ABAQUS Input Files	95
B.1	Profiled Sheets in Shear	95
B.1.1	Long side Attachment Input File	95
B.1.2	All Around Attachment Input File	97
B.2	Torsional Stability	99
B.2.1	Box Girder with Open Cross-Section	99
B.2.2	Box Girder with Closed Cross-Section	103
B.2.3	Box Girder with Partly Closed Cross-Section	106
B.2.4	Example of Assembly	109

Chapter 1

Introduction

In June 2002 bridge Y1504¹ over Gide älv collapsed during construction. The result of this collapse is shown in Figure 1.1. The bridge was a simply supported girder bridge with a span of 65 m and a width of 7 m. The bridge was a conventional composite construction containing a flanged box whose lower part was made of a steel box on which a concrete carriageway is casted. The construction demands that the load-bearing capacity of the steel box is sufficient for carrying the self-weight during launching and for carrying the loads from casting. Other loads, such as traffic load, are jointly carried by the steel and the concrete carriageway when the construction is complete. The part of the carriageway that was situated between the flanges was intended to be cast on so called lost formwork made of profiled sheeting. These profiled sheets were at the same time designated to act as stabilising elements for the box girder during construction. The casting of the carriageway was divided into two steps where in the first step a volume of 66 m³ concrete was to be casted, covering 33 m of the central part of the bridge.



Figure 1.1: Bridge Y1504 over Gide älv after collapse (Courtesy of NCC AB).

¹working name

The casting work was initiated at the centre of the bridge and was thereafter intended to be carried on towards the abutments. When about 17 m³ concrete had been cast the bridge twisted and the midsection turned almost 90° instantaneously.

At the moment, a similar bridge, bridge Y288 over the river Ljungan, is under construction. This bridge will be closely studied in this thesis. The fundamental differences between bridge Y1504 and Y288 are that the latter has a span of 57 m and that the profiled sheeting has not been used as stabilising element in the design calculations. The casting procedures have also been altered. Instead of starting at the centre of the bridge, casting began by casting about 2 m of the ends of the carriageway, thus creating an increased torsional warping restraint for the structure.

In this chapter the aims of the thesis and an outline of its structure are presented. Furthermore, an introduction to composite bridges and the finite element method are given.

1.1 Aims of the Study

This thesis aims to study the influence of different design parameters on the lateral torsional stability of a certain type of composite bridge. For this purpose a close study of bridge Y288 over the river Ljungan is performed. A detailed description of this bridge is given in Chapter 2.

The studied parameters are: variations of thickness and attachment of the profiled sheeting to the flanges, influence of different attachment techniques to the lateral torsional stability and influence of initial horizontal rotations.

Each of these factors is assumed to have a considerable impact on the torsional rigidity of the bridge. The study is performed in order to determine their effect and whether the bridge will have sufficient lateral torsional stability during construction.

This thesis also includes an investigation of the possibilities and shortcomings of BRIGADE/Plus, a commercial program for finite element analyses.

This thesis also intends to demonstrate the potential of computational software today that can handle these types of analyses in a reasonably simple manner.

1.2 Structure of the Thesis

An overview of the general structure of this thesis is presented below.

In Chapter 2, the studied composite bridge is presented. Information about the geometry and material properties is given. A description of the program used for modelling, BRIGADE/Plus, is presented along with a comparison between BRIGADE/Plus and ABAQUS.

In Chapter 3, the loads used in the bridge design process are presented. A summary of performed engineering calculations for the lateral torsional stability is given.

In Chapter 4, a selection of common theories are discussed. The subjects are: theory of thin-walled structures, bending of thin plates, buckling of thin plates, box girder analysis and torsion of thin-walled open sections. A comparison between Timoshenko's analysis of buckling of a simply supported rectangular plate, uniformly compressed in one direction, and results from a finite element analysis of the same problem is presented.

In Chapter 5, the procedure of creating models in BRIGADE/Plus is illustrated. Different analysis procedures are described, along with a discussion about element choice and ways to improve convergence. Additionally, some of the assumptions for the model are discussed.

In Chapter 6, the design and analysis of *profiled sheeting in shear* is presented, containing the studies of influence of different attachment choices of the profiled sheeting as well as variations in thickness of them.

In Chapter 7, the design and analysis of *lateral torsional stability* is presented, containing studies of critical loads for the structure with various initial imperfections and different attachment choices of the profiled sheeting.

In Chapter 8, conclusions are stated and some recommendations for further research are suggested.

In Appendix A, some basic commands in ABAQUS are presented.

In Appendix B, the keywords from the models are given.

1.3 Composite Bridges

Steel beams supporting concrete slabs have been used to form the basic superstructure of large numbers of deck bridges for many years. Since 1945 the number of composite bridges being built has significantly increased. The pressure of steel shortage in Germany after the Second World War forced engineers to adopt the most economical design method available to be able to cope with the large amount of reconstruction of bridges and buildings destroyed. New codes of practice in other countries, the publications of papers describing the results of experimental work and eventually the publication of text books have all helped to make engineers familiar with the composite construction [14].

Composite bridges are structures that combine materials like steel, concrete, timber or masonry in some combination. The behaviour of the composite structure is heavily influenced by the properties of its component materials. For example, the use of a concrete slab on a steel girder uses the strength of concrete in compression and the high tensile strength of steel. Looking at the basic behaviour of a composite structure there are two fundamental effects that need to be considered: the

differences between the materials and the connection of the two materials. Stronger, stiffer materials like steel attract proportionally more load than materials such as concrete. If there is no connection then the materials will behave independently, omitting the positive effects, but if adequately connected the materials act as one whole structure.

Most common composite structures are either precast, prestressed concrete beams with an cast concrete slab or steel girders with a concrete slab. Composite structures can be used for a wide range of structures such as foundations, substructures, superstructures and for a diverse range of bridge structures like tunnels, viaducts, footbridges and cable stayed bridges.

Steel-concrete composite box girders may advantageously be used for bridges with long spans, for bridges with significant horizontal curvature or simply for aesthetic reasons. The boxes may be complete steel boxes with an overlay slab or an open box where the concrete slab closes the top of the box.

The open top form of box girders, consisting of steel webs and a bottom flange, has only small top flanges sufficient for stability during concreting. The advantages of this form are that access to all parts of the section is available, which, e.g., facilitates welding, and that the web can be inclined which allows a larger span in the transverse direction of the bridge. A disadvantage of the open box is that the high torsional stiffness of a closed section is not present during construction until the concrete slab has gained strength, which makes it more sensitive to lateral instability during construction.

The stresses induced by the loads will depend upon the magnitude of the load and its eccentricity, the box geometry and the number and stiffness of diaphragms. The use of a box form will aid the distribution of eccentric loads. Vertical loads that act eccentrically with respect to the centre line in a box girder results in twisting of the box section. Twisting moment is resisted by pure shear stresses in the walls of a box. Longitudinal normal stresses arising from the relative warping of the section under torsion are not considered in theory of pure torsion. However, these stresses can attain very large values when the closed cross-sections are flexible. For example, considering a general loading on a box section, as shown in Figure 1.2, in which a single vertical eccentric load is replaced by sets of forces representing vertical, torsional and distortional loading. The general loading in Figure 1.2 can be represented as two different components of loading, one causing bending and the other causing torsion as shown in Figures 1.2(b) and 1.2(c), respectively. The torsional loading component can be subdivided further into a pure torsional component and a distortional component as shown in Figures 1.2(d) and 1.2(e), respectively. Although the pure torsional component will normally result in negligible longitudinal stresses, the distortional component will always tend to deform the cross-section, thus creating distortional stresses in the transverse direction and warping stresses in the longitudinal direction. The distortion of the cross-section will be resisted by cross frames and diaphragms and hence an accurate analysis involves evaluating the distortional warping and shear stresses and the associated distortional bending stresses in the transverse frames [14].

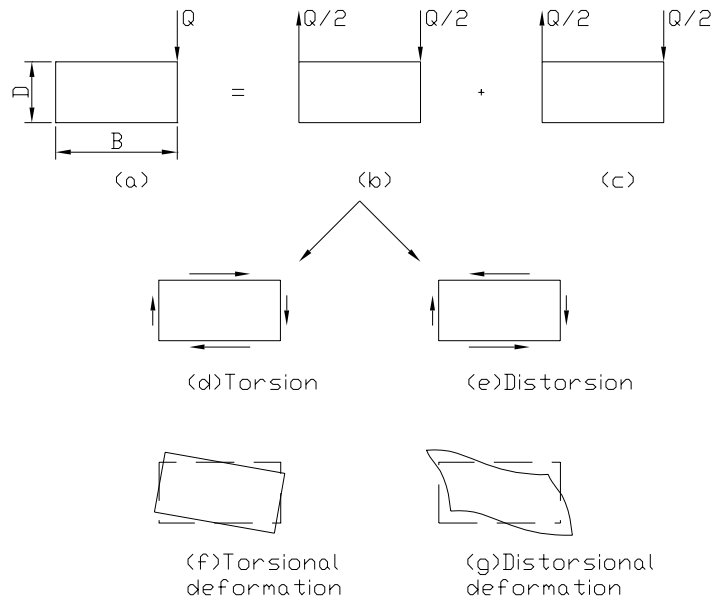


Figure 1.2: Idealisation of eccentric loading in box girder (from [14]).

Where composite action can be achieved, certain structural advantages appear. In comparison with the non-composite case the advantages may be summarised as: a reduction in steel area required, an increase in the overload capacity and a reduction in construction depth. The first two factors will lead to a reduction in the steel weight required to support a given load and the composite structures will show economy over their non-composite counterparts [13].

1.4 Finite Element Method

The finite element method as we know it today seems to have originated with Courant in 1943 [9]. Courant determined the torsional rigidity of a hollow shaft by dividing the cross-section into triangles and interpolating a stress function ϕ linearly over each triangle from the values of ϕ at nodes.

The name *finite element* was coined by Clough in 1960. Many new elements for stress analysis were soon developed. In 1963, finite element analysis acquired respectability in academia when it was recognised as a form of the Rayleigh-Ritz method. Thus finite element analysis was seen not just as a special trick for stress analysis but as a widely applicable method having a sound mathematical basis. The first textbook about finite element analysis appeared in 1967 and today there exists an enormous quantity of literature about finite element analysis [19].

General-purpose computer programs for finite element analysis emerged in the late 1960's and early 1970's. Since the late 1970's, computer graphics of increasing power have been attached to finite element software, making finite element analysis

attractive enough to be used in actual design. Previously it was so tedious that it was used mainly to verify a design already completed or to study a structure that had failed. Computational demands of practical finite element analysis are so extensive that computer implementation is mandatory. Analyses that involve more than 100 000 degrees of freedom are not uncommon [9].

Finite element analysis, also called the finite element method, is a method for numerical solution of field problems. A field problem requires determination of the spatial distribution of one or more dependent variables. Mathematically, a field problem is described by differential equations or by an integral expression. Either description may be used to formulate finite elements.

Individual finite elements can be visualised as small pieces of a structure. In each finite element a field quantity is allowed to have only a simple spatial variation, e.g. described by polynomial terms up to x^2 , xy and y^2 . The actual variation in the region spanned by an element is almost certainly more complicated, hence a finite element analysis provides an *approximate solution*.

In more and more engineering situations today, we find that it is necessary to obtain approximate numerical solutions to problems, rather than exact closed-form solutions.

Elements are connected at points called nodes and the assemblage of elements is called a finite element structure. The particular arrangement of elements is called a mesh. How the finite element method works can be summarised in the following general terms [11]:

1. *Discretise the continuum.* The first step is to divide the continuum or solution into elements. A variety of element shapes may be used and different element shapes may be employed in the same solution region.
2. *Select interpolation functions.* The next step is to assign nodes to each element and then choose the type of interpolation function to represent the variation of field variable over the element.
3. *Find the element properties.* Once the finite element model has been established the matrix equation expressing the properties of the individual elements is ready to be determined.
4. *Assemble the element properties to obtain the system equations.* The matrix equations expressing the behaviour of the elements must be combined to form the matrix equations expressing the behaviour of the entire solution region or system.
5. *Solve the system equations.* The assembly process of the preceding step gives a set of simultaneous equations that can be solved to obtain the unknown nodal values of the field variable.

Finite element analysis has advantages over most other numerical analysis methods,

including versatility and physical appeal. The major advantages of finite element analysis can be summarised as [9]:

- Finite element analysis is applicable to any field problem.
- There is no geometric restriction. The body analysed may have any shape.
- Boundary conditions and loading are not restricted.
- Material properties are not restricted to isotropy and may change from one element to another or even within an element.
- Components that have different behaviours, and different mathematical descriptions, can be combined.
- A finite element analysis closely resembles the actual body or region.
- The approximation is easily improved by grading the mesh.

Some disadvantages may be mentioned as well:

- It is fairly complicated, making it time-consuming and expensive to use.
- It is possible to use finite element analysis programs while having little knowledge of the analysis method or the problem to which it is applied. Finite element analyses carried out without sufficient knowledge may lead to results that are worthless and some critics say that most finite element analysis results are worthless [9].

Chapter 2

Studied Bridge and Used Computational Tools

2.1 Bridge Y288 over Ljungan

The studied composite bridge, bridge Y288 over Ljungan, is situated at Erikslund in Ånge municipality in central Sweden. The bridge is a simply supported box girder bridge with a span of 57 m and a width of 7 m. The girder is a conventional composite construction containing a flanged box whose lower part is made of a steel channel on which a concrete carriageway is cast [17]. Representative cross-sections are given in Figure 2.1. The steel box is provided with diaphragms c/c 7125 mm. It is made in two parts which are transported to the construction site where they are welded together and launched. The part of the carriageway that is situated between the flanges is cast on so called “lost form” of profiled sheeting. The bridge, which is built by the construction company PEAB, has been designed by the engineering consulting company Tyréns AB on request of the Swedish National Road Administration, Vägverket.

The materials chosen in the design are specified as follows [1, 2, 6]:

- Steel S275J2G3:

$$f_{yk} = \begin{cases} 275 \text{ MPa} & \text{for } 0 < t < 16 \text{ mm} \\ 265 \text{ MPa} & \text{for } 16 < t < 40 \text{ mm} \end{cases}$$

$$f_{uk} = 410 \text{ MPa}$$

- Steel S420M:

$$f_{yk} = \begin{cases} 420 \text{ MPa} & \text{for } 0 < t < 16 \text{ mm} \\ 400 \text{ MPa} & \text{for } 16 < t < 40 \text{ mm} \end{cases}$$

$$f_{uk} = 500 \text{ MPa}$$

- Profiled steel sheeting, Rydab 45-950 F:

$$f_{yk} = 320 \text{ MPa}$$

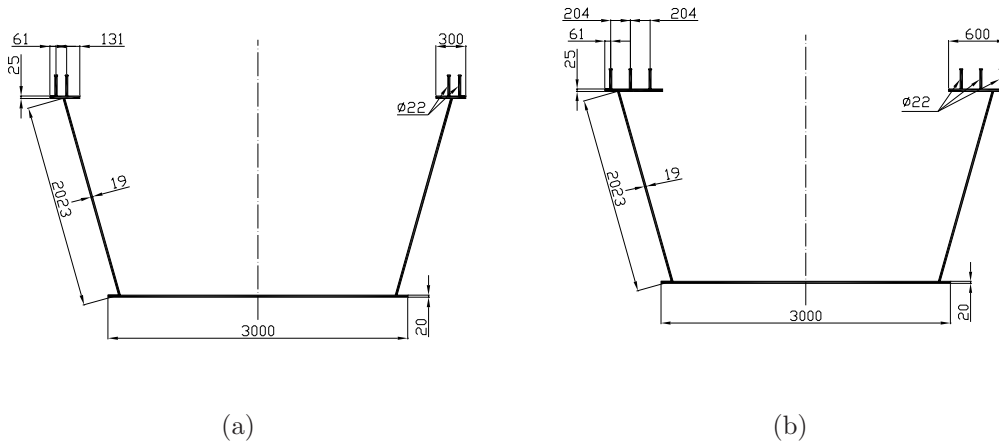


Figure 2.1: (a) Cross-section of the box girder midsection and, (b) cross-section of the box girder ends.

- Concrete BTG K40:

$$\begin{aligned} f_{cck} &= 28.5 \text{ MPa} \\ f_{ctk} &= 1.95 \text{ MPa} \\ f_{cc} &= 15.8 \text{ MPa} \\ f_{ct} &= 1.08 \text{ MPa} \\ E_c &= 32 \text{ GPa} \end{aligned}$$

The reinforcement and wooden formwork have negligible effect upon the mechanical behaviour of the bridge during construction and only their addition to the dead load is studied.

2.2 Computational Tools

A general description of BRIGADE/Plus is given, presenting an insight to how the program works and the possibilities it provides. Beside this description a comparison of BRIGADE/Plus and ABAQUS/Standard is given.

2.2.1 BRIGADE/Plus

BRIGADE/Plus is a general-purpose finite element program providing powerful analysis features in an interactive and visual environment. The geometry definition of each part is parametric and feature based, which allows quick modifications. Parts can be created in numerous ways and they are then assembled together to create the analysis model. Section and material properties can be defined and assigned to regions of the parts. The program offers a range of analysis procedures, such

as: static stress analysis, eigenvalue buckling analysis and collapse and postbuckling analysis.

There are also possibilities to take nonlinear behaviour into consideration, including geometric, material and contact nonlinearity. The loading can be created combining concentrated, distributed and pressure loads and body forces. BRIGADE/Plus contains advanced algorithms for automatic meshing regions and the density of the mesh can be controlled by applying mesh seeds globally and locally. The program also includes an extensive element library, including element families such as:

- Solid elements
- Shell elements
- Membrane elements
- Beam elements
- Truss elements
- Spring elements
- Rigid elements

Finally BRIGADE/Plus provides a suite of postprocessing features in order to enable efficient interpretation of results [3].

2.2.2 Comparison of BRIGADE/Plus and ABAQUS

The differences between ABAQUS/Standard [10] and BRIGADE/Plus [3] can be done by describing the way in which BRIGADE/Plus is created. BRIGADE/Plus consists, in short, of three parts

- A solver based on ABAQUS/Standard
- GUI (Graphical User Interface) based on ABAQUS/CAE
- Technology developed at Scanscot Technology

The solver is a subset of ABAQUS/Standard where functionalities only interesting to other industries than the construction industry have been removed. The corresponding functionalities have also been removed from the GUI of BRIGADE/Plus.

Functionalities concerning e.g. moving loads and advanced load combinations that is available in BRIGADE/Standard today will soon be available in BRIGADE/Plus.

The advantages of BRIGADE/Plus are:

- It is particularly developed for the construction industry.

- Possibilities to apply moving loads and advanced load combinations will be provided.

The major disadvantage concerns the removed functionalities which might be needed to create the desired models. Then, of course, the full ABAQUS version is a more suitable choice [4].

Chapter 3

Loads and Engineering Analysis

3.1 Loads Acting on the Bridge

The loads and load combinations that are considered in the engineering design process for a bridge are defined in accordance with the Swedish design code BRO94, [18], as: the dead load, the surfacing, the earth pressure, the traffic loads, the braking forces, the load on the road embankment and the additional earth pressure.

These loads are all, of course, important to consider while designing the structure but the calculations of these loads are beyond the scope of this thesis. Instead, due to the low torsional warping restraint of the bridge during construction, the loads acting on the structure during construction are of greater interest. These loads can be divided into:

- dead loads
- live loads

where the dead loads consist of the steel box girder self-weight, the formwork and the reinforcement, while the live loads are wind and concrete during casting. The contributions of these loads are described in subsequent sections.

3.1.1 Dead Loads

Construction design calculations have been used for calculations of the bridge self-weight.

Box Girder

The box girder self-weight is given by its cross-sectional area multiplied by its length. The cross-sectional area is divided into three sections where the steel area, $A_S(x)$

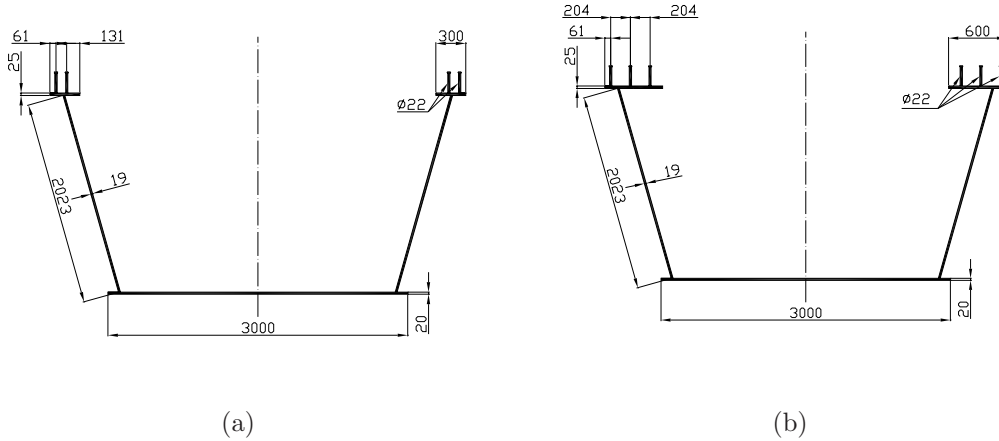


Figure 3.1: (a) Cross-section of the box girder midsection and, (b) cross-section of the box girder ends.

is [15]:

$$A_S(x) = \begin{cases} 0.15233986 \text{ m}^2 & \text{if } 0 < x \leq 10 \text{ m} \\ 0.20633676 \text{ m}^2 & \text{if } 10 < x < 47 \text{ m} \\ 0.15233986 \text{ m}^2 & \text{if } 47 \leq x < 57 \text{ m} \end{cases}$$

Representative cross-sections are shown in Figure 3.1, displaying their dimensions. The total self-weight for the box girder is given as:

$$Q_{\text{steel}} = \int_0^L \frac{q_s(x)}{g\gamma} dx = 92.4 \cdot 10^3 \text{ kg}$$

where γ is a load factor, g is the gravity and $q_s(x)$ is the load-intensity.

$$\begin{aligned} \gamma &= 1.00 \\ g &= 9.81 \text{ m/s}^2 \end{aligned}$$

$$q_s(x) = \rho A_S(x) g \gamma + 150 g \gamma = 7850 \cdot A_S(x) \cdot 9.81 \cdot 10^{-6} \cdot 1.00 + 150 \cdot 9.81 \cdot 10^{-6} \cdot 1.00$$

with $\rho = 7850 \text{ kg/m}^3$ and the contribution from diaphragms = 150 kg/m.

Formwork

The bridge is assumed to be loaded by the wooden formwork over the full length by:

$$q_{\text{formwork}} = 5 \text{ kN/m}$$

Reinforcement

The contribution from the reinforcement is included in the concrete weight. The weight of the concrete, including the reinforcement, is 2400 kg/m³.

3.1.2 Live Loads

The live loads that act upon the bridge during construction, that significantly affect the mechanical behaviour, are the wind load and the cast concrete.

Wind Load

The wind load has been calculated according to the Swedish regulations [5]. Its impact on the bridge is given by:

$$Q_{\text{wind}} = \int_0^L q_{\text{wind}}(x) dx = 170 \text{ kN}$$

where:

$$q_{\text{wind}}(x) = \psi \gamma_{\text{wind}} \mu_{\text{tot}} q_{k,\text{wind}} H_{\text{bridge}} = 2.99 \text{ kN/m}$$

with $\mu_{\text{tot}} = 2.0$, $q_{k,\text{wind}} = 0.5 \text{ kN/m}^2$, $\psi \gamma_{\text{wind}} = 1.3$ and $H_{\text{bridge}} = 2.3 \text{ m}$

Cast Concrete

The casting is performed in two or three stages, depending on whether warping restraint casting of bridge ends is performed or not.

The casting of the midsection of the bridge is performed in several steps, where about 10 m^3 of concrete is cast per step. The cast concrete will contribute to the loads with

$$q_{\text{casting}} = \rho g A_c(x) = 24 \cdot 2.032 = 48.768 \text{ kN/m}$$

where $\rho g = 24 \text{ kN/m}^3$ and $A_c(x)$ is the concrete carriageway cross-sectional area.

The concrete is cast starting from one end of the midsection and proceeds towards the other end, as shown in Figure 3.2.



Figure 3.2: Casting of bridge Y288. (1) is the starting-point for the casting of the central part and (2) is the end-point. The starting-point and end-point are located 14.25 m from the ends of the bridge.

3.2 Engineer Calculations of Stability

Calculations concerning loads acting on the completed bridge are performed according to existing codes and regulations. More relevant for this study though are calculations concerning the bridge response to loads during construction. The risk of lateral instability is imminent until the concrete has hardened and it is therefore vital to check the stability during construction. These calculations for bridge Y288 over the river Ljungan were carried out using second-order differential equations considering assumed imperfections. The imperfections are assumed to exist as an initial rotation $\phi_0(x)$ and as an initial inclination in the horizontal plane $v_0(x)$. The initial rotation is assumed to be sinusoidal with a maximum of about 0.3%, or 1° and the initial inclination is also assumed sinusoidal with a maximum amplitude of 30 mm.

The response of the bridge is governed by the following differential equations:

$$\frac{d^2}{dx^2} \left(EK_w \frac{d^2\phi}{dx^2} \right) - \frac{d}{dx} \left[(GK_v + K_{wC}) \frac{d\phi}{dx} \right] - \frac{d}{dx} \left[\frac{d}{dx} \left(M_y \frac{dv}{dx} \right) + \frac{d}{dx} \left(M_z \frac{dw}{dx} \right) \right] = m_{\text{twist}} \quad (3.1a)$$

$$EI_z \frac{d^2v}{dx^2} + M_y(\phi + \phi_0) = M_z(x) \quad (3.1b)$$

where K_w is the sector moment of inertia (m^6), GK_v is the torsional rigidity (Nm^2) and K_{wC} is the Wagner coefficient (Nm^2).

From these equations the rotations, deflections and stresses are calculated, and subsequently the ultimate load. For a complete understanding of the calculations see [15].

Chapter 4

Thin-Walled Structures

In this chapter a brief literature review of thin-walled structures and an overview of bending and buckling of thin plates is presented together with the theories of torsion of thin-walled open sections. Finally an analysis by Timoshenko of buckling of a simply supported rectangular plate is presented and compared with results from a finite element analysis of the same problem made in BRIGADE/Plus.

A thin-walled structure is defined as a structure that is made from thin plates joined along their edges. The plate thickness is small compared to other cross-sectional dimensions which are in turn often small compared to the overall length [16].

There are several reasons why thin-walled structures must be given special consideration in their analysis and design. In a thin-walled beam the shear stresses and strains are much larger relative to those in a solid rectangular beam.

When certain thin-walled structures are twisted there is a so-called *warping* of the cross-section and the Bernoulli hypothesis¹ is violated. The term warping is defined as the out-of-plane distortion of the cross-section of a beam in the direction of its longitudinal axis. This is further discussed in section 4.5.

Thin-walled structures are also susceptible to local buckling if the in-plane stresses reach their critical values. If this happens, the geometry of the cross-section changes, in contrast to overall buckling where the cross-sectional form is retained, as in the case of a pin-ended column. However, if a thin-walled column is made sufficiently long it may suffer overall buckling before it buckles locally. This means that thin-walled structures must be designed against both local and overall buckling. Theory and experiments show that these two phenomena can interact and when this happens the buckling load can decrease below the values of the individual loads.

¹The Bernoulli hypothesis states that plane sections remain plane over the entire cross-section, from Jakob Bernoulli (1654–1705)

4.1 Brief Literature Review

There is an extensive amount of literature dealing with the theory of thin-walled structures and it is beyond the scope of this thesis to review this literature to any larger extent. However, a brief review of some literature on the elastic buckling of thin-walled structures is given below.

The membrane theory of plates was first studied by Euler (1766) and the flexural theory by Bernoulli (1789) and Navier (1823). The theory for combined membrane and flexural effects was developed by Kirchhoff (1877) and Saint-Venant (1883). At this state, the governing equation for thin isotropic plates loaded laterally with q per unit area and in-plane forces N_x , N_z and N_{xz} per unit length was

$$D \left[\frac{\partial^4 w}{\partial x^4} + 2 \frac{\partial^4 w}{\partial x^2 \partial z^2} + \frac{\partial^4 w}{\partial z^4} \right] = q + N_x \frac{\partial^2 w}{\partial x^2} + 2N_{xz} \frac{\partial^2 w}{\partial x \partial z} + N_z \frac{\partial^2 w}{\partial z^2} \quad (4.1)$$

where w is the lateral deflection [12].

At the turn of the twentieth century the equation governing the buckling of flat plates was available and it was known that it forms the basis of an eigenvalue problem. At that time it was not recognised that as the plate buckles the values of N_x , N_z and N_{xz} at a given point would vary because of the stretching of the plate. The next development which overcame this deficiency was due to Föppl (1907) who introduced the stress function Φ and paved the way for von Karman (1910) to derive the governing equations for perfectly flat plates [12]:

$$D \left[\frac{\partial^4 w}{\partial x^4} + 2 \frac{\partial^4 w}{\partial x^2 \partial z^2} + \frac{\partial^4 w}{\partial z^4} \right] = \frac{\partial^2 \Phi}{\partial z^2} \frac{\partial^2 w}{\partial x^2} + \frac{\partial^2 \Phi}{\partial x^2} \frac{\partial^2 w}{\partial z^2} - 2 \frac{\partial^2 \Phi}{\partial x \partial z} \frac{\partial^2 w}{\partial x \partial z} + q \quad (4.2)$$

$$\frac{\partial^4 \Phi}{\partial x^4} + 2 \frac{\partial^4 \Phi}{\partial x^2 \partial z^2} + \frac{\partial^4 \Phi}{\partial z^4} = Et \left[\left(\frac{\partial^2 w}{\partial x \partial z} \right)^2 - \frac{\partial^2 w}{\partial x^2} \frac{\partial^2 w}{\partial z^2} \right] \quad (4.3)$$

These equations enabled the post-buckling behaviour of perfectly flat plates to be studied.

The von Karman large-deflection equations for flat isotropic plates with in-plane loading were modified to account for anisotropy by Rostovtsev (1940) and later the effect of initial imperfections were included resulting in the following simultaneous equations:

$$D_x \frac{\partial^4 w}{\partial x^4} + 2H \frac{\partial^4 w}{\partial x^2 \partial z^2} + D_z \frac{\partial^4 w}{\partial z^4} = \frac{\partial^2 \Phi}{\partial z^2} \frac{\partial^2 (y+w)}{\partial x^2} + \frac{\partial^2 \Phi}{\partial x^2} \frac{\partial^2 (y+w)}{\partial z^2} - 2 \frac{\partial^2 \Phi}{\partial x \partial z} \frac{\partial^2 (y+w)}{\partial x \partial z} + q \quad (4.4)$$

$$\frac{1}{t_z E_z} \frac{\partial^4 \Phi}{\partial x^4} + 2 \left(\frac{1}{K_{xz}} - \frac{\nu_x}{t_x E_x} - \frac{\nu_z}{t_z E_z} \right) \frac{\partial^4 \Phi}{\partial x^2 \partial z^2} + \frac{1}{t_x E_x} \frac{\partial^4 \Phi}{\partial z^4} = \frac{\partial^2 y}{\partial z^2} \frac{\partial^2 w}{\partial x^2} + 2 \frac{\partial^2 y}{\partial x \partial z} \frac{\partial^2 w}{\partial x \partial z} - \frac{\partial^2 y}{\partial x^2} \frac{\partial^2 w}{\partial z^2} - \frac{\partial^2 w}{\partial z^2} \frac{\partial^2 w}{\partial x^2} + \left(\frac{\partial^2 w}{\partial x \partial z} \right)^2 \quad (4.5)$$

These appear to be the most general equations currently available for solving plate buckling problems [12].

Bryan (1891) was the first to solve the problem of a simply supported rectangular plate with two opposite sides carrying uniform compressive loads. The same problem was later solved by Timoshenko (1907). This is described in detail in section 4.6 alongside a comparison of results from Timoshenko's analysis and finite element analysis in BRIGADE/Plus. Timoshenko also analysed many other cases of flat plates with different boundary conditions. Following the advent of the finite difference and the relaxation technique and later with the increasing use of computers and finite elements it has become relatively easy to solve this problem for a wide variety of plate shapes and stress distributions.

4.2 Bending of Thin Plates

The structural analysis of a plate is carried out by considering the state of stresses at the middle plane of the plate. All the stress component are expressed in terms of the deflection $w(x, y)$ of the plane. This deflection function has to satisfy a linear partial differential equation which, together with its boundary condition, completely defines $w(x, y)$.

Figure 4.1 shows a plate element cut from a plate whose middle plane coincides with the xy plane. The middle plane of the plate is subjected to a lateral load of intensity q . It can be shown, by considering the equilibrium of the plate element, that the stress resultants are given as:

$$M_x = -D \left(\frac{\partial^2 w}{\partial x^2} + \nu \frac{\partial^2 w}{\partial y^2} \right) \quad (4.6)$$

$$M_y = -D \left(\frac{\partial^2 w}{\partial y^2} + \nu \frac{\partial^2 w}{\partial x^2} \right) \quad (4.7)$$

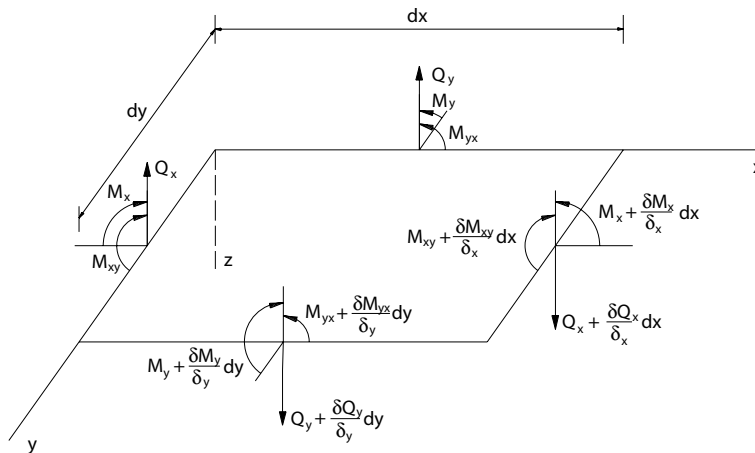


Figure 4.1: Plate element (from [14]).

$$M_{xy} = -M_{yx} = D(1 - \nu) \frac{\partial^2 w}{\partial x \partial y} \quad (4.8)$$

$$V_x = \frac{\partial^3 w}{\partial x^3} + (2 - \nu) \frac{\partial^3 w}{\partial x \partial y^2} \quad (4.9)$$

$$V_y = \frac{\partial^3 w}{\partial y^3} + (2 - \nu) \frac{\partial^3 w}{\partial y \partial x^2} \quad (4.10)$$

$$Q_x = -D \frac{\partial}{\partial x} \left(\frac{\partial^2 w}{\partial x^2} + \frac{\partial^2 w}{\partial y^2} \right) \quad (4.11)$$

$$Q_y = -D \frac{\partial}{\partial y} \left(\frac{\partial^2 w}{\partial x^2} + \frac{\partial^2 w}{\partial y^2} \right) \quad (4.12)$$

$$R = 2D(1 - \nu) \frac{\partial^2 w}{\partial x \partial y} \quad (4.13)$$

where M_x and M_y are the bending moments per unit length in the x and y directions, respectively. M_{xy} and M_{yx} are the twisting moments per unit length. Q_x and Q_y are the shearing forces per unit length in the x and y directions, respectively. V_x and V_y are supplementary shear forces in the x and y directions, respectively and R is the corner force. $D = Eh^3/12(1 - \nu^2)$ which is flexural rigidity of the plate per unit length, E is the modulus of elasticity, h is the thickness of the plate and ν is Poisson's ratio.

The governing equation for the plate is obtained as:

$$\frac{\partial^4 w}{\partial x^4} + 2 \frac{\partial^4 w}{\partial x^2 \partial y^2} + \frac{\partial^4 w}{\partial y^4} = \frac{q}{D} \quad (4.14)$$

Any plate problem should satisfy the governing equation (4.14) and boundary conditions of the plate [14].

4.3 Buckling of Thin Plates

Buckling of a plate involves out-of-plane movement of the plate and results in bending in two planes. A significant difference between axially compressed columns and plates is apparent if their buckling characteristics are compared. For a column, buckling terminates the ability of the member to resist axial load, and the critical load is thus the failure load of the member. However, the same is not true for plates due to the membrane action of the plate. Subsequent to the critical load, plates under compression will continue to resist increasing axial force, and will not fail until a load considerably in excess of the critical load is reached. The critical load

of a plate is therefore not its failure load. Instead, the load-carrying capacity of a plate must be determined by considering its postbuckling behaviour.

To determine the critical in-plane loading of a plate by the concept of neutral equilibrium a governing equation in terms of biaxial compressive forces N_x and N_y and constant shear force N_{xy} as shown in Figure 4.2 can be derived as:

$$D \left(\frac{\partial^4 w}{\partial x^4} + 2 \frac{\partial^4 w}{\partial x^2 \partial y^2} + \frac{\partial^4 w}{\partial y^4} \right) + N_x \frac{\partial^2 w}{\partial x^2} + N_y \frac{\partial^2 w}{\partial y^2} + 2N_{xy} \frac{\partial^2 w}{\partial x \partial y} = 0 \quad (4.15)$$

Numerical methods of analysis of plates, which include both geometric and material non-linearities are available today and these analyses are capable of assessing the ultimate strength and post-critical stiffness of plates with fabrication imperfections.

A square element, as shown in Figure 4.3, whose edges are oriented at 45° to the edges of a plate subjected to pure shear, experiences tensile stresses on two opposing edges and compressive ones on the other two. These compressive stresses induce a form of local buckling with elongated bulges oriented at about 45° to the plate edges. As with the compressive loading, a thin plate loaded in shear can support an applied stress well in excess of the elastic critical one. This is due again to the resistance to in-plane deformation. As the applied shear stress is increased beyond τ_{cr} the plate buckles elastically and retains little stiffness in the direction in which the compressive component acts. However, the inclined tensile component is still resisted fully by the plate. The inclined buckles become progressively narrower and the plate acts like a series of bars in the tension direction, developing a so-called tension field. Further increase of applied stress causes plastic deformation in the part of the tension field, which rotates to line up more closely with the plate diagonal. Tension field action is particularly important in plate and box girders, in which the function of the web plates is primarily to resist shear [14].

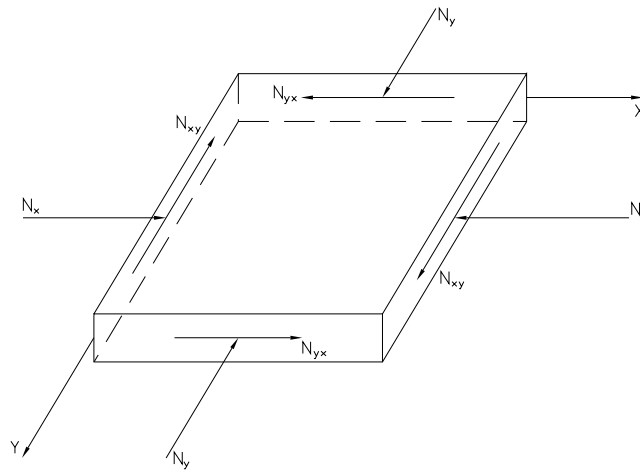


Figure 4.2: Plate subjected to in-plane forces.

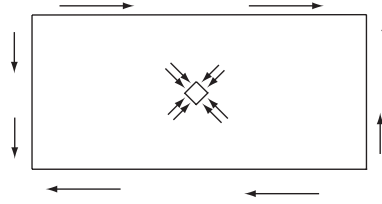


Figure 4.3: Plate subjected to pure shear; stresses on square element at 45° .

4.4 Plate and Box Girder Analysis

The high bending moments and shearing forces associated with the carrying of large loads over long spans as in the case of bridges frequently necessitates the use of fabricated plate and box girders. In their simplest form, plate and box girders can be considered as an assemblage of webs and flanges. In order to reduce the self-weight of these girders and thus achieve economy, slender plate sections are employed. Hence local buckling and postbuckling reserve strength of plates are important design criteria. Flanges in a box girder and webs in plate and box girders are often reinforced with stiffeners to allow for efficient use of thin plates. The designer has to find a combination of plate thickness and stiffener spacing that will result in the most optimal section with reduced weight and fabrication cost. There are some difficulties that are usually encountered by designers of plated structures [14]:

- The engineer's simple 'plane sections remain plane' theory of bending is no longer adequate, even for linear elastic analysis.
- Non-linear elastic behaviour caused by the buckling of plates can be of great importance and must be allowed for.
- Because of this complex non-linear elastic behaviour, and also because of stress concentration problems, some yielding may occur at loads which are quite low in relation to ultimate collapse loads. While such yielding may not be of great significance as regards rigidity and strength, it means that simple maximum stress criteria are no longer sufficient.
- Because of the buckling problem in plates and stiffened panels, complete plastification is far from being realised at collapse. Hence simple plastic criteria are also not sufficient.
- Complex interactions occur between flanges, webs and diaphragms and the pattern of this interaction can change as the level of load increases.

4.5 Torsion of Thin-Walled Open Sections

Thin-walled open cross-sections composed of slender plates are particularly susceptible to lateral torsional buckling, because the torsional rigidity of such cross-sections

are low and so their resistance to torsional instability is limited.

The analysis of lateral torsional buckling behaviour of beams is more complex than that of in-plane buckling behaviour of columns because the lateral buckling problem is intrinsically three-dimensional. The problem is further complicated because the lateral (out-of-plane) deflection and twisting are coupled, so this coupling effect must be considered in the analysis

4.5.1 Uniform Torsion of Thin-Walled Open Sections

When an equal and opposite torque T is applied to the ends of a simply supported beam with a thin-walled open section, the twisting moment along the length of the members is constant and the beam is said to be under a *uniform torsion*. Under the action of the torque, warping of the cross-section will occur and plane sections of the cross-section no longer remain plane as a result of the uneven axial deformation that takes place over the entire cross-section.

For the simply supported beam, in which warping of all the cross-sections is unrestrained, the applied torque is resisted only by shear stresses developed in the cross-section. These stresses act parallel to the edge of the component plates of the cross-section, as shown in Figure 4.4. The distribution of these shear stresses is the same for all thin-walled, open cross-sections. The magnitude of these shear stresses will be proportional to the distance from the midline of the component plate. These shear stresses are called *Saint-Venant shear stresses* and the associated torsion is referred to as *Saint-Venant torsion*, T_{sv} . The angle of twist γ over the length L caused by the Saint-Venant torsion is given by

$$\frac{\gamma}{L} = \frac{T_{sv}}{GJ} \quad (4.16)$$

where γ/L is the angle of twist per unit length, G is the shear modulus and J is the torsional constant of the cross-section.

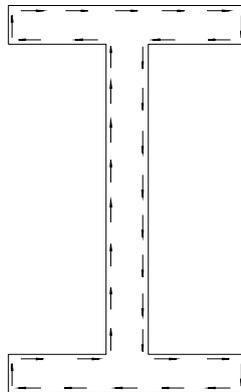


Figure 4.4: Saint-Venant shear stress distribution in an I-section (from [7]).

The rate of twist is expressed as

$$\frac{d\gamma}{dz} = \frac{T_{sv}}{GJ} \quad (4.17)$$

where z is the coordinate axis along the length of the beam. Equation (4.17) can be written as

$$T_{sv} = GJ \frac{d\gamma}{dz} \quad (4.18)$$

The Saint-Venant torsion expressed in Equation (4.18) is also referred to as *uniform* or *pure torsion*.

4.5.2 Non-Uniform Torsion of Thin-Walled, Open Sections

Consider a cantilever beam subjected to a torque applied at the free end. At the free end the cross-section is free to warp, so the applied torque is resisted only by Saint-Venant torsion. At the fixed end, however, warping is prevented. As a result, in addition to Saint-Venant torsion, there exists another type of torsion known as *warping restraint torsion* in the cross-section. If the cross-section is prevented from warping, axial strain and axial stresses must be induced in the cross-section, in addition to the shear stresses. These induced axial stresses are in self-balance because no external axial force is applied to the beam.

The resultant of these axial stresses in the two flanges constitutes a pair of equal moments called the *bi-moment*, M_f , acting oppositely in each of the two planes of the flanges.

The development of these bending moments, or bi-moments, in the flanges in the cross-section is shown in Figure 4.5. Since warping is prevented at the fixed end, the two flanges of the beam must bend in opposite directions as the cross-section rotates under the action of the applied torque. The bending of the flanges will thus induce bending moments M_f at the fixed end. The bending moment can be expressed in terms of the lateral displacement u_f as

$$M_f = EI_f \frac{d^2 u_f}{dz^2} \quad (4.19)$$

where E is the modulus of elasticity, I_f the moment of inertia of one flange about the y axis of the cross-section, and u_f the lateral displacement of the flange. Associated with the bending moment in one flange is the shear force V_f given by

$$V_f = -\frac{dM_f}{dz} = -EI_f \frac{d^3 u_f}{dz^3} \quad (4.20)$$

The shear forces are present in both flanges of the I-section. They are equal in magnitude but act in opposite directions, as shown in Figure 4.6. This pair of shear

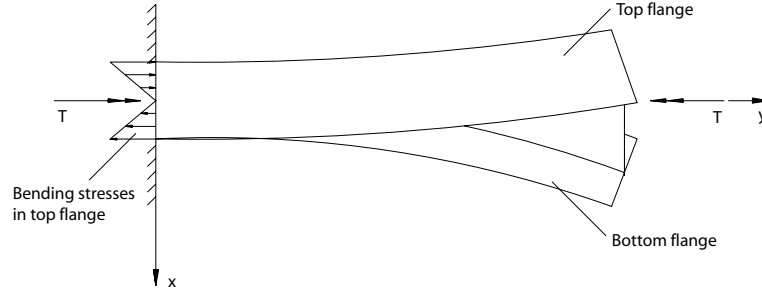


Figure 4.5: Bending of flanges due to warping restraint at the fixed end (from [7]).

forces constitute a couple acting on the cross-section. The resulting torsion, which is referred to as the *warping restraint torsion* or *non-uniform torsion*, is given by

$$T_w = V_f h \quad (4.21)$$

where h is the distance between the lines of action of the shear forces. Equation (4.21) can be expressed as

$$T_w = -EI_f \frac{h^2}{2} \frac{d^3 \gamma}{dz^3} = -EC_w \frac{d^3 \gamma}{dz^3} \quad (4.22)$$

where

$$C_w = \frac{I_f h^2}{2} \quad (4.23)$$

is called the *warping constant* of the I-section. The warping constant is different for different cross-sections.

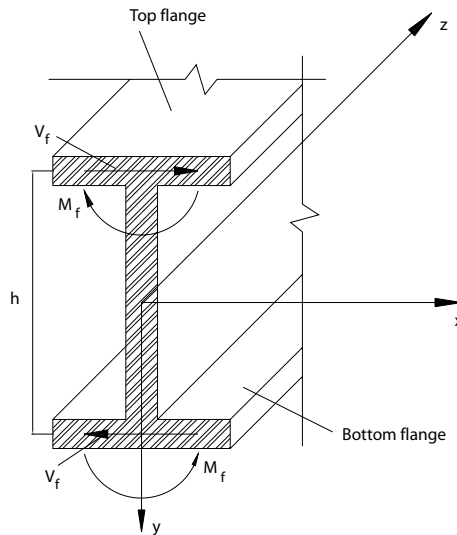


Figure 4.6: Moment and shear developed at the fixed-end cross-section of an I-section (from [7]).

If warping is restrained, the applied twisting moment will be resisted by both Saint-Venant torsion and warping restraint torsion.

$$T = T_{sv} + T_w \quad (4.24)$$

or

$$T = GJ \frac{d\gamma}{dz} - EC_w \frac{d^3\gamma}{dz^3} \quad (4.25)$$

Equation (4.25) represents the internal twisting moment that will develop in the cross-section when the member is twisted. The first term represents the resistance of the cross-section to twisting and the second term represents the resistance of the cross-section to warping.

Saint-Venant torsion is always present when a member is subjected to twisting and rotates. Warping restraint torsion will develop if a cross-section is prevented from warping when it is being twisted [7].

4.6 Buckling of Simply Supported Rectangular Plate

A comparison between Timoshenko's theory and results obtained by BRIGADE/Plus is presented in this section. The comparison has been made for buckling of a simply supported rectangular plate that is uniformly compressed in one direction. First, results, and how they are achieved, using Timoshenko's theory [16] are presented. Then, these results are compared with the results from the finite element analysis using BRIGADE/Plus.

A rectangular plate is compressed in its middle plane by forces uniformly distributed along the sides $x = 0$ and $x = a$, as shown in Figure 4.7.

The magnitude of the compressive force per unit edge length is denoted by N_x . By gradually increasing N_x , one arrive at the condition where the flat form of equilibrium of the compressed plate is disturbed and buckling occurs. The corresponding critical value of the compressive force can be found in this case from a consideration of the energy of the system. The deflection surface of the buckled plate can be represented by the double series

$$w = \sum_{m=1}^{\infty} \sum_{n=1}^{\infty} a_{mn} \sin \frac{m\pi x}{a} \sin \frac{n\pi y}{b} \quad (4.26)$$

The strain energy of bending in this case is

$$\Delta V = \frac{\pi^4 ab}{8} D \sum_{m=1}^{\infty} \sum_{n=1}^{\infty} a_{mn}^2 \left(\frac{m^2}{a^2} + \frac{n^2}{b^2} \right)^2 \quad (4.27)$$

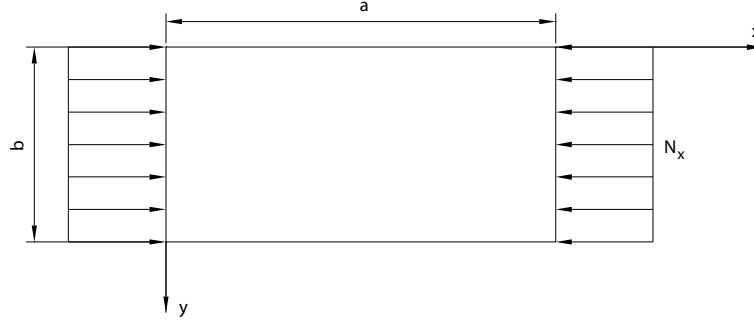


Figure 4.7: Simply supported rectangular plate uniformly compressed in one direction.

The work done by compressive forces during buckling of the plate will be

$$\frac{1}{2}N_x \int_0^a \int_0^b \left(\frac{\partial w}{\partial x} \right)^2 dx dy = \frac{\pi^2 b}{8a} N_x \sum_{m=1}^{\infty} \sum_{n=1}^{\infty} m^2 a_{mn}^2 \quad (4.28)$$

Thus, the equation for determining the critical value of compressive forces, becomes

$$\frac{\pi^2 b}{8a} N_x \sum_{m=1}^{\infty} \sum_{n=1}^{\infty} m^2 a_{mn}^2 = \frac{\pi^4 ab}{8} D \sum_{m=1}^{\infty} \sum_{n=1}^{\infty} a_{mn}^2 \left(\frac{m^2}{a^2} + \frac{n^2}{b^2} \right)^2 \quad (4.29)$$

from which

$$N_x = \frac{\pi^2 a^2 D \sum_{m=1}^{\infty} \sum_{n=1}^{\infty} a_{mn}^2 \left(\frac{m^2}{a^2} + \frac{n^2}{b^2} \right)^2}{\sum_{m=1}^{\infty} \sum_{n=1}^{\infty} m^2 a_{mn}^2} \quad (4.30)$$

It can be shown that Equation (4.30) becomes a minimum if all coefficients a_{mn} , except one, are taken equal to zero. Thus

$$N_x = \frac{\pi^2 a^2 D}{m^2} \left(\frac{m^2}{a^2} + \frac{n^2}{b^2} \right)^2 \quad (4.31)$$

The smallest value of N_x will be obtained by taking n equal to 1. The physical meaning of this is that a plate buckles in such a way that there can be several half-waves in the direction of compression but only one half-wave in the perpendicular direction. Thus the expression for the critical value of the compressive force becomes

$$N_{x,cr} = \frac{\pi^2 D}{a^2} \left(m + \frac{1}{m} \frac{a^2}{b^2} \right)^2 \quad (4.32)$$

The first factor in this expression represents the Euler load for a strip of unit width and of length a . The second factor indicates in what proportion the stability of the continuous plate is greater than the stability of an isolated strip. The magnitude of this factor depends on the magnitude of the ratio a/b and also on the number

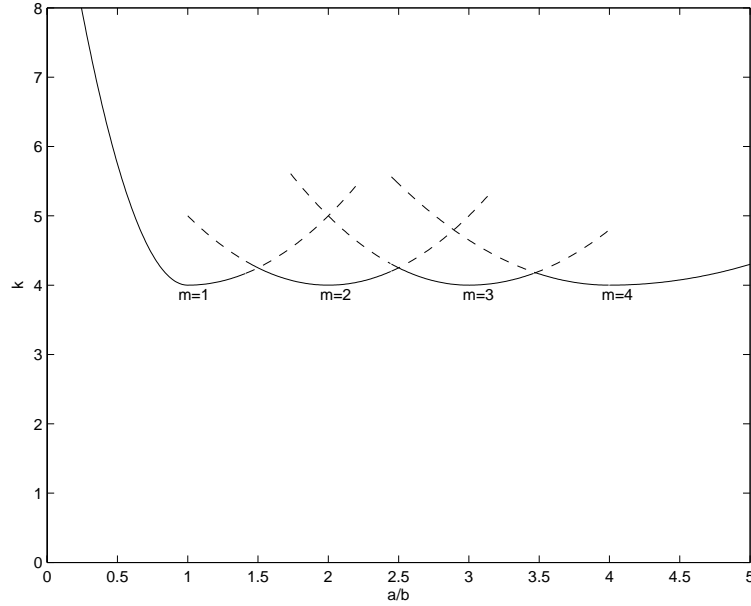


Figure 4.8: Buckling stress coefficients for uniaxially compressed plate [14].

m , which gives the number of half-waves into which the plate buckles. The critical load, with $m = 1$, can be written as

$$N_{x,\text{cr}} = \frac{\pi^2 D}{b^2} \left(\frac{b}{a} + \frac{a}{b} \right)^2 \quad (4.33)$$

Equation (4.33) can be represented in the form

$$N_{x,\text{cr}} = k \frac{\pi^2 D}{b^2} \quad (4.34)$$

in which k is a numerical factor, the magnitude of which depends on the ratio a/b . This factor is represented in Figure 4.8 by the curve marked $m = 1$. Assuming that the plate buckles into two half-waves and that the deflection surface is represented by

$$w = a_{21} \sin \frac{2\pi x}{a} \sin \frac{\pi y}{b} \quad (4.35)$$

provides an inflection line dividing the plate in halves and each half is in exactly the same condition as a simply supported plate of length $a/2$. Using Equation (4.33) for calculating the critical load and substituting a with $a/2$ in it gives

$$N_{x,\text{cr}} = \frac{\pi^2 D}{b^2} \left(\frac{2b}{a} + \frac{a}{2b} \right)^2 \quad (4.36)$$

The second factor in this expression, depending on the ratio a/b , is represented in Figure 4.8 by the curve $m = 2$. The curve $m = 2$ is obtained from the curve

$m = 1$ by keeping the ordinates unchanged and doubling the abscissas. Proceeding further in the same way and assuming $m = 3$, $m = 4$ and so on, the series of curves shown in Figure 4.8 are obtained. Having these curves, the critical load and the number of half-waves for any value of the ratio a/b can be determined by taking the corresponding point on the axis of abscissas and to choose the curve having the smallest ordinate for that point. In Figure 4.8 the portions of the curves defining the critical values of the load are shown by full lines. For very short plates the curve $m = 1$ gives the smallest ordinate. Beginning with the point of intersection of the curves $m = 1$ and $m = 2$, the second curve has the smallest ordinate, i.e., the plate buckles into two half-waves. Beginning from the point of intersection of the curves $m = 2$ and $m = 3$, the plate buckles into three half-waves, and so on. The transition from m to $m + 1$ half-waves occurs when the two corresponding curves have equal ordinates, i.e., when

$$\frac{mb}{a} + \frac{a}{mb} = \frac{(m+1)b}{a} + \frac{a}{(m+1)b} \quad (4.37)$$

or

$$\frac{a}{b} = \sqrt{m(m+1)} \quad (4.38)$$

After the number of half-waves m in which the plate buckles has been determined, the critical load is calculated from Equation (4.33).

The critical value of the compressive stress is then given by

$$\sigma_{\text{cr}} = \frac{N_{x,\text{cr}}}{h} = \frac{k\pi^2 E}{12(1-\nu^2)} \frac{h^2}{b^2} \quad (4.39)$$

where h is the thickness of the plate.

4.6.1 Comparison of Theory and BRIGADE/Plus

A comparison of this theory and results provided by BRIGADE/Plus is given below for three plates with ratios of a/b of 1, 2 and 3. Hence, for these ratios, the critical value of compressive stress is equal for all of the plates, since the value of k is 4 (in accordance with Figure 4.8). This value is

$$\sigma_{\text{cr}} = \frac{N_{x,\text{cr}}}{h} = \frac{\pi^2 E}{3(1-\nu^2)} \frac{h^2}{b^2} \quad (4.40)$$

All of these comparisons are made for plates with a width of 1 m and a thickness of 10 mm. The modulus of elasticity is assumed $E = 206.9$ GPa and $\nu = 0.3$. The models have been made of different number of elements and different element types, giving an indication of the influence of different modelling parameters. The load is applied as concentrated forces at 9, 17 and 65 points along the plate width depending on the mesh size. The load is applied as consistent nodal loads for two

of the models: the one with load applied at 9 nodes and a mesh of 256 elements/m² and the one with load applied at 65 nodes and a mesh of 4096 elements/m². For the other models the load is not applied to all nodes along the edge, which leads to a less accurate result. Their magnitudes are 1 N, 0.5 N and 0.125 N, respectively, giving a total applied load of 8 N along each side of the plate. According to Timoshenko's theory the value of the critical buckling stresses should be

$$\sigma_{cr} = 74.8 \text{ MPa}$$

The results from BRIGADE/Plus are presented in Tables 4.1 and 4.2. In Table 4.1, the analyses have been performed using the S4R element, while Table 4.2 shows the differences for some of the analyses using other element types.

Table 4.1: Critical compressive stresses for buckling of thin plates, using S4R elements.

Elements/m ²	Applied load	Stresses (MPa)		
		aspect ratio (a/b)		
		1	2	3
256	1N on 9 nodes	69.9	68.3	67.7
1024	1N on 9 nodes	69.4	67.8	67.3
4096	1N on 9 nodes	69.2	67.6	67.1
	0.5N on 17 nodes	71.6	70.9	70.6
	0.125N on 65 nodes	73.6	73.5	73.4

Table 4.2: Critical compressive stresses for buckling of thin plates, using different element types and with 4096 elements per m².

Element type	Applied load	Stresses (MPa)		
		aspect ratio (a/b)		
		1	2	3
S4	1N on 9 nodes	69.2	67.6	67.1
	0.5N on 17 nodes	71.6	70.9	70.6
	0.125N on 65 nodes	73.6	73.5	73.4
S8R5	1N on 9 nodes	69.2	67.6	67.1
S8R	1N on 9 nodes	69.0	67.5	67.0

In Figures 4.9-4.11 the first buckling mode for ratio a/b equal to 1, 2 and 3, respectively, are shown.

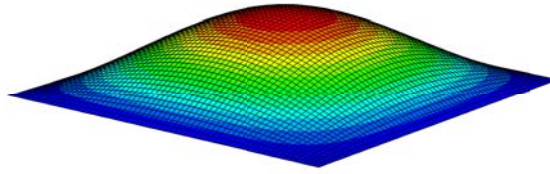


Figure 4.9: First buckling mode for thin rectangular plate uniformly compressed in one direction. Aspect ratio $a/b = 1$.

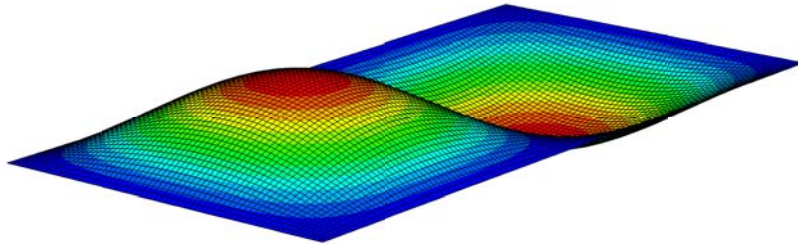


Figure 4.10: First buckling mode for thin rectangular plate uniformly compressed in one direction. Aspect ratio $a/b = 2$.

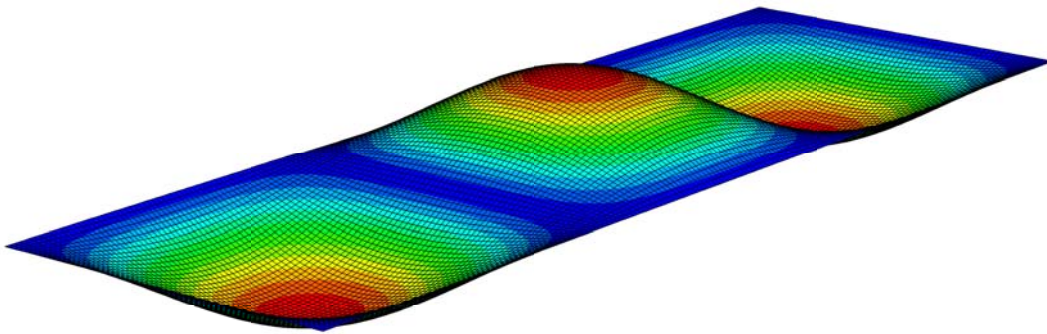


Figure 4.11: First buckling mode for thin rectangular plate uniformly compressed in one direction. Aspect ratio $a/b = 3$.

There is a small deviation in the results from BRIGADE/Plus and the analytical ones. This is because in the models the load is applied as concentrated forces along the edges of the plate while there is a uniform compressive force acting in the theoretical solution. It is also shown that the numerical solution from BRIGADE/Plus tends to approach the theoretical when the load is applied to more nodes. The best result is reached for the model with a mesh of 4096 elements/m² and the load applied as consistent nodal load at 65 nodes. The discrepancy from the analytical solution in this case is only 1.6%.

The models give the best results for the ratio $a/b = 1$, due to the increased margin of error when the model becomes larger. With more elements a more accurate result is found. But more elements require more computational costs, hence the number of elements should be chosen in such a way that the accuracy is satisfactory with as low as possible computational cost.

Which type of element to use is not an obvious choice. There is no direct correlation between an element using more nodes and a more accurate result, at least not when a reasonably dense mesh is used. Instead the emphasis should lie in choosing an element type that provides the most accurate result in the least computational time.

Chapter 5

Creating Models in BRIGADE/Plus

The procedure of creating finite element models in BRIGADE/Plus are explained in this chapter. Aspects like choice of elements and analysis procedure are discussed. The buckling phenomenon is studied closely and an explanation of made assumptions is given.

5.1 Modelling Procedures in BRIGADE/Plus

BRIGADE/Plus offers a wide range of possibilities for finite element analysis of various problems. Here are the ones used to analyse bridge Y288 over Ljungan presented. The models have been created in a procedure as follows:

1. The parts that form the model were drawn in the GUI.
2. The different parts were given material properties, such as modulus of elasticity, density, thickness and Poisson's ratio.
3. The parts were assembled to form the structure that was analysed.
4. Dividing the analysis into steps, there are two different types of steps: general analysis steps and linear perturbation steps. General analysis steps define sequential events: the state of the model at the end of one general step provides the initial state for the start of the next general step. Linear perturbation analysis steps provide the linear response of the model about the state reached at the end of the last general analysis step. For each step in the analysis it is possible to choose whether ABAQUS will account for nonlinear effects from large displacements and deformations or not. If the displacements in a model due to loading are relatively small during a step, the effects may be small enough to be ignored. However, in cases where the loads on a model result in large displacements, nonlinear geometric effects can become important.

General analysis steps and linear perturbation steps are further discussed in section 5.3 and 5.4, respectively.

5. The assembled parts were connected to each other. These connections were created using the *tie constraint* and *surface-to-surface contact* interactions. The tie constraint ties two separate surfaces together so that there is no relative motion between them. It constrains each of the nodes on the slave surface to have the same value of displacement as the point on the master surface to which it is closest. The surface-to-surface contact interaction establishes an interaction between two surfaces, thus preventing them from sliding through each other.
6. Loads and boundaries were specified. Loads can be applied as concentrated forces, pressure loads and gravity loads. The boundaries can be defined as symmetry/antisymmetry/encastre boundaries or displacement/rotational boundaries, and can be applied to nodes or surfaces.
7. The model was meshed. Applying a mesh to the model involves choices of element type and size. There is a variety of element types to choose from and their size may vary for different parts of the model. The choice of element is further discussed in section 5.5.
8. The model is submitted for analysis.
9. A critical evaluation of the results needs to be done by the user. The program provides an enormous amount of results and it is vital that these are interpreted correctly.

5.2 Buckling in General

Buckling means loss of the stability of an equilibrium configuration, without fracture or separation of the material or at least prior to it [9]. Generally there are two types of buckling: *Bifurcation buckling* and *Snap-trough buckling*. Bifurcation buckling is the kind of buckling familiar from elementary column theory. For an axial compressive load of magnitude P_{cr} , called the critical load, the straight prebuckling configuration ceases to be a stable state of equilibrium and an alternative buckled configuration is also possible. Buckling may also appear without bifurcation, as a limit point, where there is no alternative and infinitesimally close equilibrium configuration.

A *primary path* is the original load-displacement line or curve and its extension. The *secondary path* is the alternative path that originates when the critical load is reached. The two paths intersect at the *bifurcation point*. Past the bifurcation point, the primary path is unstable. Although it is possible mathematically that the structure follows the primary path, a real structure will follow the secondary path instead. If the secondary path has a positive derivative (rises), the structure has post-buckling strength. A limit point is a maximum on a load-displacement curve.

It is not a bifurcation point because there is no immediate adjacent equilibrium configuration. When a limit point load is reached under increasing load, snap-through buckling occurs, as the structure assumes a new configuration by suddenly moving. A collapse load is the maximum load a structure can sustain without gross deformation. It may be greater or less than the computed bifurcation buckling load as shown in Figure 5.1.

Figure 5.1 shows possible behaviours when loads are applied to a structure. Here P is the load magnitude and D is the displacement. The material is assumed to remain linearly elastic and loads are gradually applied.

In Figure 5.1(a) the prebuckling path is linear. At bifurcation, two very closely spaced equilibrium positions are possible. Thereafter, for $P > P_{cr}$, a real (imperfect) structure follows the secondary path. Since the postbuckling path rises, the structure can be said to have postbuckling strength. In this case, P_{cr} characterises a local buckling action that has little to do with overall strength. The structure will collapse at the limit point, which is considerably greater than the critical load.

Figure 5.1(b) describes a different type of behaviour. The structure has a nonlinear prebuckling path and the postbuckling path falls, hence the structure has no postbuckling strength. Closely spaced primary and falling secondary paths implies that the structure is *imperfection sensitive*. Imperfection sensitivity means that small changes in load directions, geometry and/or boundary conditions strongly affect the collapse load.

If knowledge of the structural behaviour of the model is little or none, one must anticipate that a computed bifurcation buckling load may be far above or far below the actual collapse load, imperfections may be influential and that prebuckling nonlinearities may be important [8].

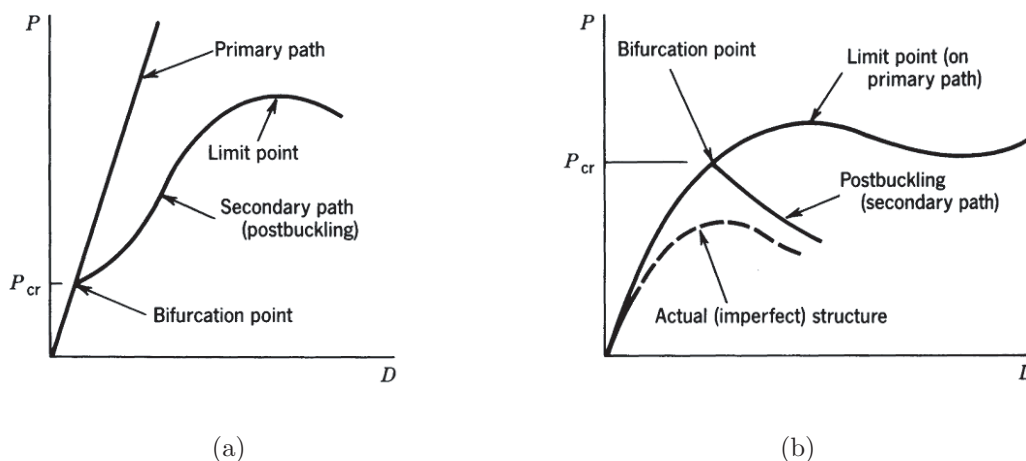


Figure 5.1: Possible load versus displacement behaviour of thin-walled structures (from [8]).

5.3 General Static Analysis

A general analysis step is one in which the effects of any nonlinearities present in the model can be included. General analysis steps define sequential events: the state of the model at the end of one general step provides the initial state for the start of the next general step.

Nonlinear stress analysis problems can contain up to three sources of nonlinearity: material nonlinearity, geometric nonlinearity and boundary nonlinearity.

It is possible to define a problem as a small-displacement analysis by ignoring the geometric nonlinearity—the kinematic relationships are linearised. The alternative to a small-displacement analysis is to include large-displacement effects by including the NLGEOM parameter on the *STEP option.

In some geometric nonlinear analyses, buckling or collapse may occur. When the loading can be considered proportional (the loading over the complete structure can be scaled with a single parameter), a special approach—called the “modified Riks method”—can be used. In other unstable analyses the instabilities are local (e.g., surface wrinkling, material instability or local buckling), in which case global load control methods such as the Riks method are not appropriate.

5.4 Linear Eigenvalue Buckling Prediction

The response in a linear analysis step is the linear perturbation response about the *base state*. The base state is the current state of the model at the end of the last general analysis step prior to the linear perturbation step. If the first step of an analysis is a perturbation step, the base state is determined from the initial conditions.

Linear perturbation analyses can be performed from time to time during a fully nonlinear analysis by including the linear perturbation steps between the general response steps. The linear perturbation response has no effect as the general analysis is continued. If geometric nonlinearity is included in the general analysis upon which a linear perturbation study is based, stress stiffening or softening effects and load stiffening effects are included in the linear perturbation analysis.

In an eigenvalue buckling problem the loads for which the model stiffness matrix becomes singular are searched, so that the problem

$$\mathbf{K}^{\text{MN}}\nu^{\text{M}} = \mathbf{0}$$

has nontrivial solutions. \mathbf{K}^{MN} is the tangent stiffness matrix when the loads are applied, and the ν^{M} are nontrivial displacement solutions. Eigenvalue buckling is generally used to estimate the critical buckling loads of stiff structures, e.g. structures carrying their loads primarily by axial or membrane action. However, even when the response of a structure is nonlinear prior to collapse, a general eigenvalue buckling

analysis can provide useful estimates of collapse mode shapes. Some structures have many buckling modes with closely spaced eigenvalues, which can cause numerical problems. In these cases it often helps to apply enough preload, just below the buckling load, before performing the eigenvalue extraction. In many cases a series of closely spaced eigenvalues indicates that the structure is imperfection sensitive. An eigenvalue buckling analysis will not give accurate predictions of the buckling load for imperfection sensitive structures; the static Riks procedure should be used instead. Sometimes negative eigenvalues are reported in an eigenvalue buckling analysis. In most cases such negative eigenvalues indicate that the structure would buckle if the load were applied in the opposite direction.

The eigenvalues given in a linear eigenvalue prediction are linear to the applied load in the step. Hence, the structure will buckle at a load equal to the applied load, in the linear eigenvalue prediction step, multiplied with the obtained eigenvalue. For example, if an applied pressure load of 3 kN/m² gives an eigenvalue of 20, the structure will buckle at a pressure load of 60 kN/m².

5.4.1 The BUCKLE Command

An eigenvalue buckling step is defined by the *BUCKLE command. The buckling command may be set to predict eigenvalues using two different methods of calculations, Lanczos or subspace. Generally the Lanczos eigensolver is said to be faster when a large number of eigenmodes is required from a structure with many degrees of freedom. The subspace eigensolver can be faster for a smaller system. Both methods may be used for different steps in the same analysis. The Lanczos solver can be set to predict eigenvalues in a numeric range, i.e. the minimum and maximum limits may be prescribed. The subspace iteration does not offer the possibility to define a minimum limit. The Lanczos eigensolver cannot be used in cases where the stiffness matrix is indefinite, i.e. if a model is preloaded above the bifurcation load, if it contains contact pairs and contact elements, if it contains hybrid elements of connector element, etc. [10].

5.4.2 The IMPERFECTION Command

Imperfections are usually introduced by perturbations in the geometry. ABAQUS offers three ways to define an imperfection: as a linear superposition of buckling eigenmodes, from the displacements of a *STATIC analysis, or by specifying the node number and imperfection values directly. The usual approach involves two analysis runs with the same model definition:

1. An eigenvalue buckling analysis is performed on the “perfect” structure to establish probable collapse modes and to verify that the mesh discretises those modes accurately.
2. In the second analysis run imperfections in the geometry are introduced by

addition of the buckling modes to the “perfect” geometry using the *IMPERFECTION option. The imperfection has the form

$$\Delta \mathbf{x}_i = \sum_{i=1}^M \omega_i \phi_i$$

where ϕ_i is the i^{th} eigenmode and ω_i is the associated scale factor. The magnitudes of the perturbations are typically a few percent of a relative structural dimension such as a beam cross-section or shell thickness.

3. A geometrically nonlinear load-displacement analysis of the structure containing the imperfections is performed using the Riks method. In this way the Riks method can be used to perform postbuckling analyses of “stiff” structures that show linear behaviour prior to buckling, if perfect.

5.5 Elements

Given a structural geometry, with two dimensions considerably greater than the third and a relatively complex design, the use of *shell elements* is a suitable choice. ABAQUS shell elements assume that plane sections perpendicular to the plane of the shell remain plane [10].

There are three different classes of shell elements, distinguished by the applicability of the element to thin and thick shell problems. General-purpose shell elements are valid for use with both thick and thin shell problems and they also consider finite membrane strains. The general-purpose elements are: S4, S4R, S3/S3R, SAX1, SAX2 and SAX2T. The special-purpose shell elements fall into two categories: thin-only shell elements, including STRI3, STRI65, S4R5, S8R5, S9R5 and SAXA, and thick-only shell elements, including S8R and S8RT. For thick shells, transverse shear flexibility is important, while it is negligible for thin shells.

ABAQUS uses numerical integration to calculate the stresses and strains independently at each integration point through the thickness of the shell, thus allowing nonlinear material behaviour. By default, ABAQUS uses five section points through the thickness of a homogeneous shell.

Throughout the modelling in this thesis the S4R element has been used most frequent. The S4R element is a 4-node, quadrilateral, stress/displacement shell element with reduced integration.

5.6 Improving Convergence

In nonlinear problems the challenge is always to obtain a convergent solution in the least possible computational time. ABAQUS offers two approaches for controlling incrementation. Direct user control, whereby the user specifies the increment

scheme. Automatic control, whereby the user defines the step and, in some procedures, specifies certain tolerances or error measures. ABAQUS then automatically select the increment size against the response in the step.

Some static problems can be naturally unstable, for a variety of reasons. Instability may also be caused by localised buckling behaviour or by material instability. The static, general analysis procedures in ABAQUS can stabilise this type of problem if the STABILIZE parameter is included on the procedure option.

5.7 Assumptions

Some simplifying assumptions are consistently made while producing finite element models. A general attitude towards these are to make as few as possible and to make them in a manner that they do not affect the correctness of the analysis. Some of the assumptions made here are described below:

- Abutments

The abutments are assumed to be completely rigid, hence they do not deform from the loads applied upon them. They have therefore been omitted from the model and boundary conditions have been applied directly to the box girder bearings.

- Loads from cast concrete

When casting the midsection of the bridge the, concrete is assumed to be equally distributed over the whole section, providing an even pressure on the flanges.

- Camber

The fabricated box girder has a camber (initial elevation) at mid-span. This is omitted and the model is made level in the horizontal plane.

Chapter 6

Profiled Sheeting in Shear

Two models have been created for analysis. One model for a close study of the effects of the attachment of the profiled sheeting to the top flanges of the box girder and of the thickness of these profiled sheets. This one will be described in this chapter, where the study of the influence of how the profiled sheeting is attached is presented in section 6.1 and the study of the effects of variations in thickness of the profiled sheets is presented in section 6.2. The other model aims to study the global behaviour of the bridge, emphasising the effects of initial geometrical imperfections and it will be described in Chapter 7.

6.1 Profiled Sheet Attachment

This model symbolises a part of the bridge, containing five profiled sheets and parts of the underlying top flanges of the box girder. Two analyses were performed, one where the profiled sheeting was attached along the long sides only and one where it was attached along all sides. Dimensions and material properties of the profiled sheets and the underlying top flanges are given in Table 6.1. The long and short plate and the profiled sheet are shown in Figure 6.1. In Figures 6.2 and 6.3, the models are shown when the profiled sheets are attached along the long sides only and along all sides, respectively.

Table 6.1: Dimensions and material properties.

Part	Outer dimensions (mm ²)	Thickness (mm)	Modulus of elasticity (GPa)	Poisson's ratio (-)
Long plate	4500 × 300	30	210	0.3
Short plate	300 × 2700	30		
Profiled sheet	950 × 2800	0.86		

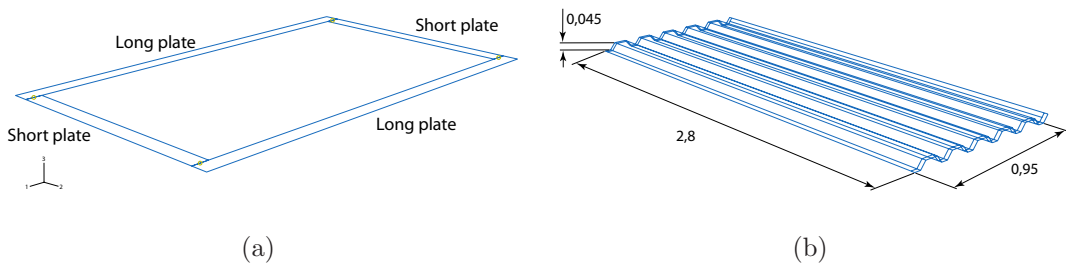


Figure 6.1: (a) Long and short plate. (b) Profiled sheet with dimensions.

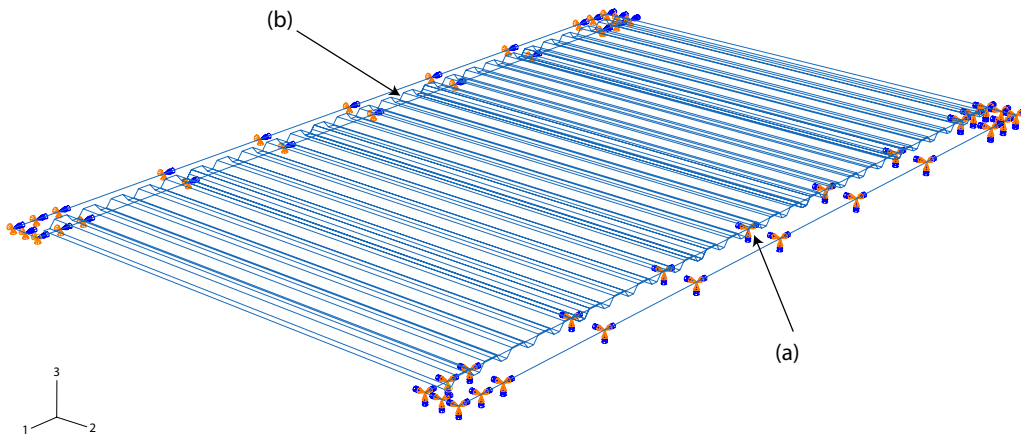


Figure 6.2: The model for analysis of profiled sheet attachment along the long sides only. Plate (a) is lock in all translational degrees of freedom. Plate (b) is free to move in its axial direction. Concentrated forces are applied to plate (b), in two or four nodes.

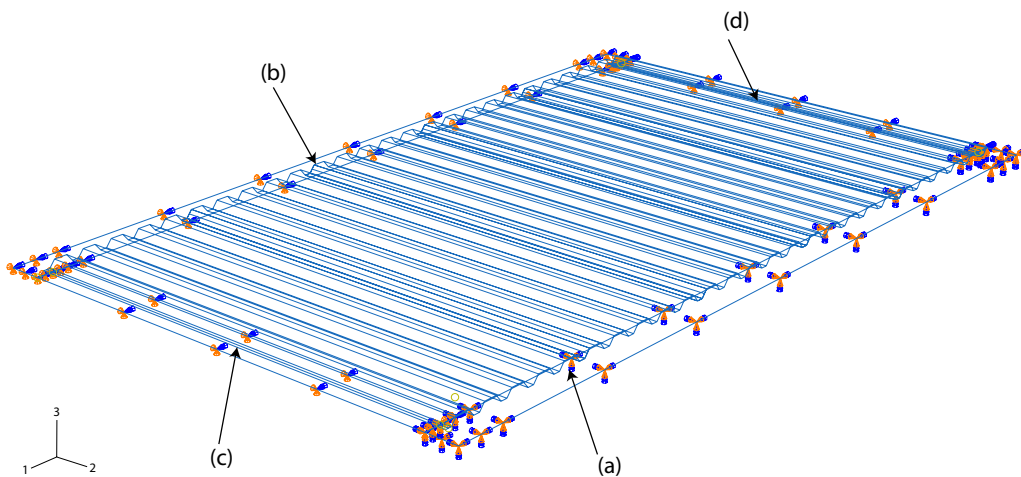


Figure 6.3: The model for analysis of profiled sheet attachment along all sides. Plate (a) is lock in all translational degrees of freedom. Plate (b) is free to move in its axial direction. Plates (c) and (d) are lock in translation out of its plane. Concentrated forces are applied to plate (b), in two or four nodes.

In the first analysis the profiled sheets are attached to the top flanges along the long sides with a tie-interaction. This ties one node in each profile-bottom of the profiled sheets to the surface of the top flange. In addition to this, a surface-to-surface contact interaction is included between these parts. This to prevent an unrealistic movement of the profiled sheets where it slides through the top flange. One of the top flanges is given a fixed support, locking all of its degrees of freedom. The other is free to move in its axial direction and a force is applied to it in this direction. The application of this force gives rise to similar action upon the structure as an incipient torsion of the box girder. Three different meshes have been analysed providing an indication of the reliability of the results from the analyses¹.

In the second analysis there are, besides the interactions already defined, additional tie-interactions along the short sides. Here nodes with c/c 400 mm on the outer profiled sheets are tied to the additional top flanges to create an all around attachment. There is also an surface-to-surface contact interaction between the short side top flanges and the part of the profiled sheets that are in contact. Otherwise the model is created equally to the first one, regarding boundaries, loads and mesh.

6.2 Profiled Sheet Thickness

In this analysis, the same model as in the first analysis was used, i.e. the profiled sheets are attached along the long sides only (as shown in Figure 6.2), and the thickness of the sheets was altered. The analysis is performed for three different thicknesses: 0.774 mm, 0.86 mm and 0.946 mm. The thickness 0.86 mm is the thickness of the profiled sheet that is used in the bridge and 0.774 mm and 0.946 mm represent a decrease and an increase of 10%, respectively.

6.3 Results

The evaluation of the results focuses mainly on the stresses that arise in the transverse direction in the profiled sheeting.

Sheets subjected to transverse shear forces will show stress-concentrations at the edges, as shown in Figure 6.4. If the sheets are attached along all sides, these stresses will decrease compared to if the sheets are attached only along two sides, as shown in Figure 6.5.

The results of the study concerning the influence of the profiled sheet attachment are displayed in Tables 6.2-6.4 and those of the study concerning the influence of the profiled sheet thickness are shown in Tables 6.6-6.7. Some remarks on the results and analysis procedure are presented below:

¹If one model with, e.g., 1000 elements and one with 2000 elements are studied, and they give similar results one can say that the mesh is sufficient accurate. The errors from bad meshing are small enough.

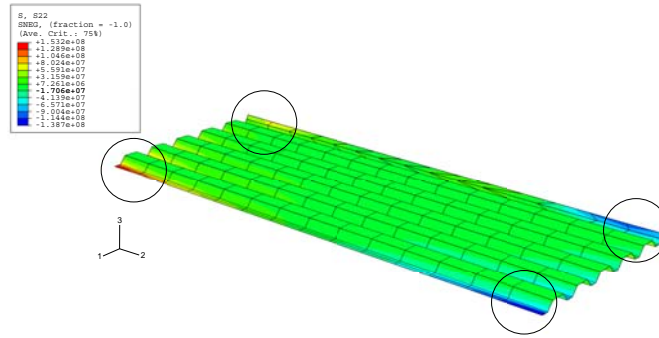


Figure 6.4: Transverse stresses for profiled sheet attached at two sides.

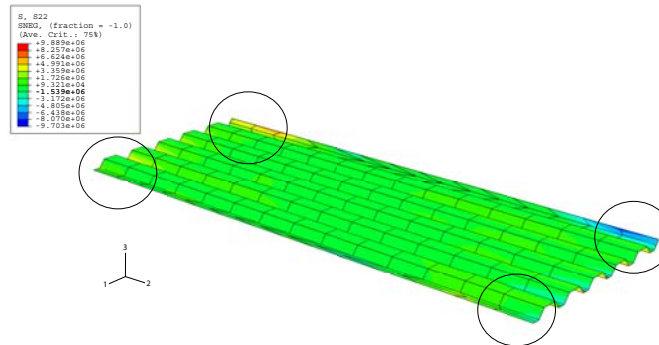


Figure 6.5: Transverse stresses for profiled sheet attached along all sides.

- The magnitude of applied forces are not particularly interesting. Instead it is the differences in stresses, tensions and their distribution between the models that are of interest.
- The stresses that arise at the outer profile bottoms of the sheets for the case where the sheets are attached only along the long sides are substantially reduced for the case where the sheets are attached along all four sides. This is shown in Figures 6.4 and 6.5.
- When the profiled sheets are attached along all outer boundaries the stress distribution is much more favourable in terms of the ability of the structure to resist applied forces. Hence, this type of attachment creates a more stable structure.
- For the model with an all around attachment, an average reduction of 94% in stresses and tensions is attained. Hence, a considerably stronger structure is provided with an overall, all around attachment of the profiled sheeting than when it is attached only along two sides.
- If a 10% thinner profiled sheeting is attached, an average increase of about 20% of the stresses and tensions is attained. If a 10% thicker profiled sheeting is attached, an average decrease of about 15% of the stresses and tensions is attained.

Table 6.2: Results from analysis of influence of trapezoidal sheet attachment with a model composed of 2078/2138 elements.

	Applied load			
	20000 N at two nodes		10000 N at four nodes	
	Longside	Around	Longside	Around
$\sigma_{\text{Mises,max}}$ (MPa)	313.7	15.0	312.9	23.2
$\sigma_{11,\text{max}}$ (MPa)	187.9	9.3	187.6	15.4
$\sigma_{11,\text{min}}$ (MPa)	-361.5	-17.2	-360.4	-26.7
$\sigma_{22,\text{max}}$ (MPa)	180.0	7.5	177.9	10.5
$\sigma_{22,\text{min}}$ (MPa)	-162.4	-7.1	-161.4	-11.4
$\sigma_{12,\text{max}}$ (MPa)	85.7	4.2	85.7	6.3
$\sigma_{12,\text{min}}$ (MPa)	-33.5	-6.2	-33.9	-3.3
$\epsilon_{11,\text{max}}$ ($\cdot 10^{-6}$)	910.3	45.4	909.7	66.5
$\epsilon_{11,\text{min}}$ ($\cdot 10^{-6}$)	-1491	-71.8	-1488	-110.9
$\epsilon_{22,\text{max}}$ ($\cdot 10^{-6}$)	771.3	27.6	762.3	39.9
$\epsilon_{22,\text{min}}$ ($\cdot 10^{-6}$)	-652.6	-30.3	-644.9	-44.2
$\epsilon_{12,\text{max}}$ ($\cdot 10^{-6}$)	1061	52.5	1061	78.5
$\epsilon_{12,\text{min}}$ ($\cdot 10^{-6}$)	-414.4	-76.8	-419.5	-40.6
u_{max} (mm)	14.9	0.7	14.9	1.1

Table 6.3: Results from analysis of influence of trapezoidal sheet attachment with a model composed of 4260/4368 elements.

	Applied load			
	20000 N at two nodes		10000 N at four nodes	
	Longside	Around	Longside	Around
$\sigma_{\text{Mises,max}}$ (MPa)	474.0	27.3	473.4	28.5
$\sigma_{11,\text{max}}$ (MPa)	244.6	16.0	244.8	17.8
$\sigma_{11,\text{min}}$ (MPa)	-517.7	-29.5	-516.3	-31.0
$\sigma_{22,\text{max}}$ (MPa)	251.0	13.7	248.4	13.8
$\sigma_{22,\text{min}}$ (MPa)	-215.4	-10.2	-213.0	-10.8
$\sigma_{12,\text{max}}$ (MPa)	158.2	9.2	158.3	9.6
$\sigma_{12,\text{min}}$ (MPa)	-56.2	-6.4	-55.6	-5.9
$\epsilon_{11,\text{max}}$ ($\cdot 10^{-6}$)	961.4	62.4	962.6	71.2
$\epsilon_{11,\text{min}}$ ($\cdot 10^{-6}$)	-2287	-131.4	-2284	-137.6
$\epsilon_{22,\text{max}}$ ($\cdot 10^{-6}$)	1069	46.8	1057	47.1
$\epsilon_{22,\text{min}}$ ($\cdot 10^{-6}$)	-891.2	-42.3	-881.6	-45.3
$\epsilon_{12,\text{max}}$ ($\cdot 10^{-6}$)	1958	114.1	1960	118.8
$\epsilon_{12,\text{min}}$ ($\cdot 10^{-6}$)	-696.1	-79.2	-688.8	-72.9
u_{max} (mm)	15.9	0.9	15.9	1.0

Table 6.4: Results from analysis of influence of trapezoidal sheet attachment with a model composed of 10320/10752 elements.

	Applied load			
	20000 N at two nodes		10000 N at four nodes	
	Longside	Around	Longside	Around
$\sigma_{\text{Mises,max}}$ (MPa)	634.0	29.4	635.1	26.9
$\sigma_{11,\text{max}}$ (MPa)	270.4	13.4	270.0	11.7
$\sigma_{11,\text{min}}$ (MPa)	-661.7	-30.2	-660.3	-27.9
$\sigma_{22,\text{max}}$ (MPa)	308.9	10.7	311.8	9.5
$\sigma_{22,\text{min}}$ (MPa)	-256.2	-8.2	-253.6	-7.8
$\sigma_{12,\text{max}}$ (MPa)	212.9	10.0	213.2	10.2
$\sigma_{12,\text{min}}$ (MPa)	-95.5	-11.0	-95.3	-6.0
$\epsilon_{11,\text{max}}$ ($\cdot 10^{-6}$)	1152	57.9	1150	50.4
$\epsilon_{11,\text{min}}$ ($\cdot 10^{-6}$)	-3003	-138.4	-3003	-126.7
$\epsilon_{22,\text{max}}$ ($\cdot 10^{-6}$)	1316	36.6	1329	37.0
$\epsilon_{22,\text{min}}$ ($\cdot 10^{-6}$)	-1061	-36.5	-1050	-33.3
$\epsilon_{12,\text{max}}$ ($\cdot 10^{-6}$)	2636	123.7	2640	126.0
$\epsilon_{12,\text{min}}$ ($\cdot 10^{-6}$)	-1183	-136.6	-1180	-74.8
u_{max} (mm)	16.2	0.7	16.2	0.7

Table 6.5: Results from analysis of influence of profiled sheet thickness with a model having a two-sided attachment of the profiled sheeting composed of 2078 elements.

	Sheet thickness (mm)		
	0.86	0.774	0.946
$\sigma_{\text{Mises,max}}$ (MPa)	312.9	377.0	263.8
$\sigma_{11,\text{max}}$ (MPa)	187.6	218.2	168.6
$\sigma_{11,\text{min}}$ (MPa)	-360.4	-434.1	-304.0
$\sigma_{22,\text{max}}$ (MPa)	177.9	208.9	154.3
$\sigma_{22,\text{min}}$ (MPa)	-161.4	-191.9	-138.3
$\sigma_{12,\text{max}}$ (MPa)	85.7	100.1	74.4
$\sigma_{12,\text{min}}$ (MPa)	-33.9	-41.7	-28.2
$\epsilon_{11,\text{max}}$ ($\cdot 10^{-6}$)	909.7	1031	810.9
$\epsilon_{11,\text{min}}$ ($\cdot 10^{-6}$)	-1488	-1795	-1253
$\epsilon_{22,\text{max}}$ ($\cdot 10^{-6}$)	762.3	891.9	665.5
$\epsilon_{22,\text{min}}$ ($\cdot 10^{-6}$)	-644.9	-743.0	-568.4
$\epsilon_{12,\text{max}}$ ($\cdot 10^{-6}$)	1061	1239	920.7
$\epsilon_{12,\text{min}}$ ($\cdot 10^{-6}$)	-419.5	-516.1	-349.0
u_{max} (mm)	14.9	19.7	11.6

Table 6.6: Results from analysis of influence of profiled sheet thickness with a model having a two-sided attachment of the profiled sheeting composed of 4260 elements.

	Sheet thickness (mm)		
	0.86	0.774	0.946
$\sigma_{\text{Mises,max}}$ (MPa)	473.4	567.9	400.8
$\sigma_{11,\text{max}}$ (MPa)	244.8	293.1	208.0
$\sigma_{11,\text{min}}$ (MPa)	-516.3	-618.8	-437.5
$\sigma_{22,\text{max}}$ (MPa)	248.4	292.4	214.8
$\sigma_{22,\text{min}}$ (MPa)	-213.0	-247.9	-186.1
$\sigma_{12,\text{max}}$ (MPa)	158.3	186.6	135.9
$\sigma_{12,\text{min}}$ (MPa)	-55.6	-67.5	-46.9
$\epsilon_{11,\text{max}}$ ($\cdot 10^{-6}$)	962.6	1141	828.4
$\epsilon_{11,\text{min}}$ ($\cdot 10^{-6}$)	-2284	-2736	-1935
$\epsilon_{22,\text{max}}$ ($\cdot 10^{-6}$)	1057	1237	919.3
$\epsilon_{22,\text{min}}$ ($\cdot 10^{-6}$)	-881.6	-1017	-776.4
$\epsilon_{12,\text{max}}$ ($\cdot 10^{-6}$)	1960	2313	1683
$\epsilon_{12,\text{min}}$ ($\cdot 10^{-6}$)	-688.8	-835.8	-580.7
u_{max} (mm)	15.9	21.1	12.3

Table 6.7: Results from analysis of influence of profiled sheet thickness with a model having a two-sided attachment of the profiled sheeting composed of 10320 elements.

	Sheet thickness (mm)		
	0.86	0.774	0.946
$\sigma_{\text{Mises,max}}$ (MPa)	635.1	760.1	538.6
$\sigma_{11,\text{max}}$ (MPa)	270.0	326.3	227.5
$\sigma_{11,\text{min}}$ (MPa)	-660.3	-78.8	-561.9
$\sigma_{22,\text{max}}$ (MPa)	311.8	366.8	270.0
$\sigma_{22,\text{min}}$ (MPa)	-253.6	-293.4	-222.2
$\sigma_{12,\text{max}}$ (MPa)	213.2	251.4	183.2
$\sigma_{12,\text{min}}$ (MPa)	-95.3	-114.2	-80.8
$\epsilon_{11,\text{max}}$ ($\cdot 10^{-6}$)	1150	1392	973.5
$\epsilon_{11,\text{min}}$ ($\cdot 10^{-6}$)	-3003	-3585	-2553
$\epsilon_{22,\text{max}}$ ($\cdot 10^{-6}$)	1329	1559	1153
$\epsilon_{22,\text{min}}$ ($\cdot 10^{-6}$)	-1050	-1209	-924.3
$\epsilon_{12,\text{max}}$ ($\cdot 10^{-6}$)	2640	3113	2268
$\epsilon_{12,\text{min}}$ ($\cdot 10^{-6}$)	-1180	-1414	-1001
u_{max} (mm)	16.2	21.5	12.5

Chapter 7

Lateral Torsional Stability

This model is used to study the lateral torsional stability of the bridge. The influence of the profiled sheeting and its attachment, and also the influence of geometric imperfections in the box girder, mainly in shape of an initial rotation, are considered. Three different models are studied in this analysis:

- a model composed of the steel box girder only,
- a model composed of the steel box girder and all the profiled sheets, and
- a model composed of the steel box girder and all the profiled sheets, except the ones closest to the abutments. This last model is made to study what importance it has to make an all around attachment of the profiled sheets to the top flanges of the box girder. The bridge that collapsed (Y1504) had the profiled sheets attached as in this model.

The box girder is made as one homogeneous part of shell elements, with the external dimensions $57 \times 3.9 \times 2.0$ m³, as shown in Figure 7.1.

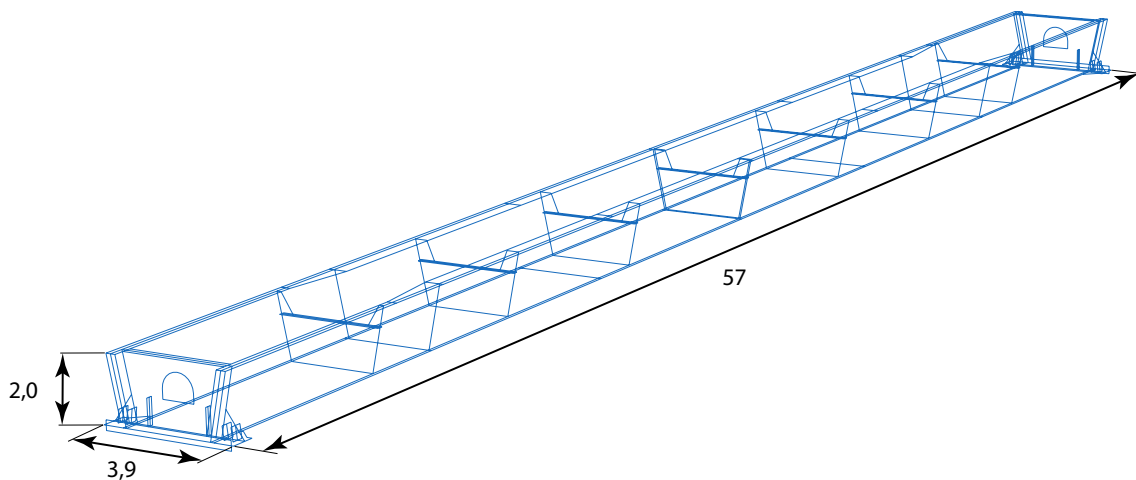


Figure 7.1: Model of steel box girder with external dimensions.

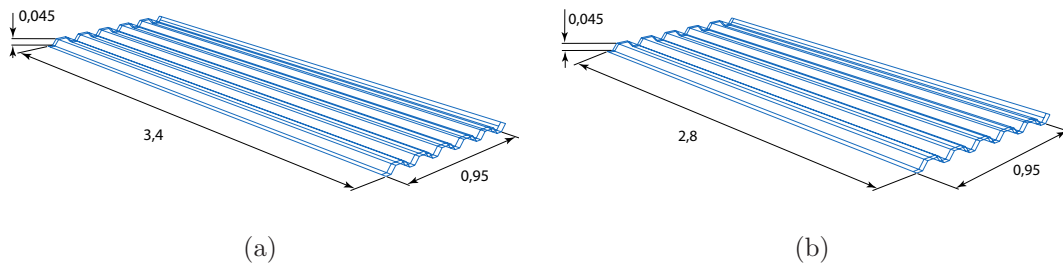


Figure 7.2: Model and dimensions of the long profiled sheet (a) and the short profiled sheet (b).

The profiled sheets are made as a homogeneous part of shell elements, with the external dimensions $0.95 \times 3.4 \times 0.045 \text{ m}^3$ or $0.95 \times 2.8 \times 0.045 \text{ m}^3$, as shown in Figure 7.2. There are 11 long profiled sheets, attached from each abutment and towards the centre of the bridge, and 38 short profiled sheets attached at the centre part of the bridge.

Dimensions and material properties for the parts are given in Table 7.1. The profiled sheets are connected to the box girder in each profile bottom with a tie-interaction, locking all translational degrees of freedom of the node in the profile bottom to the top flange of the box girder. They are also tied mutually in the same manner as for the small model. The connections for the profiled sheets are shown in Figure 7.3.

The boundary conditions are defined equally for all three models. The bearings at one end of the bridge are locked in all translational degrees of freedom while the bearings at the other end are locked only in the axial and transverse direction. Apart from the formwork and reinforcement, which are modelled as loads, the self-weight, wind load and the load from the cast concrete are applied.

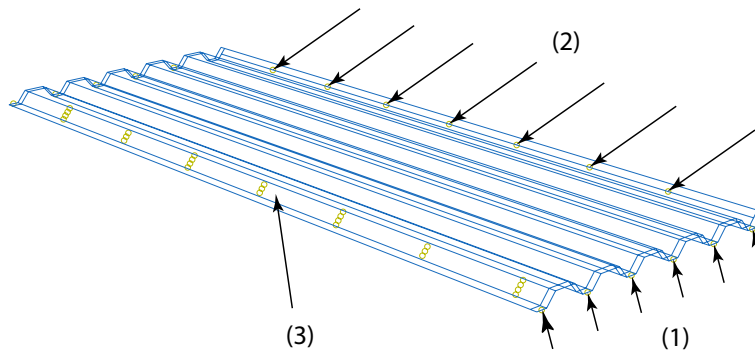


Figure 7.3: Profiled sheet with connections: (1) are the tie interactions between the profiled sheet and the box girder top flange. (2) are the slave nodes in the tie interaction between the profiled sheets, and (3) represent the master surface in the same interaction. The slave nodes in (2) are tied to the master surface of the *next* profiled sheet.

Table 7.1: Dimensions and material properties.

Part	Outer dimensions (m)	Thickness (mm)	Modulus of elasticity (GPa)	Poisson's ratio (-)
Box girder	$57 \times 3.9 \times 2$	10 – 38	210	0.3
Central profiled sheets	$0.95 \times 2.7 \times 0.045$	0.86		
Outer profiled sheets	$0.95 \times 3.3 \times 0.045$	0.86		

7.1 Implementation of Geometric Imperfections

The implementation of geometric imperfections is performed by first performing a linear eigenvalue prediction, which provides the buckling modes for the structure. These buckling modes are then added to the model as imperfections in the geometry, giving the “perfect” structure displacements that correspond to the applied eigenmodes.

In the linear eigenvalue prediction the first overall buckling mode is the most vital to find, since this buckling mode corresponds well to the form that the box girder has due to production imperfections, hence the way the bridge will deform in case of collapse. However, this particular buckling mode is not trivial to find in the model containing both the box girder and the profiled sheets because a large amount of local buckling modes, mainly in the profiled sheets, will appear prior to any overall buckling mode. In order to avoid a linear eigenvalue prediction that only provides numerous local buckling modes, a linear eigenvalue prediction can be performed on a model composed of the steel box girder only. In this way, an overall buckling mode is obtained much earlier in the analysis. The buckling modes of interest can then be implemented to the model composed of both the steel box girder and the profiled sheets, given that the node numbers are the same in both the linear eigenvalue prediction analysis and the other model.

The buckling modes of interest, i.e. mainly the first overall buckling mode but also random local buckling modes, are introduced to the structure with a suitable scaling factor providing the geometric imperfections to the structure. The scaling factor is varied in different analyses, providing an indication of the influence of the magnitude of the geometric imperfections.

7.1.1 Linear Eigenvalue Prediction

The linear eigenvalue prediction is performed using the Lanczos eigensolver. The first 100 buckling modes larger than zero are sought. Three concentrated forces at each top flange, as shown in Figure 7.4, are applied to create the perturbation.

The first overall buckling mode given by this analysis is shown in Figure 7.5. This mode, and some random local buckling modes like those in Figure 7.6, are introduced to the models with different scaling factors for the postbuckling analysis.

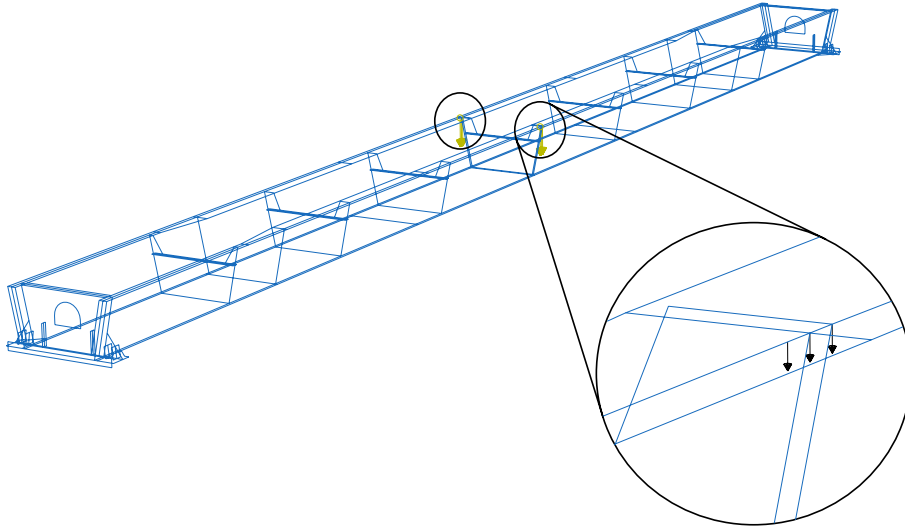


Figure 7.4: Loads in the linear eigenvalue prediction analysis.

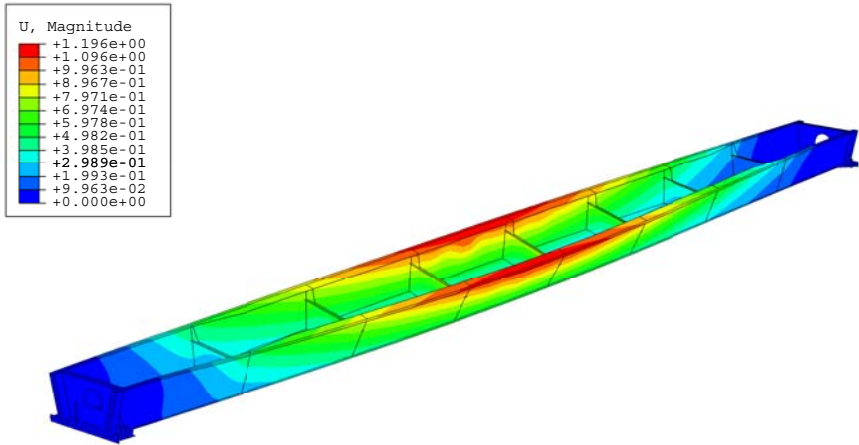


Figure 7.5: First overall buckling mode from the linear eigenvalue prediction.

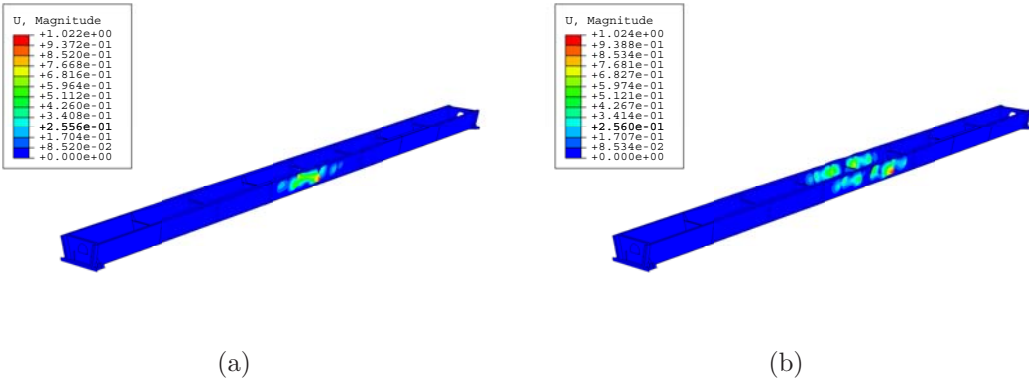


Figure 7.6: Typical local buckling modes.

7.2 Postbuckling Analysis

The postbuckling analysis aims to analyse the bridge response, regarding stresses and deformations, to the applied loads with different geometrical imperfections and different attachments of the profiled sheeting. Analyses are carried out on the three different models as described below:

- The first overall buckling mode is introduced with a scaling factor $w = 0.05$. Additionally, a few random local buckling modes are introduced with a scaling factor of $w = 0.001$. The loads are applied as:
 - A pressure load of 5 kN/m^2 at the top flanges representing the wooden formwork.
 - A pressure load of 1.5 kN/m^2 , acting transversally on the structure, representing the wind load.
 - An additional pressure load of 45 kN/m^2 at the central part of the top flanges representing the cast concrete.

The model is meshed with an approximate global element size of 0.48 meter and the S4R element is chosen. The loads from the wooden formwork and wind load are applied in a non-linear static general step, while the cast concrete is applied in a Riks step.

- Additional analyses are performed with the following changes:
 - The overall buckling mode is introduced with a scaling factor of 0.01, 0.1 and 0.2.
 - The model is meshed with an approximate global element size of 0.24 meter.

7.3 Results

First, the results from the analyses are presented individually for the models and then a comparison between these models is given.

7.3.1 Box Girder with Open Cross-Section

This model aims to demonstrate the sensitivity of a box girder with open cross-section, principally regarding its lateral torsional stability. The stresses and displacements from

the analyses are presented and compared. The displacements and stresses for the whole model are presented. Some paths, as shown in Figure 7.7, are used for a study of displacements and stresses at different stages of the analyses.

Analysis 1

This analysis is performed with a scaling factor of 0.05 for the overall buckling mode. Three local buckling modes are introduced with a scaling factor of 0.001 and the model is meshed with global seeds of 0.48.

In Figure 7.8 the von Mises stresses for the whole model are shown, in Figures 7.9-7.11 the displacements, in Figure 7.12 the stresses in the 11-direction, in Figure 7.13 the stresses in the 22-direction and

in Figure 7.14 the stresses in the 12-direction. The figures show the stresses and displacements when full load from the cast concrete is applied. The stresses are displayed in Pa and the displacements in metres.

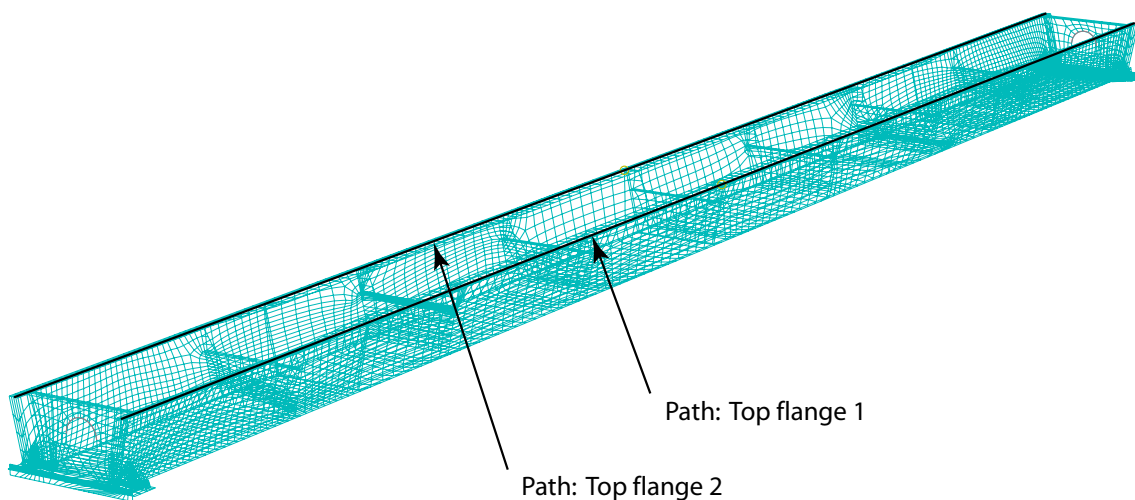


Figure 7.7: Paths for which displacements and stresses are shown.

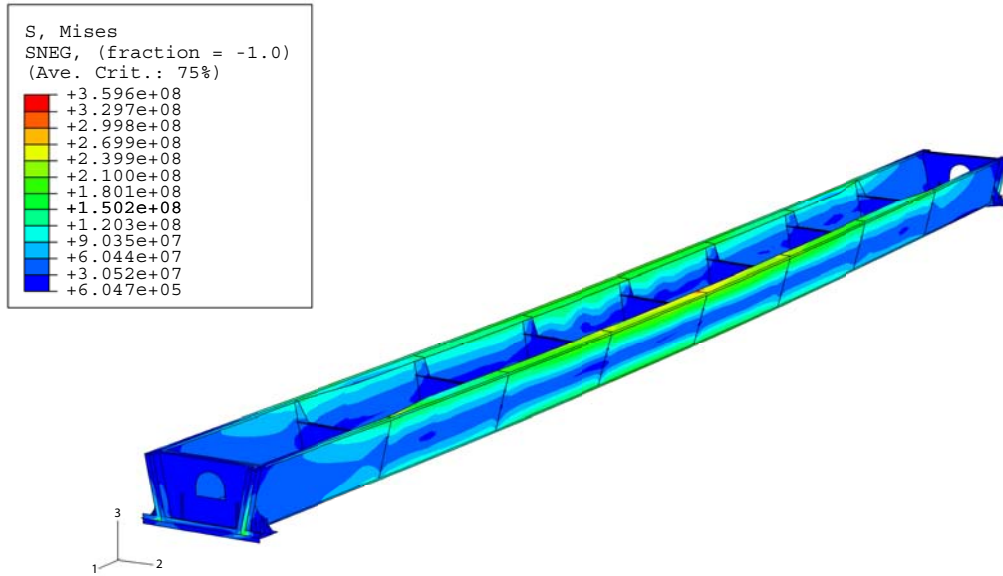
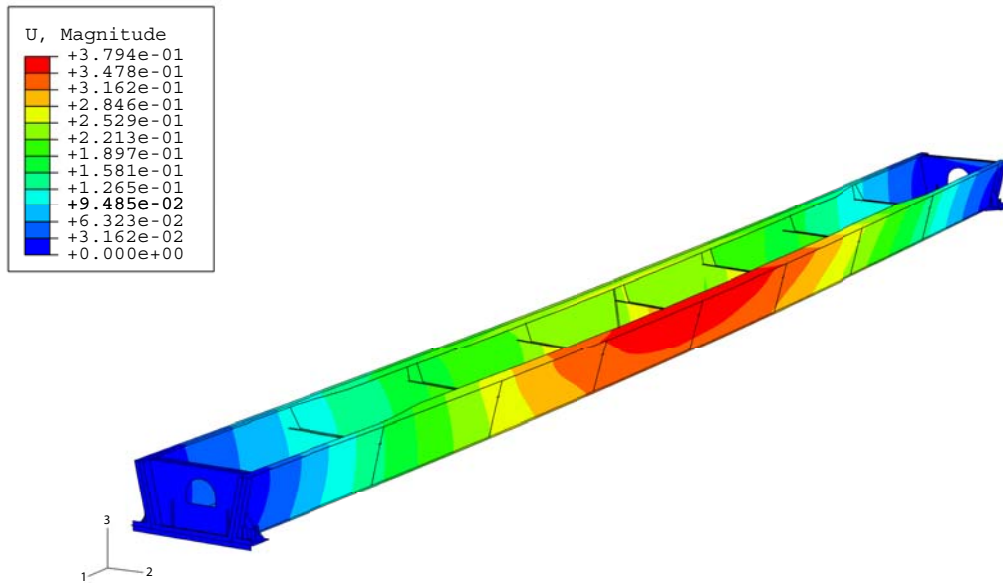


Figure 7.8: von Mises stresses.

Figure 7.9: Magnitude of displacements, $U = \sqrt{U_1^2 + U_2^2 + U_3^2}$.

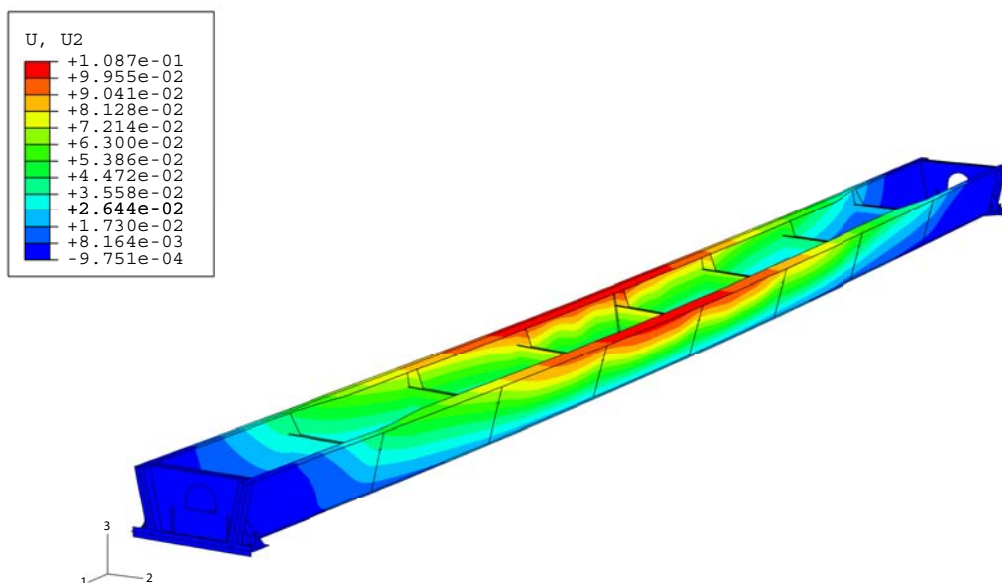


Figure 7.10: Lateral displacements, U2.

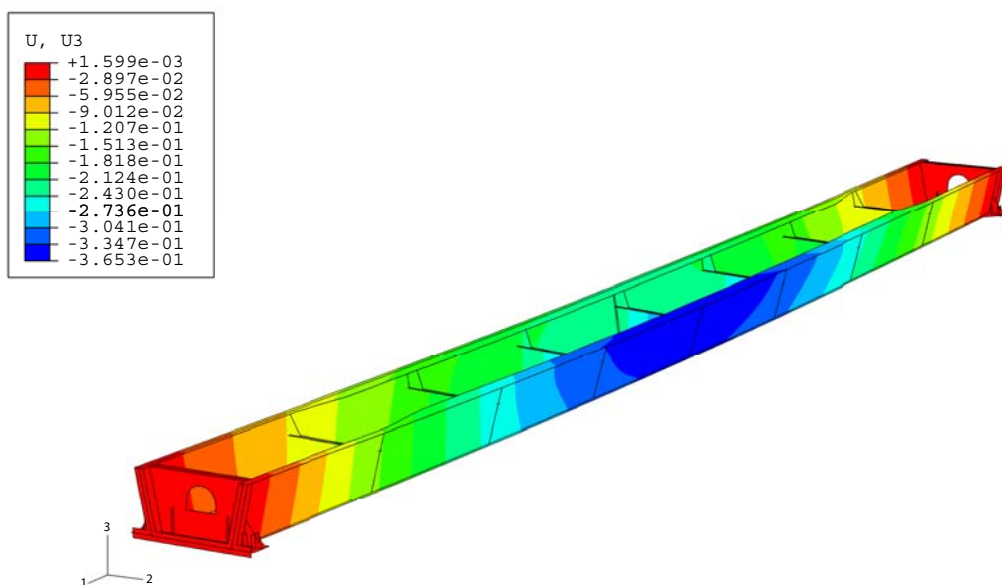


Figure 7.11: Vertical displacements, U3.

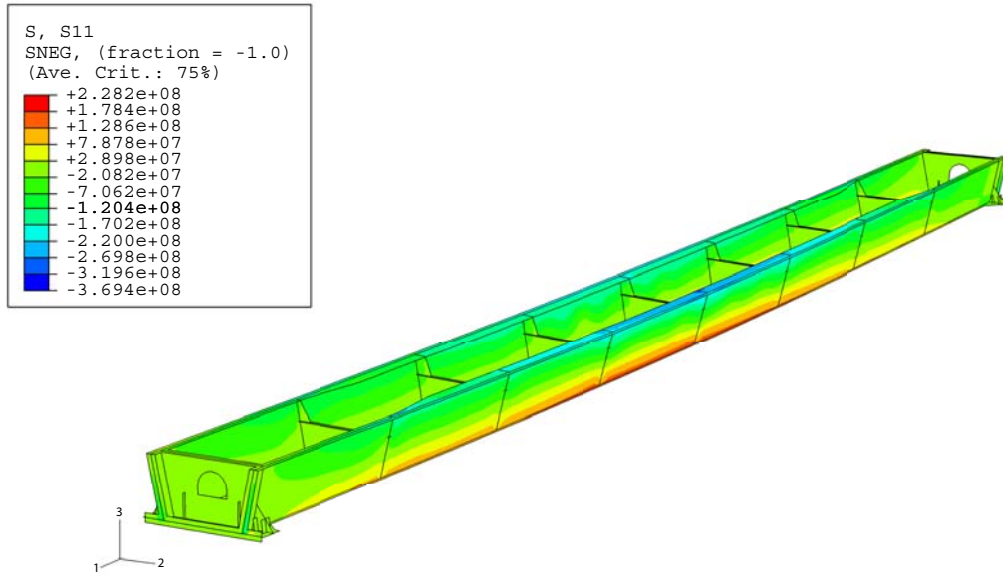


Figure 7.12: Stresses in the 11-direction.

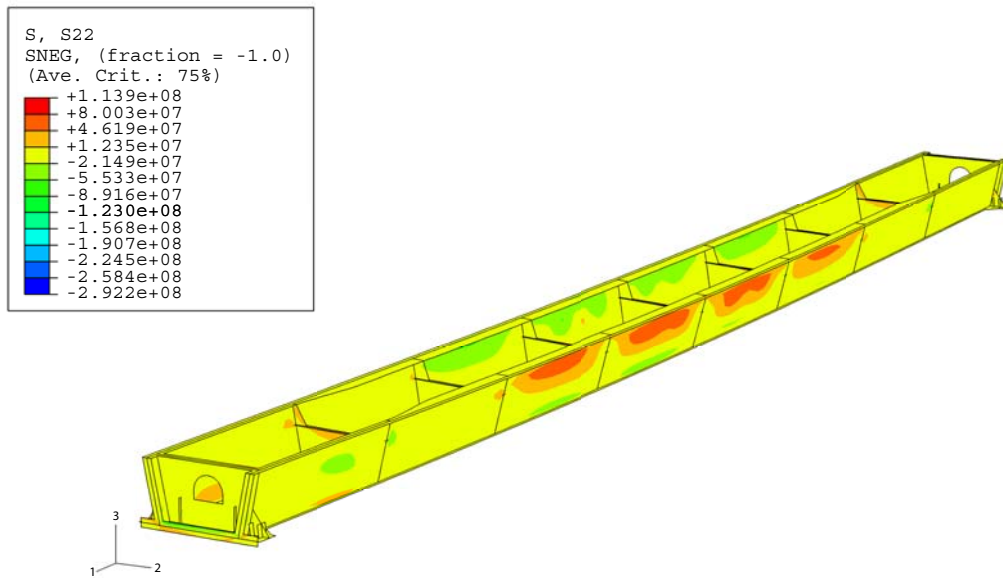


Figure 7.13: Stresses in the 22-direction.

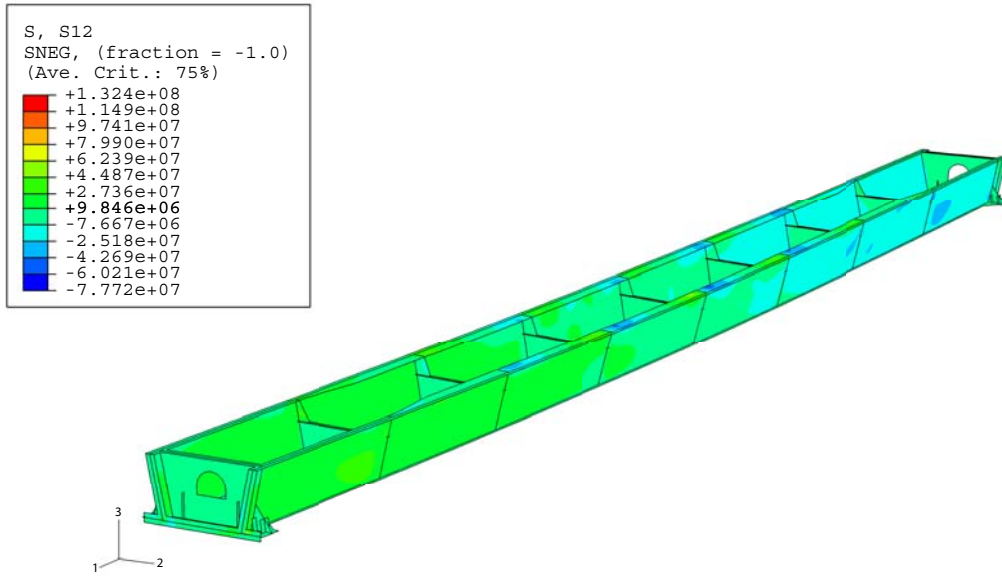


Figure 7.14: Stresses in the 12-direction.

The first path, *top flange 1*, is created in the bridge longitudinal direction at one of the top flanges. In Figure 7.15 the magnitudes of the displacements along path top flange 1 are shown. Graphs are drawn for different stages of the casting, starting when no concrete is cast and until the casting is finished. In Figure 7.16 the lateral displacements along path top flange 1 are shown.

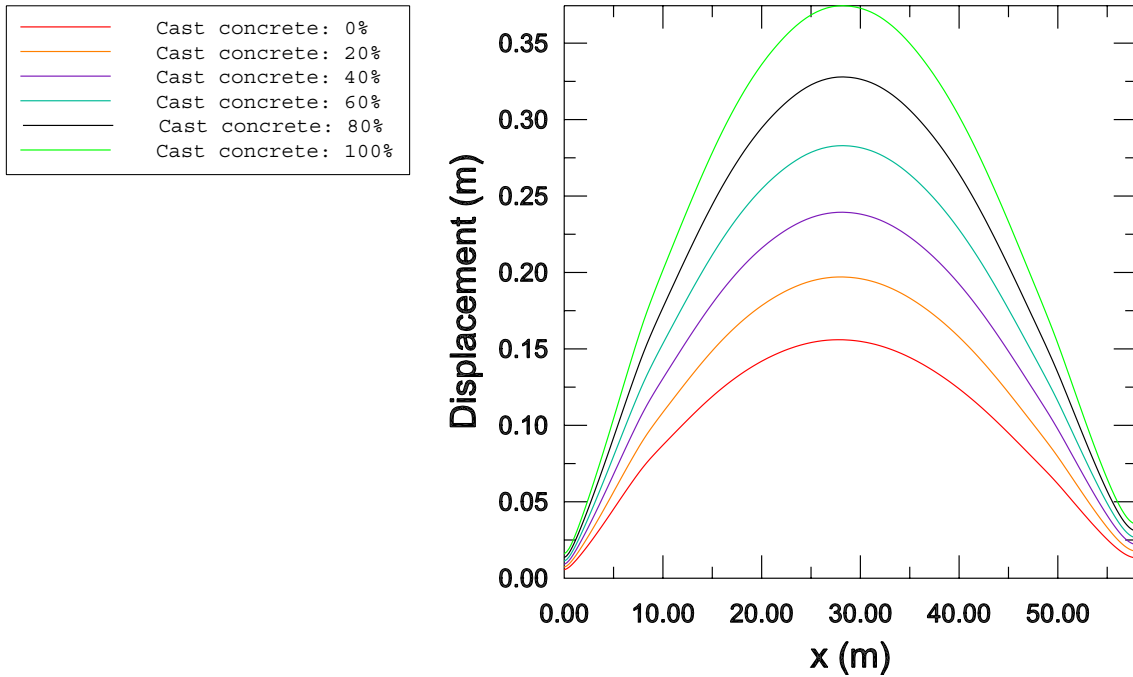


Figure 7.15: Magnitude of node displacement along path top flange 1.

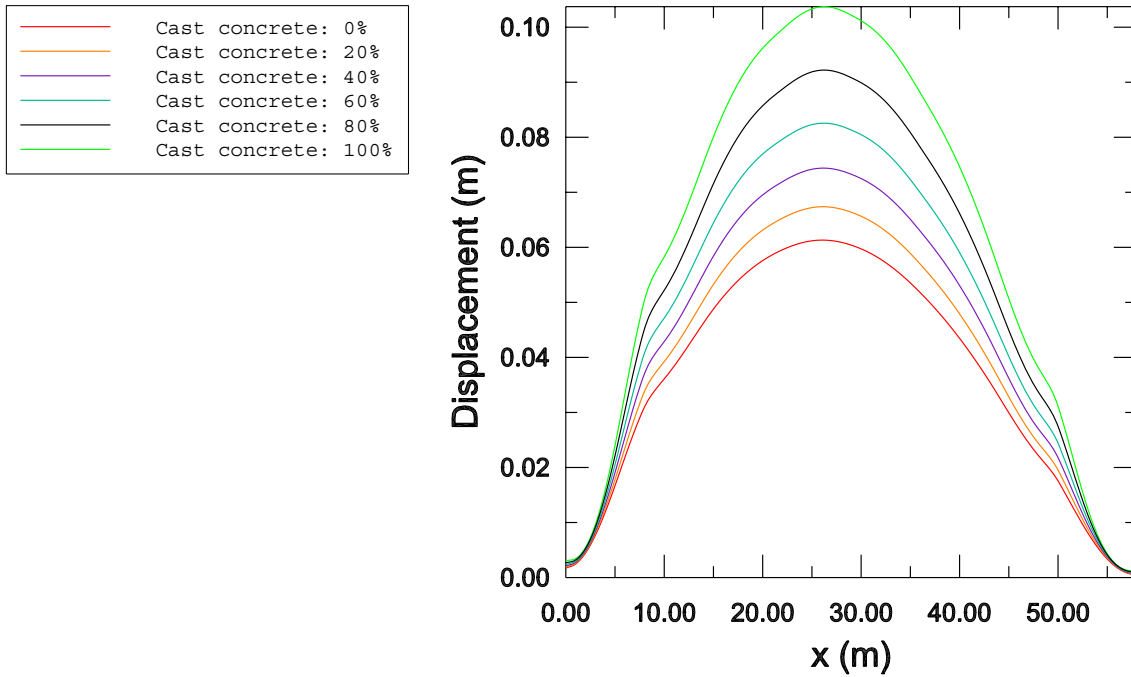


Figure 7.16: Lateral node displacement along path top flange 1.

The other top flange is also used to create a path, *top flange 2*, for which the same variables are studied. In Figure 7.17 the magnitude of the displacements along path top flange 2 are shown. In Figure 7.18 the lateral displacements along path top flange 2 are shown.

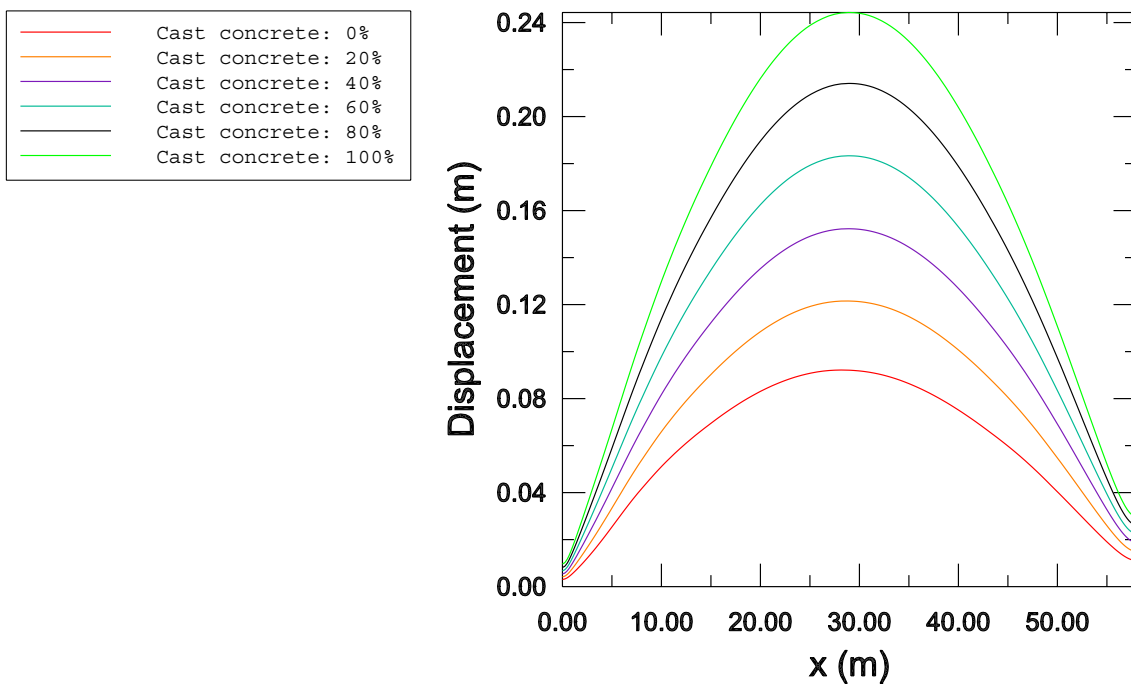


Figure 7.17: Magnitude of node displacement along path top flange 2.

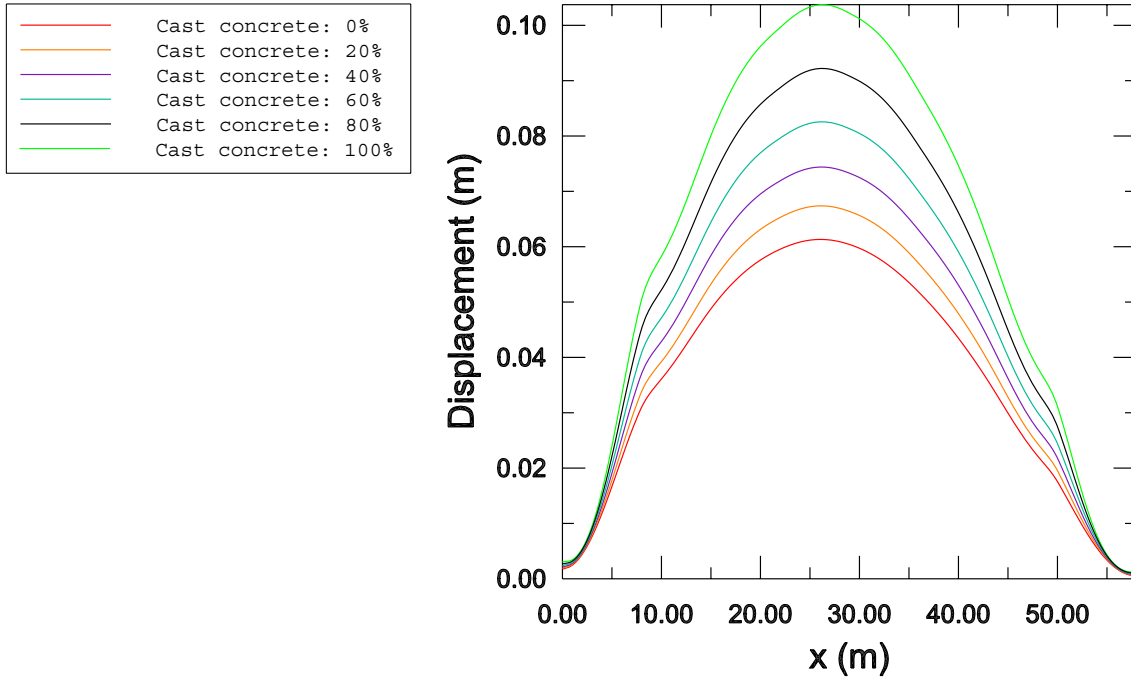


Figure 7.18: Lateral node displacement along path top flange 2.

There is an obvious difference between the magnitude of node displacement for top flange 1 and top flange 2, while their lateral displacements are almost identical. This is due to the rotation about the longitudinal axis, which makes top flange 1 descend twice as much as top flange 2.

To calculate the ultimate load for the construction, the analysis is proceeded further. Instead of stopping at a stage where the full load from the cast concrete is applied, the analysis is carried on until the ultimate load is reached. The Riks method initially adds 0.1 of the total casting load in each increment. When the applied load approaches the ultimate load, the applied load in each increment is reduced so that there still is a converging solution. As the applied load approaches the ultimate load, the displacements continue to grow and the curve shown in Figure 7.20 is obtained.

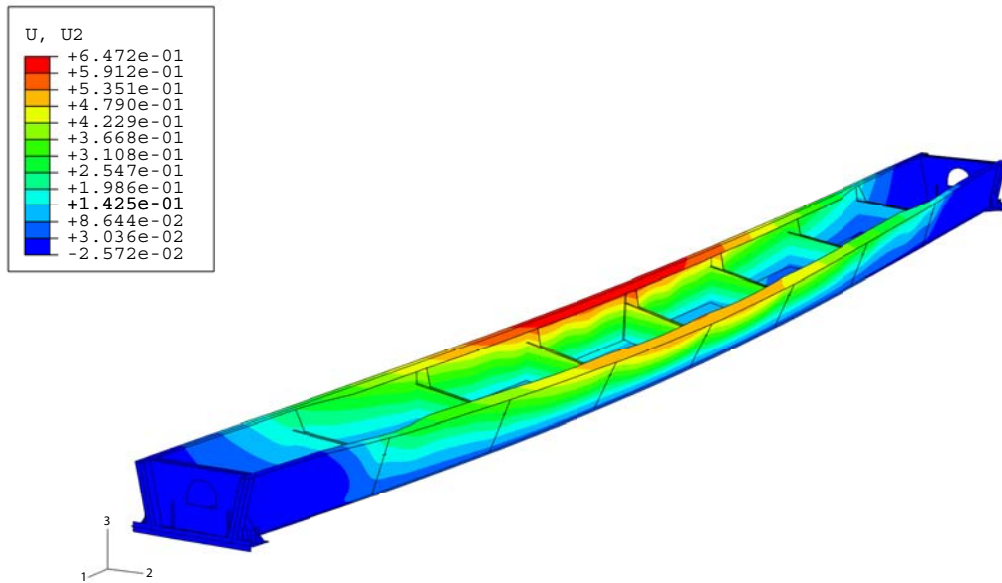


Figure 7.19: Lateral displacement at ultimate load.

In Figure 7.19 the lateral displacements when the ultimate load is applied are shown. In Figure 7.20 the maximum lateral displacement along path top flange 1 is shown on the x -axis, while the y -axis shows a load proportionality factor, λ , of the cast concrete.

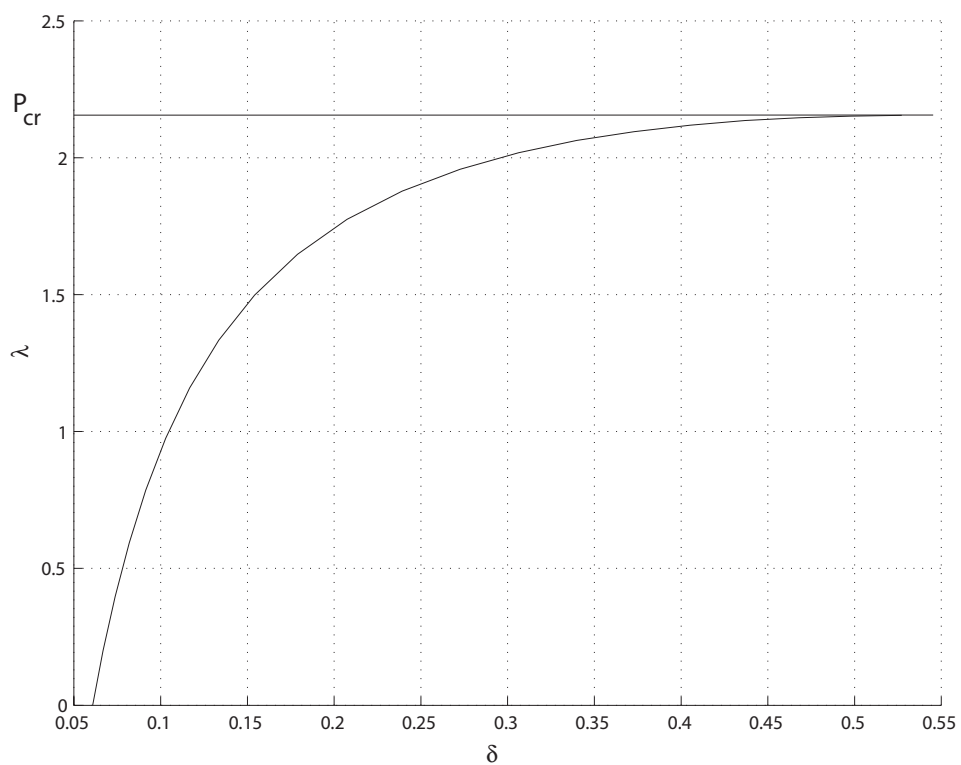


Figure 7.20: Load-displacement curve.

Plotting these displacements against a quota of the displacement divided by the applied load, Southwell plot is given. This curve is shown in Figure 7.21. From this curve, the critical load proportionality factor is given by

$$\lambda_{\text{cr}} = \frac{1}{\theta}$$

where θ is the gradient of the curve. Using the marked points in Figure 7.21 to calculate the gradient, $\theta = 0.432$ which gives $\lambda_{\text{cr}} = 2.31$. This value can also be compared with the maximum value of the critical load proportionality factor given directly by BRIGADE/Plus, which is $\lambda_{\text{cr}} = 2.16$ as shown in Figure 7.20.

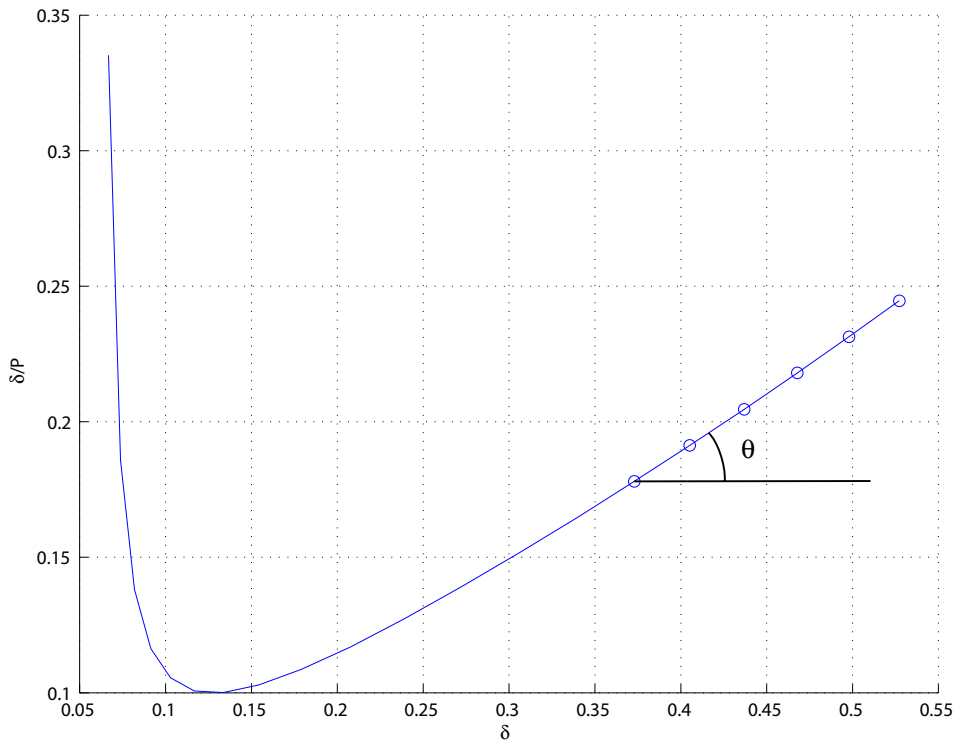


Figure 7.21: Southwell plot.

Additional analyses

Five additional analyses are performed on this model as described below:

- *Analysis 2.* This analysis is performed with a scaling factor of 0.01 for the overall buckling mode. Three local buckling modes are introduced with a scaling factor of 0.001 and the model is meshed with a global seed of 0.48.
- *Analysis 3.* This analysis is performed with a scaling factor of 0.1 for the overall buckling mode. Three local buckling modes are introduced with a scaling factor of 0.001 and the model is meshed with a global seed of 0.48.

- *Analysis 4.* This analysis is performed with a scaling factor of 0.2 for the overall buckling mode. Three local buckling modes are introduced with a scaling factor of 0.001 and the model is meshed with a global seed of 0.48.
- *Analysis 5.* This analysis is performed without any geometrical imperfections. The model is meshed with a global seed of 0.48.
- *Analysis 6.* This analysis is performed with a scaling factor of 0.05 for the overall buckling mode. Three local buckling modes are introduced with a scaling factor of 0.001 and the model is meshed with a global seed of 0.24.

The results from these analyses are compared with the results from the first analysis.

In Figure 7.22 the magnitude of the displacements along path top flange 1 are shown. Graphs are drawn for when the total load from the casting is applied for different initial imperfections. In Figure 7.23 the lateral displacements along path top flange 1 are shown.

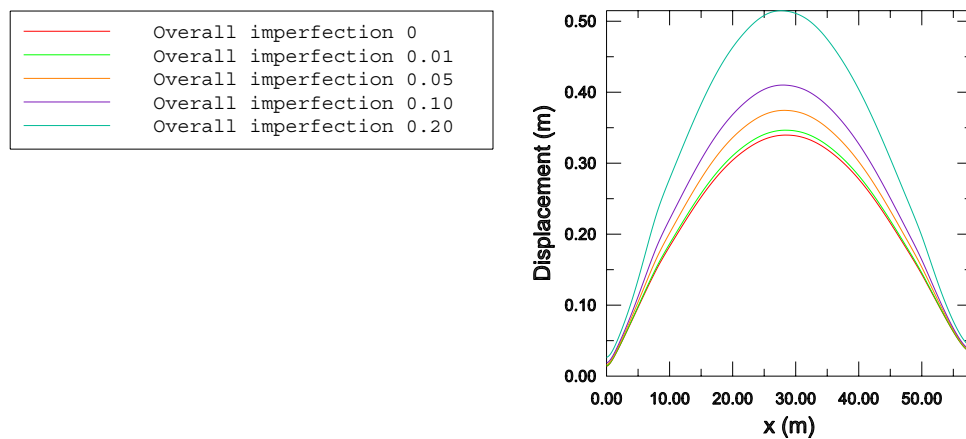


Figure 7.22: Magnitude of node displacement along path *top flange 1* for different initial imperfections.

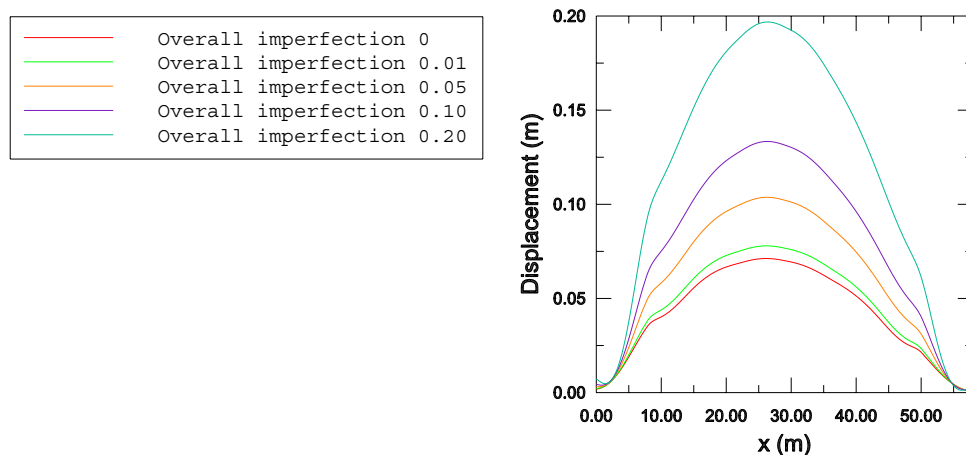


Figure 7.23: Lateral node displacement along path *top flange 1* for different initial imperfections

The maximal lateral displacements in Figure 7.23 becomes relatively larger when the initial imperfection is increased. Increasing the initial imperfection from 0.01 to 0.05 provides a growth in lateral displacement of 36%. A further increase from 0.05 to 0.1 yields an additional growth in lateral displacement of 24% and an increase from 0.1 to 0.2 finally produces a growth in lateral displacement of 52%. This clearly shows that an increased initial imperfection drastically increases the lateral displacement. In Figure 7.24 the maximum lateral displacement along path top flange 1 is shown on the x -axis, while the y -axis shows a load proportionality factor, λ , of the cast concrete. Curves are drawn for different initial imperfections. The Southwell plot for the curves of Figure 7.24 are shown in Figure 7.25.

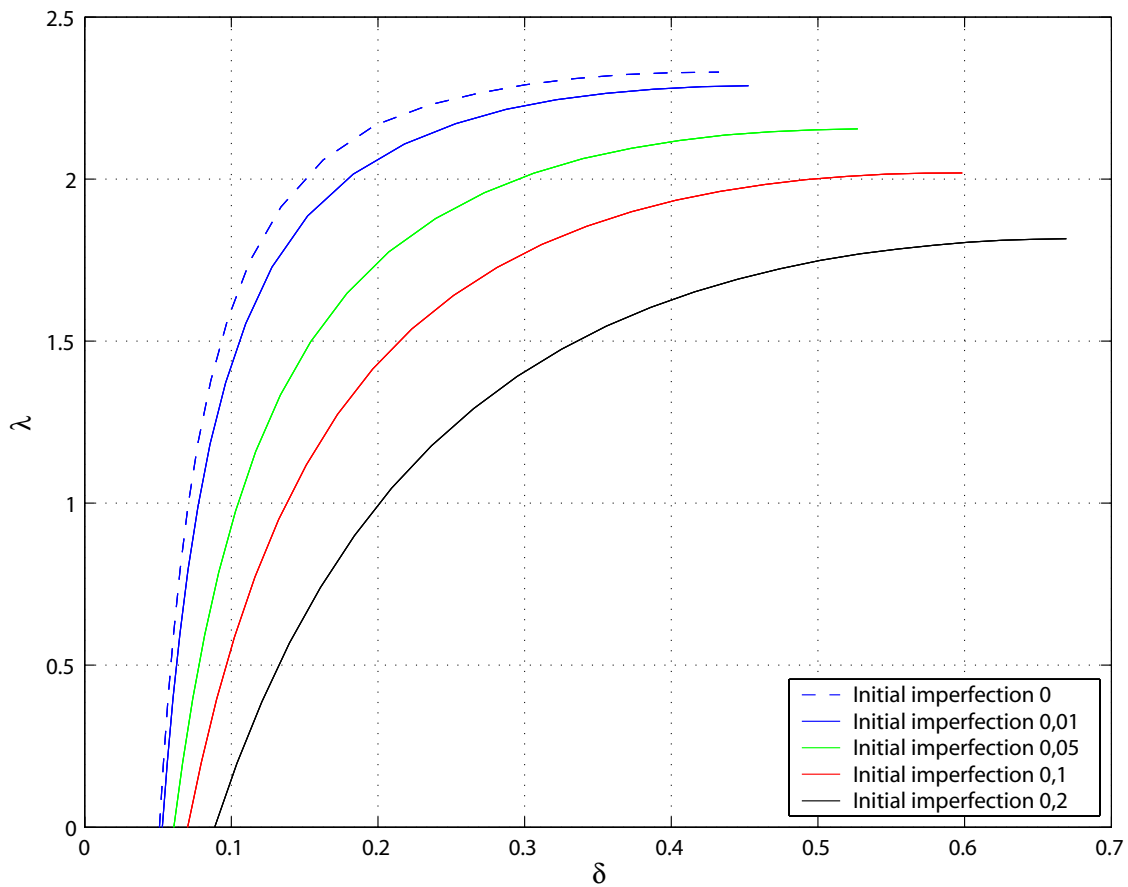


Figure 7.24: Load-displacement curves for different initial imperfections.

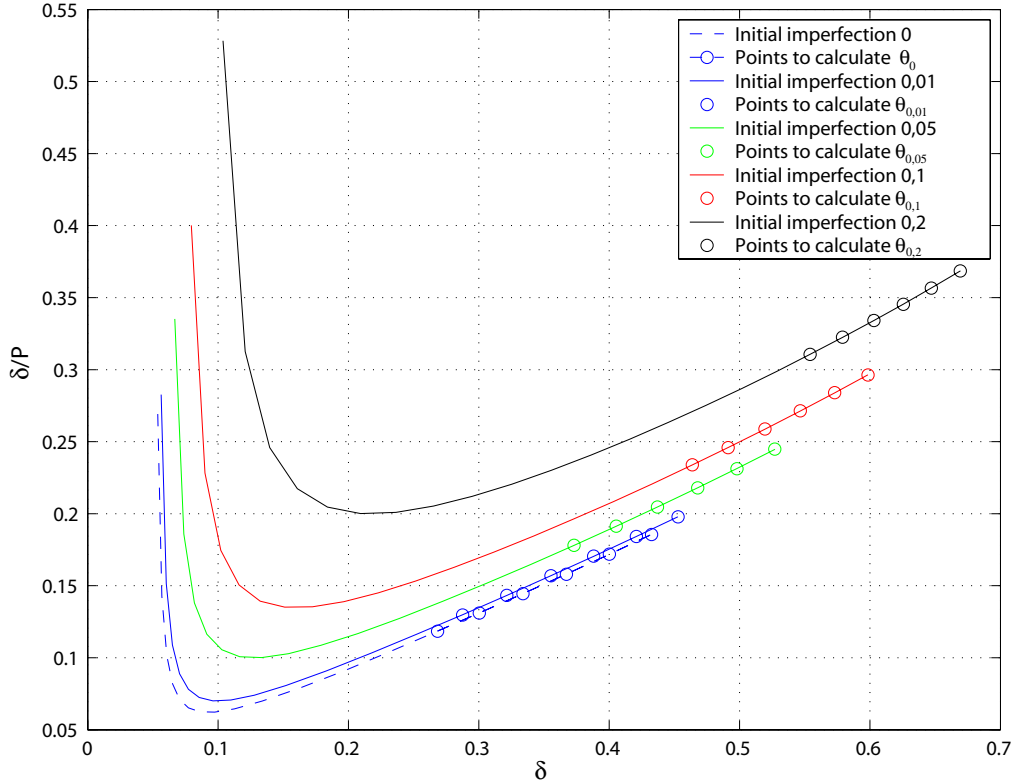


Figure 7.25: Southwell plot for various initial imperfections.

From these curves, the critical load proportionality factor is given by

$$\lambda_{cr,i} = \frac{1}{\theta_i}$$

where θ_i is the gradient of the curve i . Using the marked points in Figure 7.25 to calculate the gradient, θ_i , and the corresponding critical load proportionality factor, λ_i , gives the results presented in Table 7.2. In Figure 7.26, the axial rotation for the bridge is shown for different initial imperfections. These curves can be approximated with quadratic curves, producing the curves shown in Figure 7.27. From these curves, it is clear that an increased initial imperfection also produces a relatively larger rotation of the structure.

Table 7.2: Curve gradients and their corresponding critical load proportionality factors for various initial imperfections.

Initial imperfection, i	θ_i (rad)	λ_i (-)
0	0.409	2.446
0.01	0.412	2.427
0.05	0.432	2.314
0.1	0.464	2.153
0.2	0.503	1.988

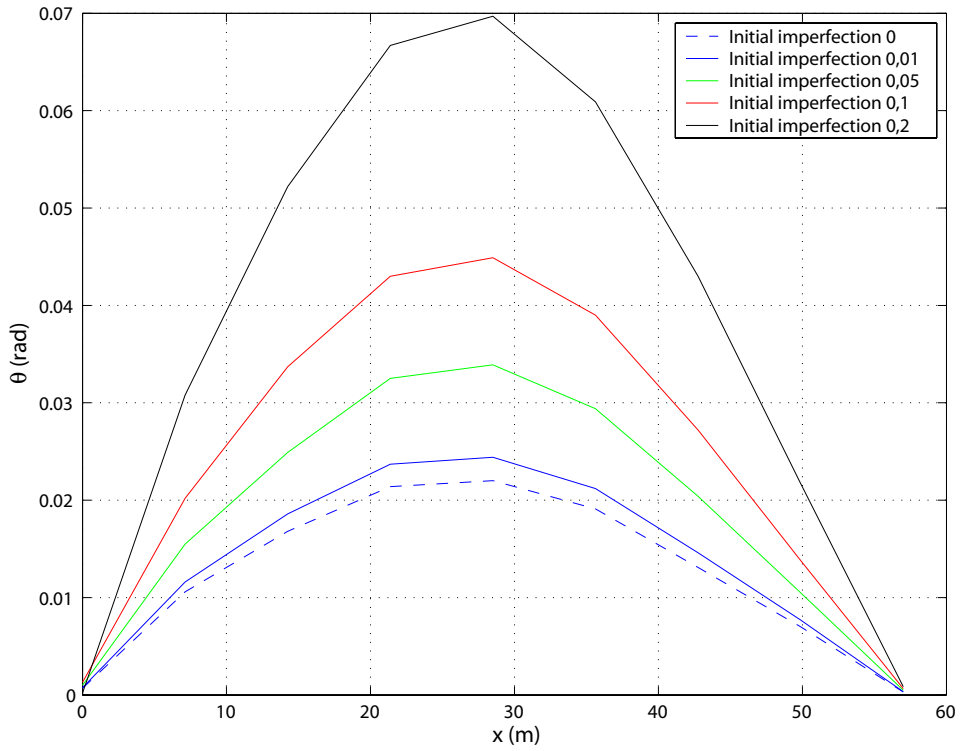


Figure 7.26: Axial rotation for various initial imperfections.

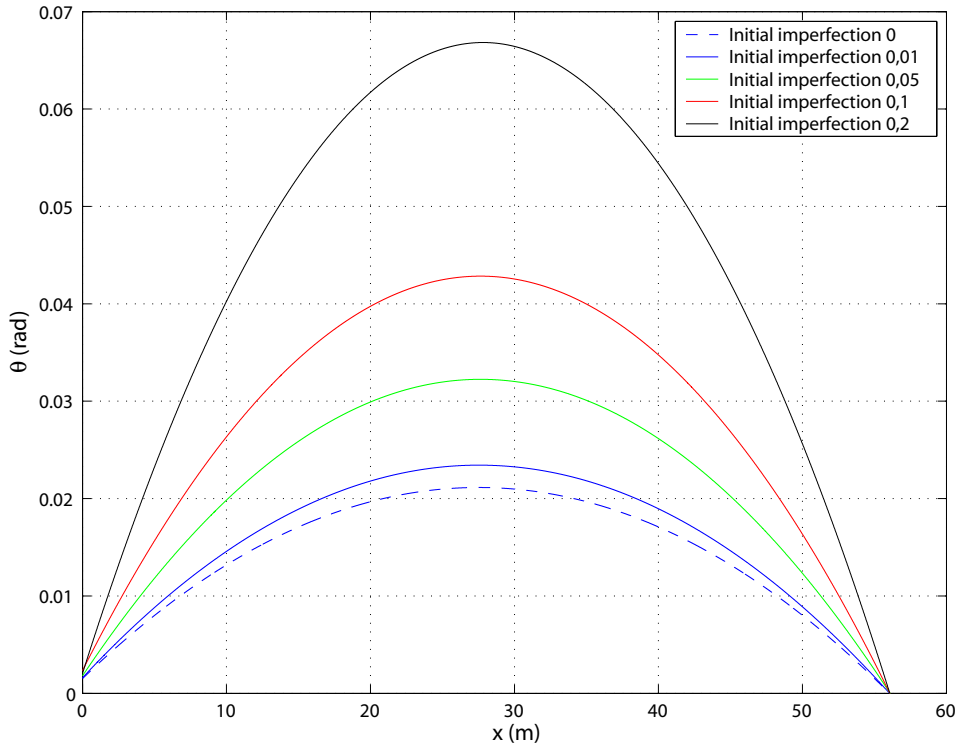


Figure 7.27: Axial rotation, approximated with quadratic curves, for various initial imperfections.

To verify that the error from bad meshing is small enough to be neglected, an analysis with an improved mesh is performed. The box girder is meshed with global seeds of 0.24. In Figure 7.28, the magnitude of the displacements and the von Mises stresses from analyses with different meshes are shown. Since the discrepancy is very small, the coarser mesh can be assumed to provide trustworthy results.

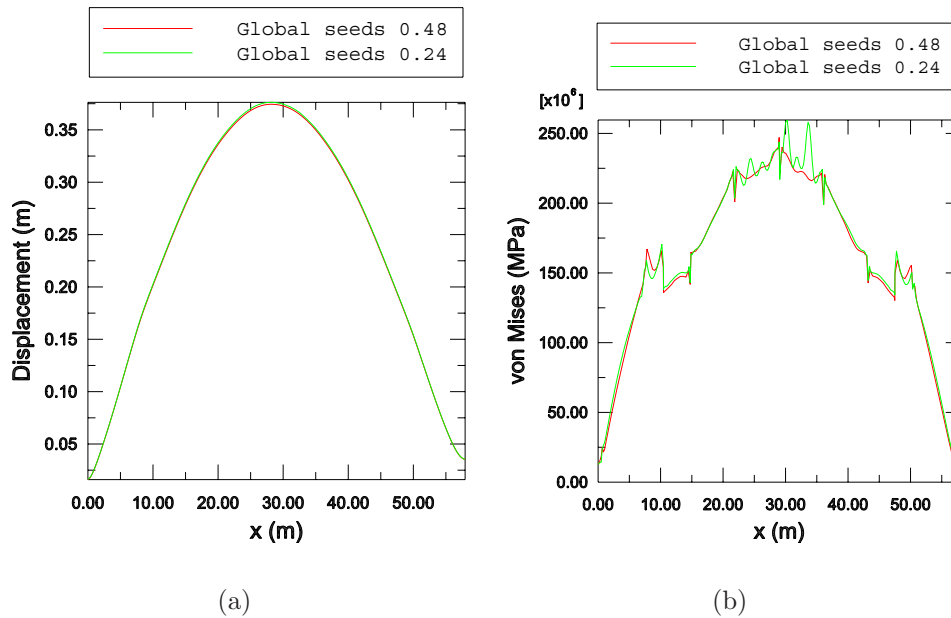


Figure 7.28: (a) Magnitude of displacements along top flange 1. (b) von Mises stresses along top flange1.

7.3.2 Box Girder with Closed Cross-Section

The same box girder as in the model with the open cross-section is used in this model. Profiled sheets are attached at the top of the box girder and given an all around attachment, producing a closed cross-section. The stresses and displacements from the analyses are presented and compared.

Analysis 1

This analysis is performed with a scaling factor of 0.05 for the overall buckling mode. Three local buckling modes are introduced with a scaling factor of 0.001 and the model is meshed with global seeds of 0.48.

In Figure 7.29 the von Mises stresses for the whole model are shown, in Figures 7.30-7.32 the displacements, in Figure 7.33 the stresses in the 11-direction, in Figure 7.34 the stresses in the 22-direction and in Figure 7.35 the stresses in the 12-direction.

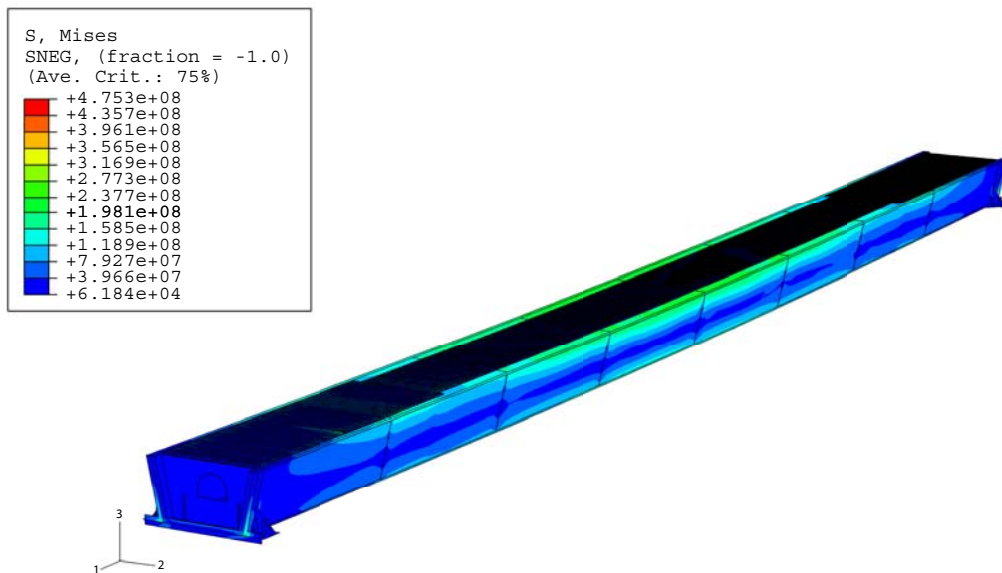


Figure 7.29: von Mises stresses.

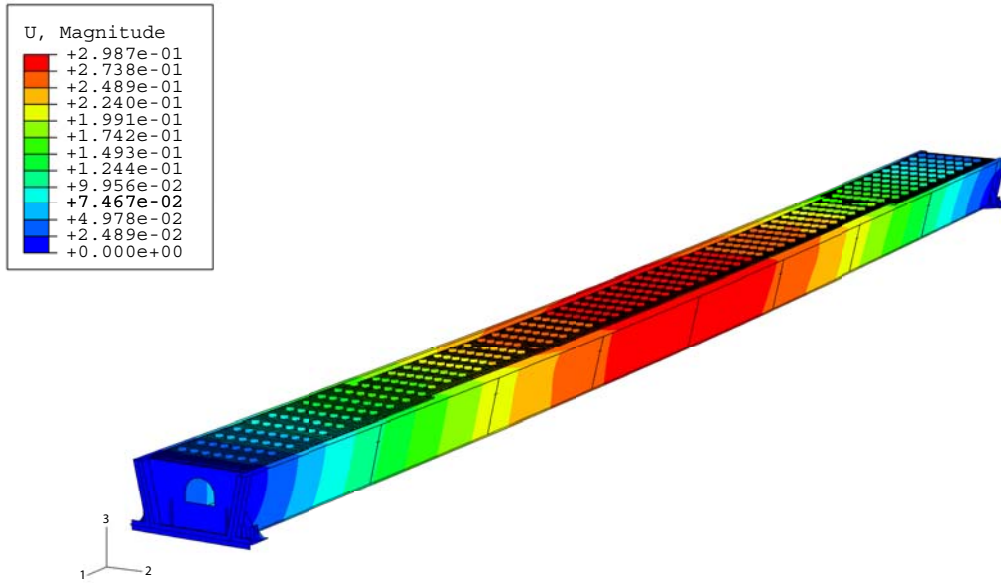


Figure 7.30: Magnitude of displacements, $U = \sqrt{U_1^2 + U_2^2 + U_3^2}$.

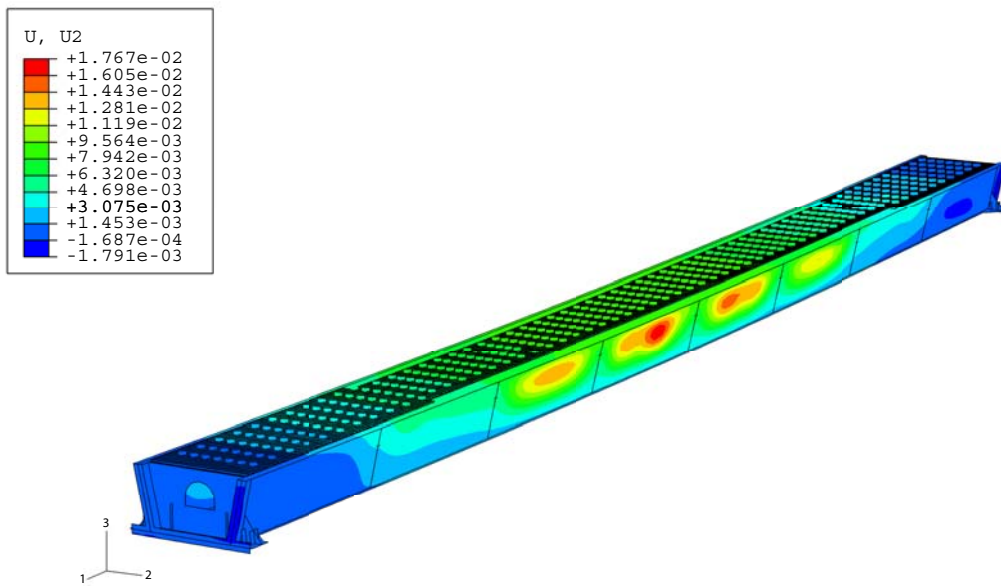


Figure 7.31: Lateral displacements, U_2 .

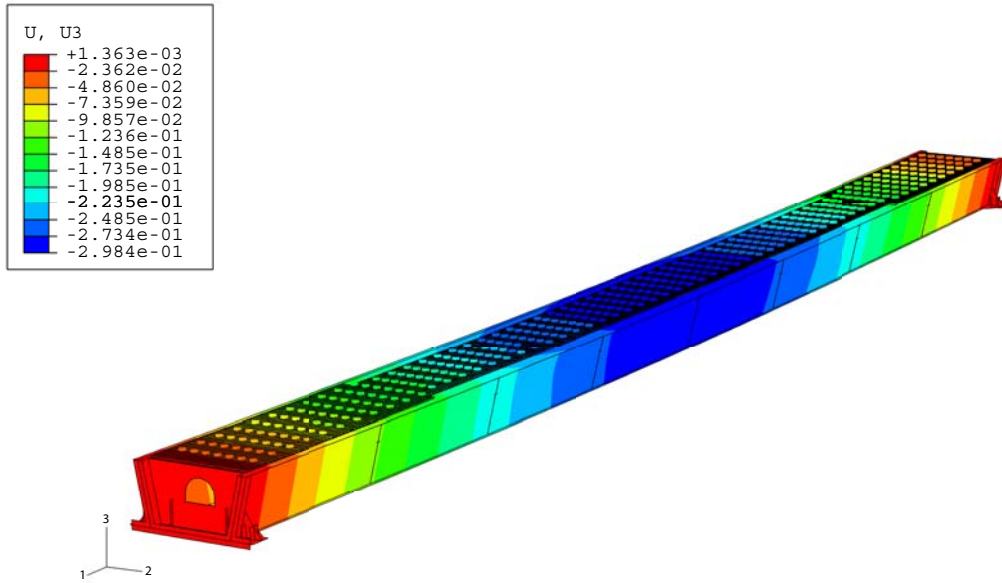


Figure 7.32: Vertical displacements, U3.

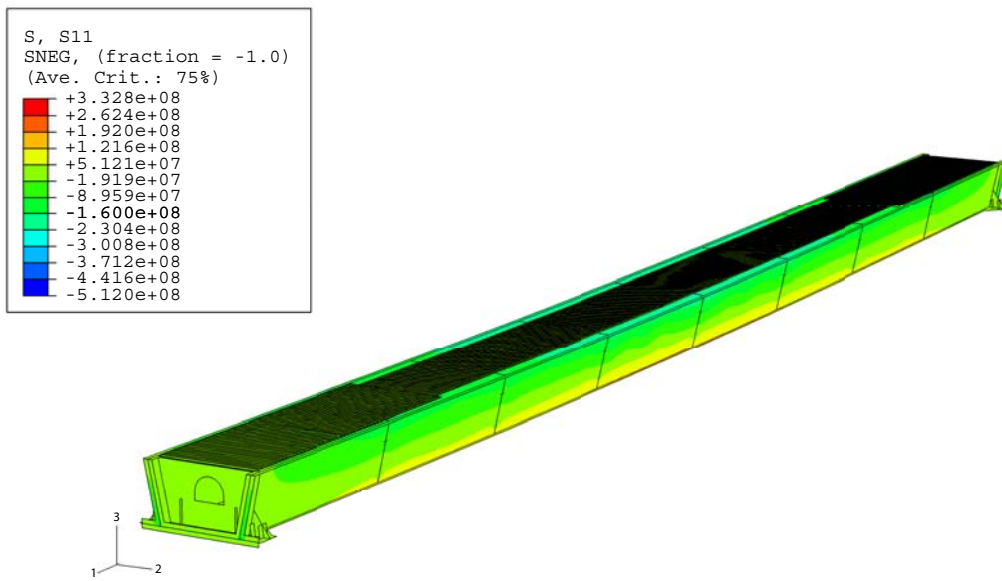


Figure 7.33: Stresses in the 11-direction.

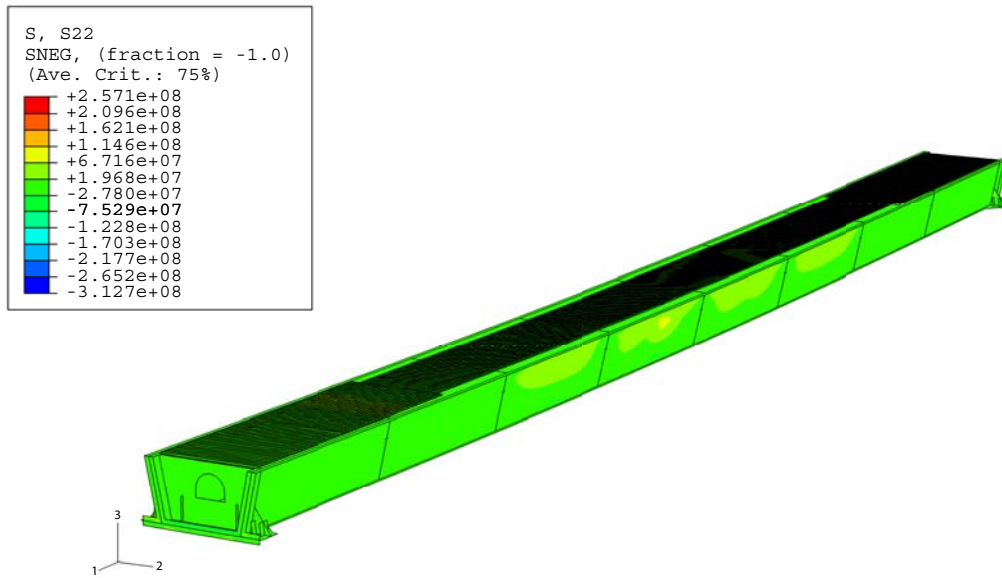


Figure 7.34: Stresses in the 22-direction.

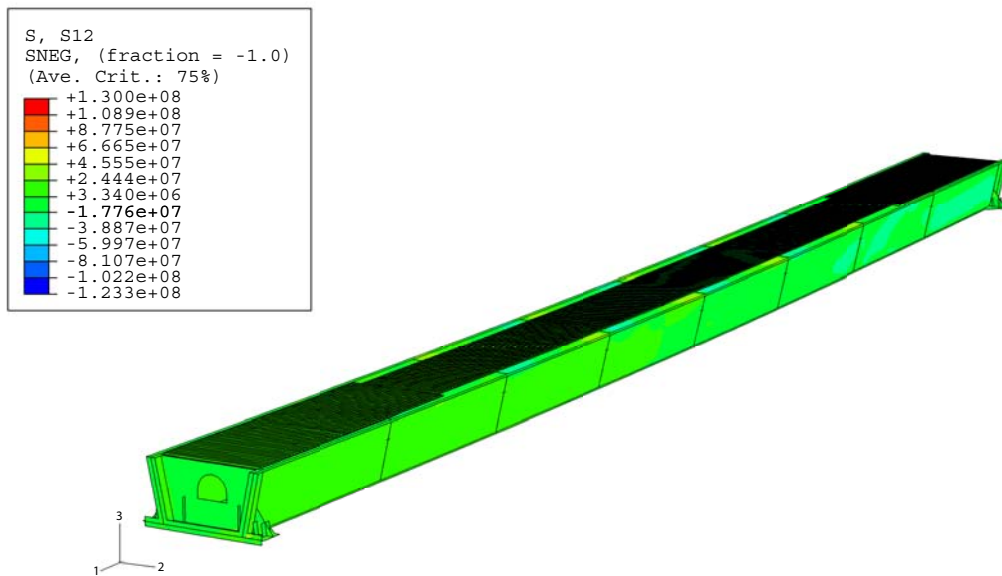


Figure 7.35: Stresses in the 12-direction.

The profiled sheeting is subjected to large stresses in the connections to the box girder, as described in Chapter 6. If these stresses become too large, bolt hole yielding will occur. The stresses at the outer part of the profiled sheeting are shown below.

In Figure 7.36 the von Mises stresses for the four outer profiled sheets are shown. In Figure 7.37 the stresses in the axial direction for the four outer profiled sheets are shown. In Figure 7.38 the stresses in the transverse direction for the four outer profiled sheets are shown.

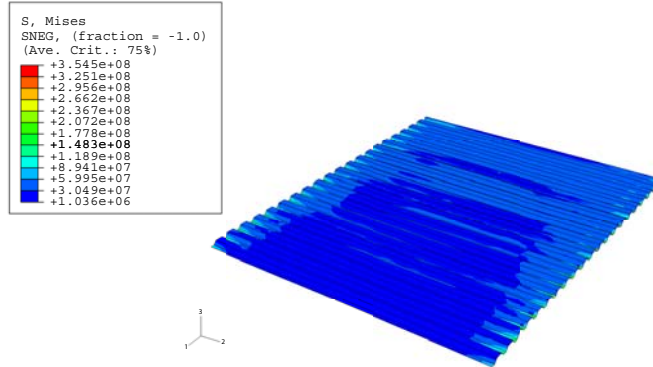


Figure 7.36: von Mises stresses.

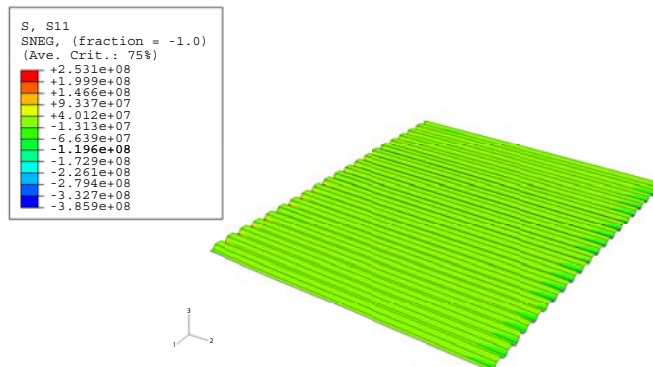


Figure 7.37: Stresses in the 11-direction.

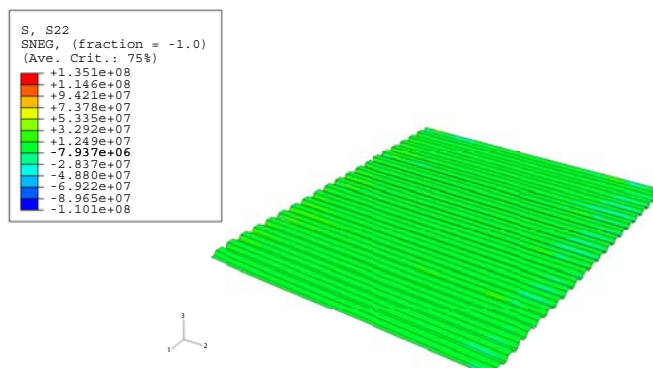


Figure 7.38: Stresses in the 22-direction.

7.3.3 Box Girder with Partly Closed Cross-Section

The same box girder as in the model with the open cross-section is used in this model. Profiled sheets are attached at the top flanges of the box girder, providing a partly closed cross-section. The stresses and displacements from the analyses are presented and compared.

Analysis 1

This analysis is performed with a scaling factor of 0.05 for the overall buckling mode. Three local buckling modes are introduced with a scaling factor of 0.001 and the model is meshed with global seeds of 0.48.

In Figure 7.39 the von Mises stresses for the whole model are shown, in Figures 7.40-7.42 the displacements, in Figure 7.43 the stresses in the 11-direction, in Figure 7.44 the stresses in the 22-direction and in Figure 7.45 the stresses in the 12-direction.

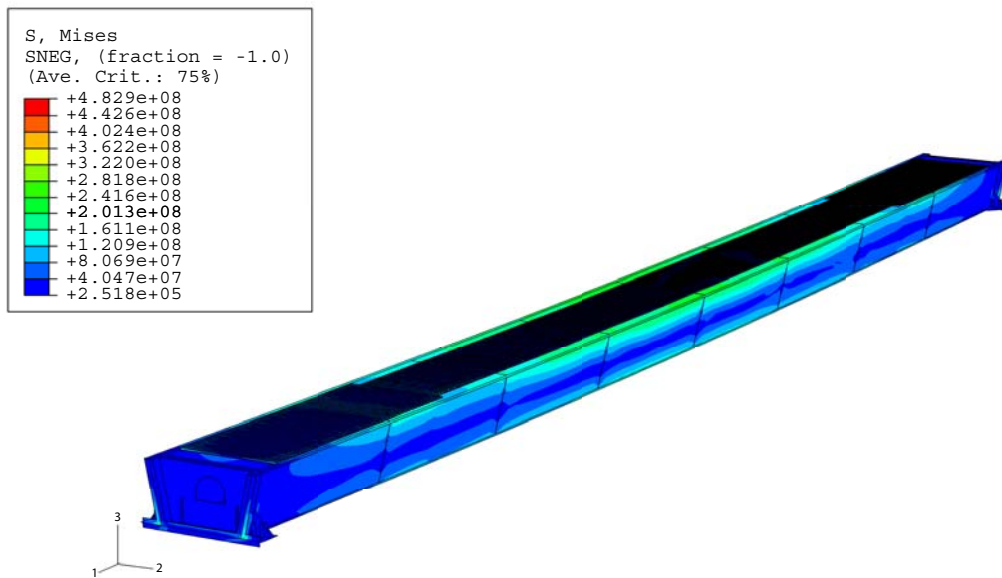


Figure 7.39: von Mises stresses.

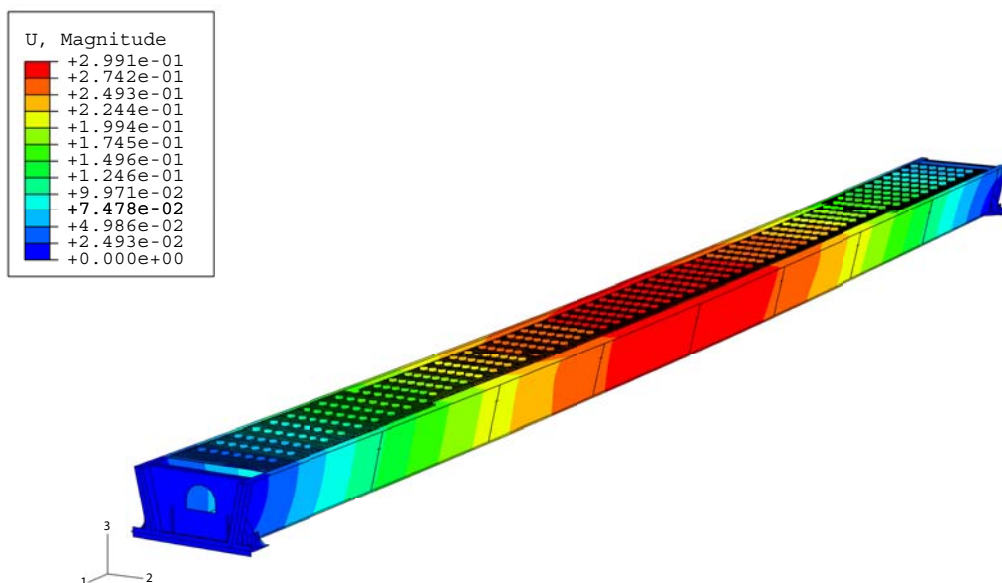


Figure 7.40: Magnitude of displacements, $U = \sqrt{U_1^2 + U_2^2 + U_3^2}$.

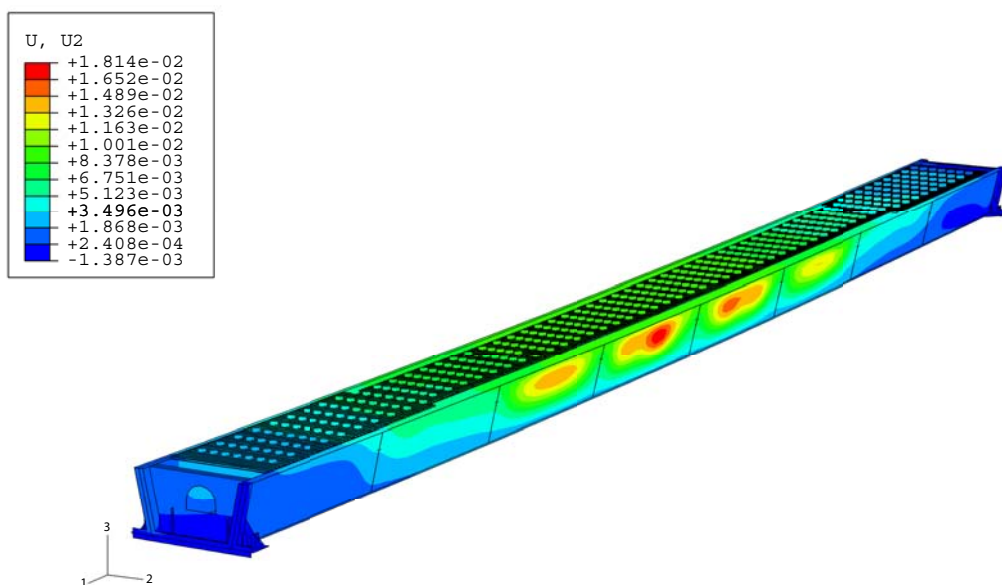


Figure 7.41: Lateral displacements, U_2 .

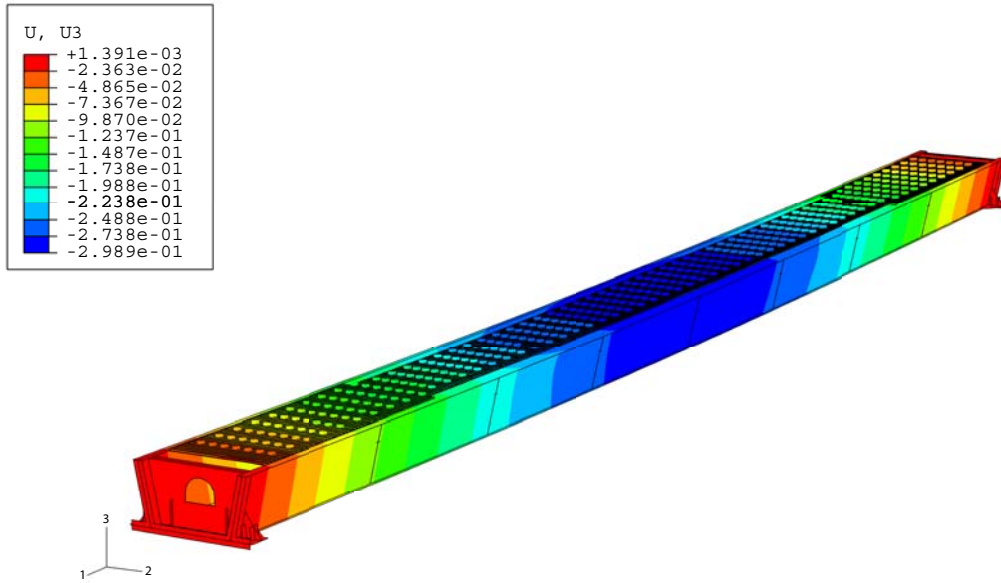


Figure 7.42: Vertical displacements, U3.

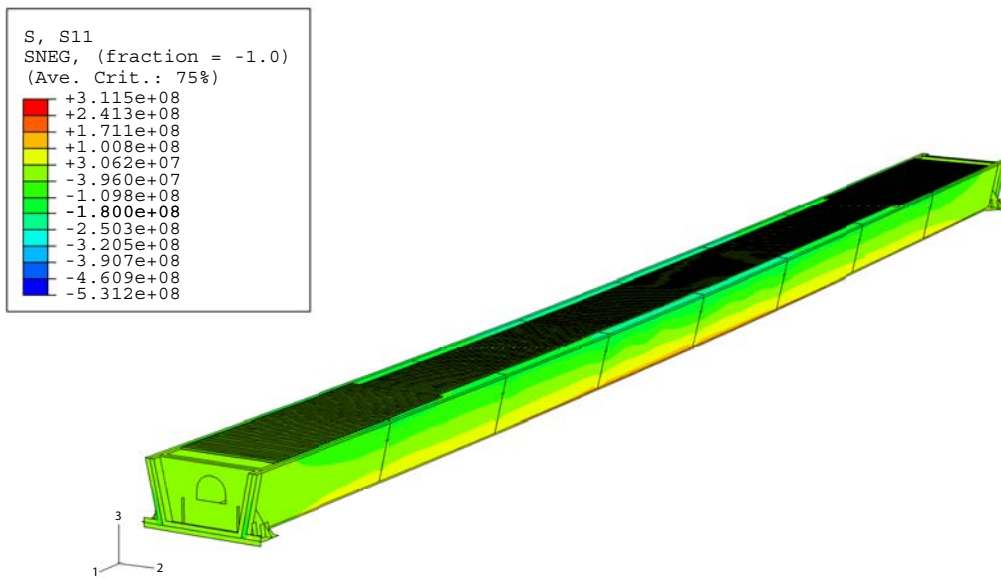


Figure 7.43: Stresses in the 11-direction.

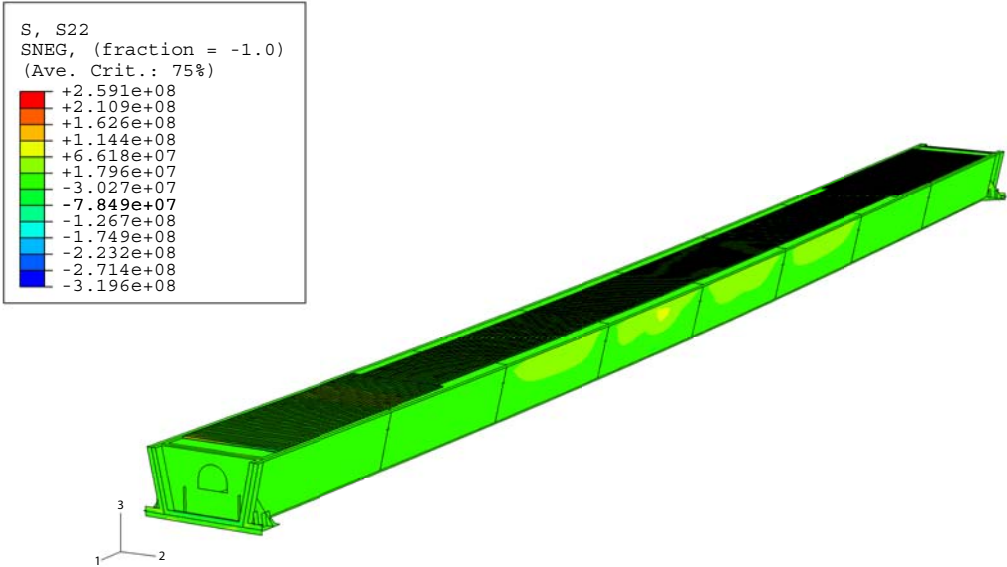


Figure 7.44: Stresses in the 22-direction.

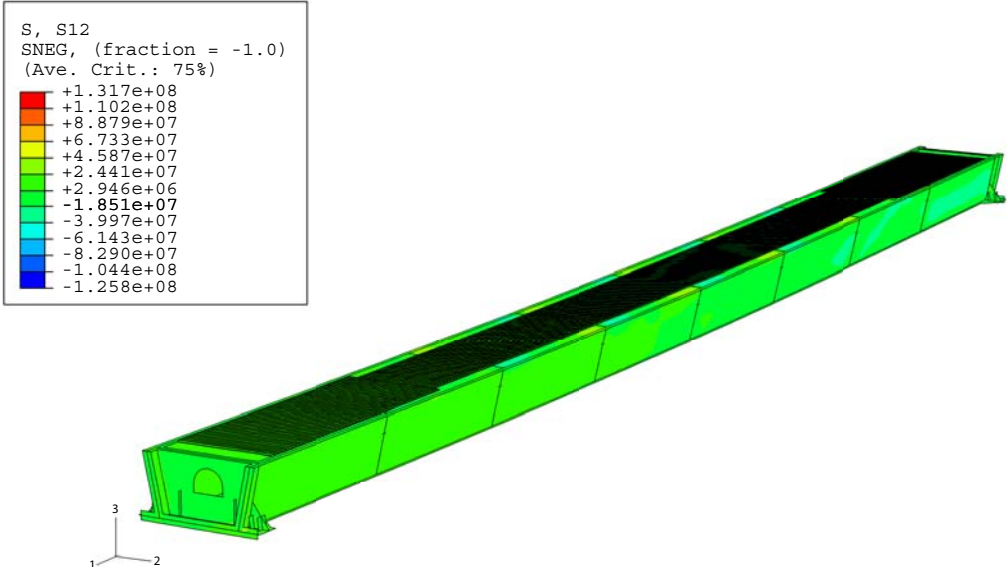


Figure 7.45: Stresses in the 12-direction.

The stresses at the outer part of the profiled sheeting are shown below. In Figure 7.46 the von Mises stresses for the three outer profiled sheets are shown. In Figure 7.47 the stresses in the axial direction for the three outer profiled sheets are shown. In Figure 7.48 the stresses in the transverse direction for the three outer profiled sheets are shown.

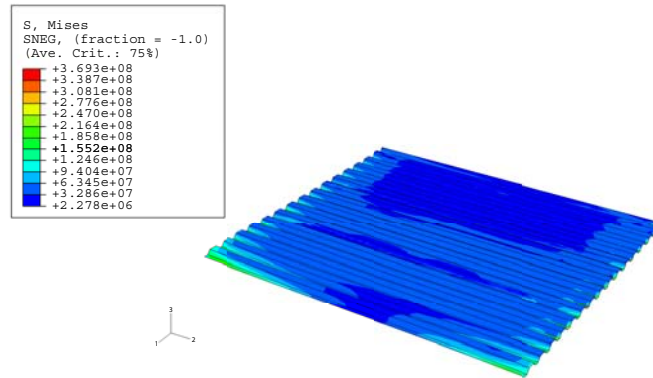


Figure 7.46: von Mises stresses.

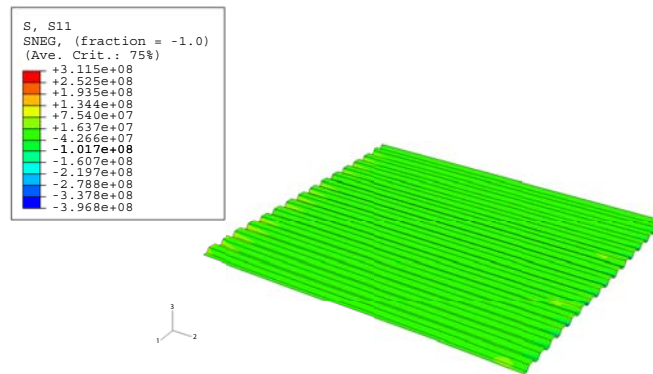


Figure 7.47: Stresses in the 11-direction.

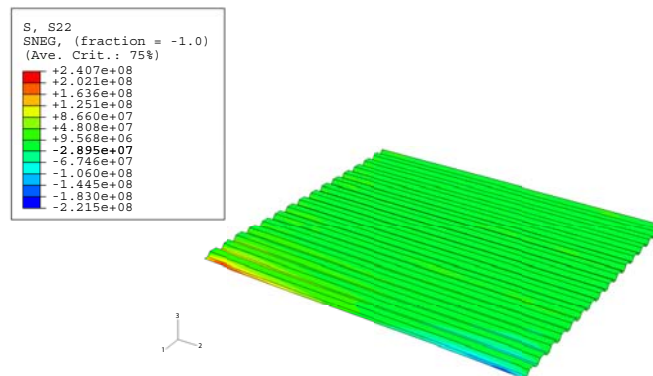


Figure 7.48: Stresses in the 22-direction.

7.3.4 Comparison of Results

From the model with a quadrilaterally connected profiled sheeting and the model with a laterally connected profiled sheeting, two main conclusions are drawn. The first is that if the profiled sheeting is only laterally attached, large axial forces appear in parts of the profiled sheeting closest to the edge, additionally straining the connections. This is demonstrated in Figure 7.49.

The other conclusion is that in both these models the stresses in the profile-bottoms of the profiled sheeting become alarmingly large, already at a relatively moderate loading. These stresses are larger for the model with a two sided attachment of the profiled sheeting than for the one with a quadrilaterally attached profiled sheeting. In Table 7.3 the stresses in the profiled sheeting are compared between the model with the closed cross-section and the partly closed cross-section.

Table 7.3: Stresses in the profiled sheeting with an initial imperfection of 0.05 when full load from cast concrete is applied.

Stresses (MPa)	Closed cross-section		Partly closed cross-section	
	All Sheets	Outer Sheets	All Sheets	Outer Sheets
von Mises	475	355	483	369
11-direction (+)	333	253	312	312
11-direction (-)	512	386	531	397
22-direction (+)	257	135	259	241
22-direction (-)	313	110	320	222

These values should be interpreted with some caution. The connections in the model have been made in such a manner that the part of the profile-bottom that is in contact with the top flange has been tied to this top flange. In the actual bridge, the profiled sheets are nailed to the top flange with one nail at each profile-bottom, providing a much more concentrated connection. Consequently, the stresses that

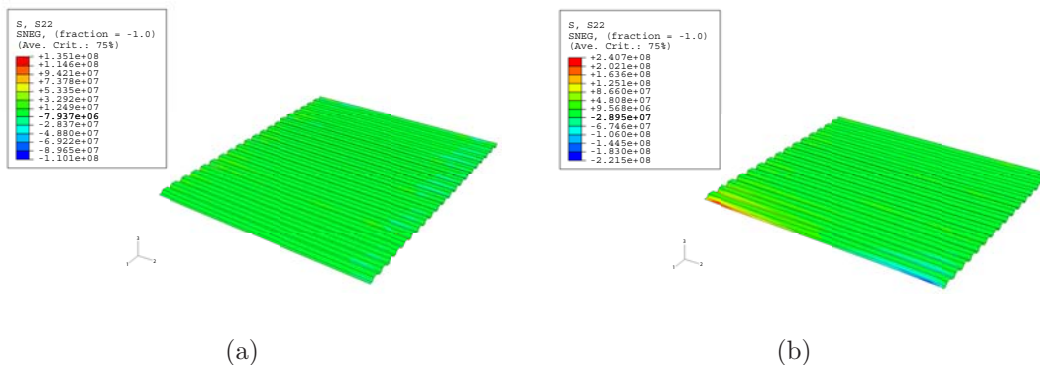


Figure 7.49: Stresses in the 22-direction for the outer profiled sheets for the model with in (a) a quadrilaterally connected profiled sheeting and in (b) a laterally connected profiled sheeting.

arise in the real bridge are probably somewhat larger than the ones given by the finite element models, thus the finite element model provides a lower bound for the stresses.

A comparison of the displacements and rotations between the three different models (open cross-section, closed cross-section and partly closed cross-section) shows that for the models with the profiled sheeting, the displacements and rotations are very small, while they are quite large for the open box girder. In Figure 7.50 the lateral displacements along top flange 1 for these three different models, with an initial imperfection of 0.05, are shown. The model with the open cross-section has a maximum lateral displacement of 0.109 m, the one with the closed cross-section 0.0177 m and the one with the partly closed cross-section 0.0181 m.

In Figure 7.51, the rotations for all three models are shown. The model with the open cross-section experiences rotations that are about ten times the rotations for the models with the profiled sheeting.

When the stresses in the profile-bottoms become too large, bolt hole yielding will occur which swiftly reduces the shearing rigidity and the continued action will be as if the box girder cross-section was open. It is therefore of great importance that the box girder with open cross-section is rigid enough to avoid a collapse. In the case of an open cross-section it is not the stresses that are the main problem, but rather rotations and lateral displacements.

The box girder with an open cross-section has been studied for various initial imperfections and comparison of the results given by the finite element models and analytical analyses considering second degree differential equations have been made [15].

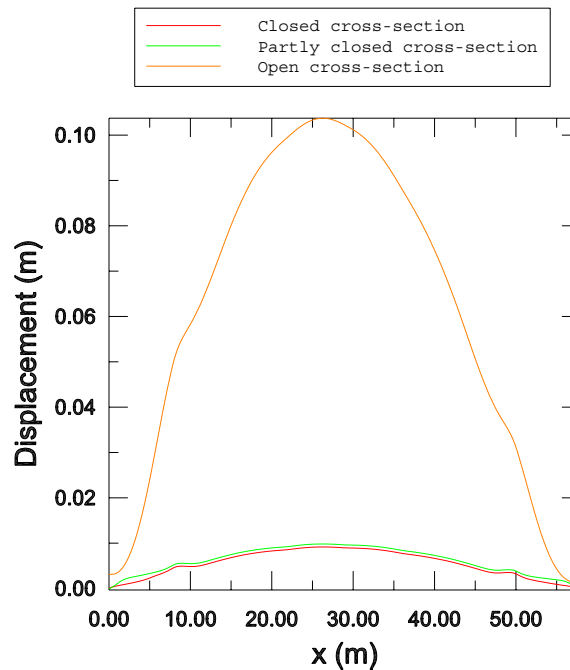


Figure 7.50: Lateral displacements along *top flange 1* for the three different models with an initial imperfection of 0.05

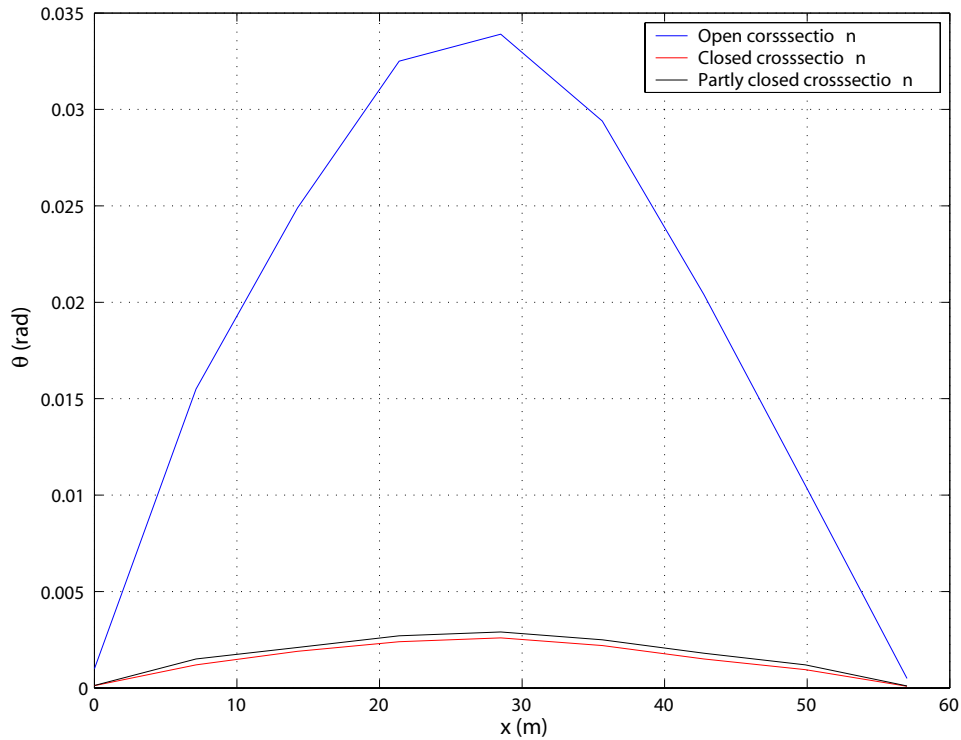


Figure 7.51: Rotations for the three different models with an initial imperfection of 0.05

The analytical analysis, with an initial imperfection of 0.05, gives an ultimate load of 2.13 times full casting load. The corresponding value from the finite element analysis is 2.15. The analyses with different initial imperfections show that relatively larger rotations and lateral displacements are obtained with an increased initial imperfection. Consequently, the ultimate load is also decreased with increased initial imperfections.

Chapter 8

Conclusions

The main objective of this thesis was to study the lateral torsional stability of bridge Y288 over river Ljungan, using finite element analysis performed in BRIGADE/Plus. A secondary objective was to examine the possible usefulness of BRIGADE/Plus for these types of designs.

8.1 Finite Element Calculations

Three different types of finite element analyses were performed: a simply supported rectangular plate uniformly compressed in one direction, profiled sheeting subjected to shear forces and finally the lateral torsional stability of the bridge.

The aim of the first analysis was to use a simple model for which analytical results were available and compare them with finite element modelling results. The analytical solution of this problem is due to Timoshenko, and the finite element analysis provided results well in accordance with the analytical results. According to Timoshenko's analytical solution, the critical buckling stress should be 74.8 MPa. The finite element analyses provided results of the critical buckling stress between 67.1 MPa and 73.6 MPa, depending on the accuracy of the model. The difference can be derived to that the load is applied as a uniformly compressive force in the analytical solution, while it was applied as a number of concentrated forces in the finite element analysis. The more concentrated forces that were applied, the more accurate were the results. The critical buckling stress of 73.6 MPa was obtained when 65 concentrated forces were applied at each side.

The analysis of the profiled sheeting in shear aimed to study the importance of different attachment techniques of the profiled sheeting. With an all around attachment, the structure is much more capable to resist shear forces. If the profiled sheeting is attached merely in one direction (here the axial direction of the bridge) large axial forces arise at the edges of the profiled sheets. This might lead to a pull through action at the fasteners, leading to a loss of the stabilising effects of the profiled sheeting which ultimately might lead to a collapse of the bridge. These force concentrations are considerably reduced with an all around attachment of the profiled sheeting.

These analyses were performed on models containing five profiled sheets and two or four plates, depending on type of attachment. When the profiled sheeting is given an all around attachment, a 94% reduction of stresses is achieved compared to when it is attached only at two sides. Large stress concentrations also appear along the free edges of the profiled sheeting for the model that has an attachment along two sides. These concentrations are avoided with an all around attachment.

Furthermore, the importance of the thickness of the profiled sheeting was studied. This study showed a clear correlation between decreased thickness and increased stresses in the profiled sheets. When a 10% thinner profiled sheeting was used, an about 20% increase of the stresses was obtained. If the profiled sheeting was made 10% thicker, the stresses were decreased about 15%. Although it is a well known fact that a thinner profiled sheeting provides a weaker structure, it is of great importance to consider the thickness in this case where the structure already is weak. An additional attenuation, from the use of too thin profiled sheeting, might give rise to a pull through action at the fasteners.

The third, and final, main aim was to study the overall behaviour of the bridge. Primarily the lateral torsional stability and how it is affected by initial imperfections and various attachment choices of the profiled sheeting was studied. When a profiled sheeting is used to create a closed cross-section, the structure becomes much more rigid compared to an open cross-section. The rotations and lateral displacements are significantly reduced when a closed cross-section is used. In order to successfully get the profiled sheeting to create a closed cross-section that is sustainable, two aspects are especially important: First, that the profiled sheeting is given an all around attachment. If it is attached along two sides only, large axial forces arise in parts of the profiled sheeting closest to the edge. These forces might lead to a pull through action at the fasteners, leading to a loss of the stabilising effect of the profiled sheeting. If that happens, the cross-section of the bridge behaves like an open, thin-walled cross-section. Second main consideration is to keep the stresses below the yield point. Even though an all around attachment is made, large stresses arise in the profile-bottoms at the connections to the top flanges of the box girder. Small initial imperfections help reduce the stresses while thicker profiled sheeting together with sturdy connections between the profiled sheeting and box girder makes the profiled sheeting more capable to resist the arisen stresses. To obtain accurate quantitative values of the arisen stresses in the profile bottoms a more detailed modelling of the connections between the profiled sheeting and the top flanges is needed. In this study, two different variants were analysed. One where a part of the surface of the profile bottom is tied to the top flange and one where just one node is tied. The former assumes a smeared-out connection that is more widespread than in reality, leading to an underestimation of the stresses. The latter produces a connection that is more concentrated than in reality, providing too large stresses. However, it can be concluded that it is vital to carefully consider both the thickness of the profiled sheeting and the way in which it is attached to the box girder.

Another aspect is that if the stabilising effect from the profiled sheeting is lost, the box girder with the open cross-section ought to be able to withstand the continued action. From the analyses of the open cross-section it was shown that the magnitude

of the initial imperfections has great influence of the bridge behaviour. An increasing initial imperfection leads to larger rotations, lateral displacements and decreasing ultimate load. What furthermore will happen, which is not shown in these models, is that if the rotations become large the wet concrete will run towards one side of the bridge, acting as an eccentric load that further increases the rotations.

Modelling Problems

Performing finite element analyses of this kind involves much time spend on trial and error before a model that provides results that are trustworthy has been created. Since this is very time-consuming it is helpful to find out about problems that others have had in order to avoid them. Therefore, one of the modelling problems that cost me a lot of time will be described below.

In the study of the lateral torsional stability geometric imperfections were to be implemented in the analysis. A linear eigenvalue buckling prediction was performed in order to find the overall buckling mode corresponding to the geometric initial imperfection of the box girder. This overall buckling mode, together with some random local buckling modes, was then implemented as an initial imperfection in a postbuckling analysis. Finding this overall buckling mode for the model with the profiled sheeting included turned out to be quite complicated. The linear eigenvalue buckling prediction only resulted in numerous local buckling modes, mainly in the profiled sheeting. To circumvent this problem, a linear eigenvalue buckling prediction was performed on the box girder without the profiled sheeting and the overall buckling mode from that analysis was implemented in the postbuckling analysis of the model with the profiled sheeting included. This course of action led to another problem, since the linear eigenvalue buckling prediction and the postbuckling analysis were performed on models with different geometric definitions. Furthermore, the connections between the profiled sheeting and the box girder in the postbuckling analysis have to be defined prior to implementing the initial imperfection from the linear eigenvalue buckling prediction. This two circumstances created vast difficulties creating a converging solution. The final solution of this problem was found when the connections were made with tie-interactions without adjusting the initial position of the slave nodes.

8.2 Suggested Direction for Further Research

It would be interesting to perform a study of the influence of the warping restraint casting at the abutments. This was originally intended to be studied in this thesis, but time constraints forced an omission of this part. Such a study would include modelling of the concrete and consideration of the action between the steel box girder and the concrete. That study could determine how much the torsional stability would be increased by an initial casting at the abutments.

A study that includes a careful modelling of the connections between the profiled

sheeting and the top flanges of the box girder would give more accurate results of the magnitude of the stresses at the connections. However, there are about 600 connections between the profiled sheeting and the top flanges, and about 420 between the profiled sheets. Thus, careful modelling these connections would be extremely time-consuming.

Bibliography

- [1] <http://www.rydab.se> (May 2003).
- [2] Letter from Skandinavisk bro- & industriteknik AB (March 2003).
- [3] <http://www.scanscot.com> (April 2003).
- [4] Private communication with Johan Kölfors at Scanscot Technology (June 2003).
- [5] BOVERKET. *Boverkets handbok om snö- och vindlast, utgåva 2*. Tryckeri Balder, Karlskrona, 1997.
- [6] BOVERKET. *Boverkets handbok om stålkonstruktioner, BSK 99*. Tryckeri Balder, Karlskrona, 1999.
- [7] CHEN, W. F., AND LUI, E. M. *Structural stability: theory and implementation*. Elsevier Science Publishing, New York, 1987.
- [8] COOK, R. D., MALKUS, D. S., AND PLESHA, M. E. *Concepts and applications of finite element analysis*, third ed. John Wiley & Sons, New York, 1989.
- [9] COOK, R. D., MALKUS, D. S., PLESHA, M. E., AND WITT, R. J. *Concepts and applications of finite element analysis*, fourth ed. John Wiley & Sons, New York, 2002.
- [10] HIBBITT, KARLSSON, AND SORENSEN. *ABAQUS/Standard User's Manual*, 6.3 ed. Hibbit, Karlsson and Sorensen Inc, Pawtucket, 2002.
- [11] HUEBNER, K. H., AND THORNTON, E. A. *The Finite Element Method for Engineers*. John Wiley & Sons, New York, 1982.
- [12] MURRAY, N. W. *Introduction to the theory of thin-walled structures*. Oxford University Press, Oxford, 1984.
- [13] OEHLERS, D. J., AND BRADFORD, M. A. *Composite Steel and Concrete Structural Members: Fundamental Behaviour*. Elsevier Science Ltd, Oxford, 1995.
- [14] RYALL, M. J., PARKE, G. A. R., AND HARDING, J. E. *Manual of Bridge Engineering*. Thomas Telford Publishing, London, 2000.

- [15] THOMASSON, P-O. MathCAD program: “Kontroll av sidostabilitet i byggskedet” (January 2003).
- [16] TIMOSHENKO, S. *Theory of Elastic Stability*. McGraw-Hill, New York, 1936.
- [17] TYRÉNS AB. Design drawings for bridge Y288 over river Ljungan at Erikslund.
- [18] VÄGVERKET. *Publikation 1994:1. Allmän teknisk beskrivning för broar, BRO 94*. Division Väg & Trafik, Borlänge, 1994.
- [19] ZIENKIEWICZ, O. C., AND CHEUNG, Y. K. *The Finite Element Method in Structural and Continuum Mechanics*. McGraw-Hill, London, 1967.

Appendix A

ABAQUS Template

A.1 Template

This template provides general information of various aspects of an ABAQUS/Standard analysis. For more detailed understanding of included, or general understanding of excluded options and parameters, see the ABAQUS manual.

- *BOUNDARY

Prescribes boundary conditions at nodes. Boundary conditions can be given as *model* input data to define zero-valued boundary conditions or as *history* input data to add, modify, or remove zero-valued or nonzero boundary conditions.

Options for this command,

Direct: Specify the node set or node number to which the boundary conditions apply, degree of freedom or the first and last of a range of degrees of freedom to be specified, and the magnitude of the boundary condition. Set the TYPE parameter to DISPLACEMENT to give a displacement history, default in ABAQUS. Set TYPE=VELOCITY to give a velocity history. Set TYPE=ACCELERATION to give an acceleration history.

Type: The type of boundary condition can be specified instead of degrees of freedom. The following boundary condition types are available:

XSYMM	Symmetry about a plane $X = \text{constant}$ (dof 1, 5, 6 = 0)
YSYMM	Symmetry about a plane $Y = \text{constant}$ (dof 2, 4, 6 = 0)
ZSYMM	Symmetry about a plane $Z = \text{constant}$ (dof 3, 4, 5 = 0)
ENCASTRE	Fully built-in (dof 1, 2, 3, 4, 5, 6 = 0)
PINNED	Pinned (dof 1, 2, 3 = 0)
XASYMM	Antisymmetry about a plane $X = \text{constant}$ (dof 2, 3, 4 = 0)
YASYMM	Antisymmetry about a plane $Y = \text{constant}$ (dof 1, 3, 5 = 0)
ZASYMM	Antisymmetry about a plane $Z = \text{constant}$ (dof 1, 2, 6 = 0)

Op: The optional parameter OP can be set to one of two values, MOD or NEW.
Set OP=MOD to modify or OP=NEW to add zero-valued or nonzero boundary conditions. If OP=NEW is used, all previously defined boundary conditions will be removed.

Examples: *BOUNDARY, TYPE=DISPLACEMENT, OP=MOD
TOP, 2, 2, 0.5E-3
BOTTOM, 1, 3, 0
RSIDE 1, 1, 0
Here the node set TOP is set to move 0.5 mm in dof 2, and the node set BOTTOM is prescribed a zero-value in dof:s 1-3.

*BOUNDARY, TYPE=DISPLACEMENT, OP=NEW
TOP, 1, 1, 3E-3
BOTTOM, ENCASTRE
By changing to OP=NEW, the node set TOP is here set to move 3 mm in dof 1, and the node set BOTTOM is prescribed a zero-value in all dof:s. Note that the node set RSIDE is left out, thus removing previously defined boundary conditions for this node set.

- *BUCKLE

Controls eigenvalue buckling estimation.

Options for this command,

Eigensolver: This parameter can be set one of two values, SUBSPACE or LANCZOS. Below follows examples of the Lanczos and the Subspace eigensolver.

Examples: *BUCKLE, EIGENSOLVER=LANCZOS
10, 0.2, 0.5,,
The first digit sets the number of eigenvalues to be estimated.
The second digit sets the minimum value of interest.
The third digit sets the maximum value of interest.
The fourth digit sets the block size. Here, this entry is omitted and a default value is created.
The fifth digit sets the maximum number of block Lanczos steps within each Lanczos run. Here, this entry is omitted and a default value is created.

*BUCKLE, EIGENSOLVER=SUBSPACE
10, 0.2, 18, 30
The first digit sets the number of eigenvalues to be estimated.
The second digit sets the maximum value of interest.
The third digit sets the number of vectors in the iteration. In general, the convergence in solving the eigenproblem is more rapid if

more vectors are carried in the iteration. The default number of vectors used is the minimum of $2n$ or $n + 8$. The fourth digit sets the maximum number of iterations. The default is 30.

- *CLOAD

Specifies concentrated forces and moments.

Options for this command,

Amplitude: Set the parameter AMPLITUDE equal to the name of the amplitude curve that defines the magnitude of the load during the step. If omitted, the reference magnitude is applied immediately at the beginning of the step or linearly over the step.

Follower: Include this parameter if the direction of the load is assumed to rotate with the rotation at this node. This parameter should be used only for large-displacement analysis and can be used only at nodes with active rotational degree of freedom, such as beams and shells.

Op: The optional parameter OP can be set to one of two values, MOD or NEW. Set OP=MOD to modify or OP=NEW to add concentrated forces. If OP=NEW is used, all previously defined concentrated forces will be removed.

Example: *CLOAD, OP=MOD
 PickedSet1330, 2, -2000
 PickedSet1330, 3, -2000
Here the node set PickedSet1330 is set to apply a concentrated force of magnitude -2000 at d.o.f. 2 and 3.

- *HEADING

This option is used to define a title to the analysis.

Example: *HEADING
 Torsional stability of box girder without profiled sheets.

- *IMPERFECTION

Introduces a geometric imperfection into a model for postbuckling analysis.

Options for this command,

FILE: Set the parameter FILE equal to the name of the results file from a previous analysis containing either the mode shapes from a *BUCKLE or *FREQUENCY analysis or the nodal displacements from a *STATIC analysis

STEP: Set the parameter STEP equal to the step number from which model or displacement data are to be read.

Examples: *IMPERFECTION, FILE=BIG-Buckle, STEP=1

1, 0.001

2, 0.001

3, 0.001

9, 0.1

The first digit sets the mode number to be introduced.

The second digit sets the scaling factor for this mode.

Here mode number 1, 2, and 3 are introduced with the scaling factor 0.001 and mode number 4 with the scaling factor 0.1.

This section deals with material properties and gives an idea of how it could look like in a input file.

- *MATERIAL, *DENSITY, and *ELASTIC

Defines material properties.

Required parameter,

Name: Set this parameter equal to the name of the parameter to be used for the material when referenced in the element property option. The name must be unique and cannot begin with a number.

Example: *MATERIAL, NAME=Steel

**

*DENSITY

7850

**

*ELASTIC

**

2.1e+11, 0.3

- *STATIC

Specifies that the step should be analysed as a static load step.

Options for this command,

Direct: Include this parameter if direct control over the time incrementation is desirable throughout the step.

Riks: Include this parameter if it is desirable to use the Riks method when performing the static load step. The load case should be proportional.

Stabilize: This parameter provides automatic stabilisation to the structure. Set this parameter equal to the dissipated energy fraction desirable. If this parameter is omitted, ABAQUS defaults to a value of 2×10^{-4} . If the FACTOR parameter is used, any value of the

dissipated energy fraction will be overridden.

This parameter cannot be used if the RIKS parameter is included.

Example: *STATIC

0.1, 1., 1e-05, 0.1

The first digit sets initial time increment.

The second digit sets the time period of the step.

The third digit sets the minimum time increment allowed.

The fourth digit sets the maximum time increment allowed.

- *STEP

Specifies a step definition. It must be followed by a procedure definition.

Options for this command,

Nl-geom: If the NLGEOM (Nonlinear Geometry) parameter is specified on the *STEP option it will be active in all subsequent steps of the analysis.

Amplitude: This parameter can be set one of two values, STEP or RAMP. By setting AMPLITUDE=STEP, Figure A.1 *a*, the loads are applied instantaneously at the start of the step. By setting AMPLITUDE=RAMP, Figure A.1 *b*, the load magnitude will vary linearly over the step.

Inc: Set this parameter equal to the maximum number of increments in the step. The default value is 100.

Example: *STEP, NLGEOM, AMPLITUDE=RAMP, INC=200

The step defined in this example states that the loading will vary linearly over the step, that large-displacement will be included in the step and that the step will consist of 200 time increments.

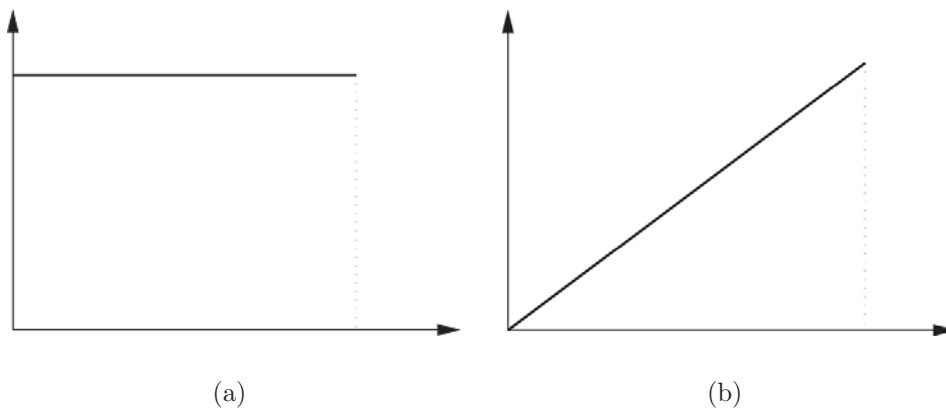


Figure A.1: Stepload and Rampload

- *TIE

Constrains each node on the slave surface to have the same value of displacement as the point on the master surface to which it is closest.

Required parameter,

Name: Set this parameter equal to the name that will be used to identify this constraint.

Options for this parameter,

Position tolerance: Set this parameter equal to the distance within which nodes on the slave surface must lie from the master surface in order to be tied. The default value for this tolerance distance is 5% of the typical element size in the master surface. If a node-based master surface is used, the default tolerance distance is based on the average distance between nodes in the master surface.

Adjust: Set ADJUST=YES (default) to move all tied nodes on the slave surface onto the master surface in the initial configuration, without any strain.

No rotation: Include this parameter if rotation degrees of freedom should not be tied. If this parameter is omitted, any existing rotation degrees of freedom will be tied if applicable, in addition to the translation degrees of freedom.

Example: *TIE, NAME=*name*
slave_surface_name, master_surface_name
*TIE, NAME=tpy9-tpy10, ADJUST=yes, NO ROTATION
PickedSet1350-CNS, PickedSurf1349
Here the node set PickedSet1350-CNS will be tied in degrees of freedom 1, 2 and 3 to PickedSurf1349. All nodes in the slave node set within the default position tolerance will be moved to the master surface.

Appendix B

ABAQUS Input Files

This template provides a summary of the input files used of the finite element analyses. The assembly has been left out from each input file to make this appendix reasonable short. An example of how the assembly might be created is given after the input files. For more detailed understanding of included, or general understanding of excluded parts of the input files, contact the author of this thesis.

B.1 Profiled Sheets in Shear

B.1.1 Long side Attachment Input File

```
*Heading
PROFILED SHEETS IN SHEAR, ATTACHED AT LONGSIDES
Units: Length - m, Force - N, Stress - N/m2
** Job name: FiveTP-26 Model name: Model-1
**
**-----DEFINING THE PARTS-----
**
*Part, name=Plate
*End Part
*Part, name=TrapSheet
*End Part
**
**-----ASSEMBLY OF THE PARTS-----
**
The assembly is left out.
*End Assembly
**
**-----MATERIAL DATA-----
**
** MATERIALS
```

```

**
*Material, name=PlattaSection
*Density
7850.,
*Elastic
2.1e+11, 0.3
*Material, name=TRP-Plåt
*Density
7850.,
*Elastic
2.1e+11, 0.3
**
**-----INTERACTION DEFINITIONS-----
**
** INTERACTION PROPERTIES
**
*Surface Interaction, name=IntProp-1
1.,
*Surface Behavior, pressure-overclosure=HARD
**
**-----BOUNDARY CONDITIONS-----
**
** BOUNDARY CONDITIONS
**
** Name: Fixlager Type: Symmetry/Antisymmetry/Encastre
*Boundary
PickedSet491, ENCASTRE
** Name: rull2 Type: Symmetry/Antisymmetry/Encastre
*Boundary
PickedSet492, XASYMM
**
** INTERACTIONS
**
** Interaction: Int-1
*Contact Pair, interaction=IntProp-1
PickedSurf505, PickedSurf504
** Interaction: Int-2
*Contact Pair, interaction=IntProp-1
PickedSurf507, PickedSurf506
** -----
**
*****
**ANALYSIS STEP - APPLYING LOADS
*****
** STEP: General
**
*Step, name=General

```

```

*Static
0.1, 1., 1e-05, 0.1
**
** LOADS
**
** Name: DisplacementLoad Type: Concentrated force
*Cload
PickedSet515, 1, 10000.
**
** OUTPUT REQUESTS
**
*Restart, write, frequency=1
**
** FIELD OUTPUT: F-Output-1
**
*Output, field, variable=PRESELECT
**
** HISTORY OUTPUT: H-Output-1
**
*Output, history, variable=PRESELECT
*El Print, freq=999999
*Node Print, freq=999999
*End Step

```

B.1.2 All Around Attachment Input File

```

*Heading
PROFILED SHEETS IN SHEAR, ATTACHED ALL AROUND
Units: Length - m, Force - N, Stress - N/m2
** Job name: FiveTParound-13 Model name: Model-1
**
**-----DEFINING THE PARTS-----
**
*Part, name=Plate
*End Part
*Part, name=PlateShort
*End Part
*Part, name=TrapSheet
*End Part
**
**-----ASSEMBLY OF THE PARTS-----
**
The assembly is left out.
*End Assembly
**

```

```

**-----MATERIAL DATA-----
**
** MATERIALS
**
*Material, name=PlattaSection
*Density
7850.,
*Elastic
2.1e+11, 0.3
*Material, name=TRP-Plåt
*Density
7850.,
*Elastic
2.1e+11, 0.3
**
**-----INTERACTION DEFINITIONS-----
**
** INTERACTION PROPERTIES
**
*Surface Interaction, name=IntProp-1
1.,
*Surface Behavior, pressure-overclosure=HARD
**
**-----BOUNDARY CONDITIONS-----
**
** BOUNDARY CONDITIONS
**
** Name: Fixlager Type: Symmetry/Antisymmetry/Encastre
*Boundary
PickedSet491, ENCASTRE
** Name: rull2 Type: Symmetry/Antisymmetry/Encastre
*Boundary
PickedSet549, XASYMM
**
** INTERACTIONS
**
** Interaction: Int-1
*Contact Pair, interaction=IntProp-1
PickedSurf505, PickedSurf504
** Interaction: Int-2
*Contact Pair, interaction=IntProp-1
PickedSurf507, PickedSurf506
** -----
**
*****
**ANALYSIS STEP - APPLYING LOADS

```

```

*****
** STEP: General
**
*Step, name=General
*Static
0.1, 1., 1e-05, 0.1
**
** LOADS
**
** Name: DisplacementLoad Type: Concentrated force
*Clload
PickedSet584, 1, 10000.
**
** OUTPUT REQUESTS
**
*Restart, write, frequency=1
**
** FIELD OUTPUT: F-Output-1
**
*Output, field, variable=PRESELECT
**
** HISTORY OUTPUT: H-Output-1
**
*Output, history, variable=PRESELECT
*El Print, freq=999999
*Node Print, freq=999999
*End Step

```

B.2 Torsional Stability

B.2.1 Box Girder with Open Cross-Section

Prebuckling Input File

```

*Heading
TORSIONAL STABILITY OF BOX GIRDER WITH OPEN CROSS-SECTION
Units: Length - m, Force - N, Stress - N/m2
** Job name: BIG-Buckle Model name: Model-1
**
**-----DEFINING THE PARTS-----
**
The assembly is left out.
*Part, name=Y288
*End Part

```

```

**
**-----ASSEMBLY OF THE PARTS-----
**
The assembly is left out.
*End Assembly
**
**-----MATERIAL DATA-----
**
*Material, name=Y288-Steel
*Density
7850.,
*Elastic
2.1e+11, 0.3
**
**-----BOUNDARY CONDITIONS-----
**
** Name: Support,Fix Type: Symmetry/Antisymmetry/Encastre
*Boundary
PickedSet888, PINNED
** Name: Support,Moveable Type: Symmetry/Antisymmetry/Encastre
*Boundary
PickedSet889, XASYMM
** -----
**
*****
** STEP - EIGENVALUE BUCKLING PREDICTION
*****
** STEP: Buckling
**
*Step, name=Buckling, perturbation
*Buckle, eigensolver=lanczos
100, 0., ,
**
** BOUNDARY CONDITIONS
**
** Name: Support,Fix Type: Symmetry/Antisymmetry/Encastre
*Boundary, op=NEW, load case=1
PickedSet888, PINNED
*Boundary, op=NEW, load case=2
PickedSet888, PINNED
** Name: Support,Moveable Type: Symmetry/Antisymmetry/Encastre
*Boundary, op=NEW, load case=1
PickedSet889, XASYMM
*Boundary, op=NEW, load case=2
PickedSet889, XASYMM
**
** LOADS

```

```

**
** Name: BucklingLoad Type: Concentrated force
*Cload
PickedSet887, 3, -25000.
**
** OUTPUT REQUESTS
**
*Restart, write, frequency=1
**
** FIELD OUTPUT: F-Output-2
**
*Output, field, variable=PRESELECT
*El Print, freq=999999
*Node Print, freq=999999
*Node File, freq=999999
U
*End Step

```

Postbuckling Input File

```

*HEADING
TORSIONAL STABILITY OF BOX GIRDER WITH OPEN CROSS-SECTION
** Job name: BIG-pb1 Model name: Model-1
**
**-----DEFINING THE PARTS-----
**
*Part, name=Y288
*End Part
**
**-----ASSEMBLY OF THE PARTS-----
**
The assembly is left out.
*End Assembly
**
**-----MATERIAL DATA-----
**
*Material, name=Y288-Steel
*Density
7850.,
*Elastic
2.1e+11, 0.3
**
**-----INTRODUCING IMPERFECTIONS-----
**
*Imperfection, file=BIG-Buckle-2, Step=1
1, 1e-3

```

```

2, 1e-3
3, 1e-3
9, 0.05
**
**-----BOUNDARY CONDITIONS-----
**
** Name: Support,Fix Type: Symmetry/Antisymmetry/Encastre
*Boundary
PickedSet889, PINNED
** Name: Support,Moveable Type: Symmetry/Antisymmetry/Encastre
*Boundary
PickedSet890, XASYMM
** -----
**
*****
** STEP 1 - APPLYING GRAVITY, FORMWORK AND WIND
*****
** STEP: General
**
*Step, name=General, nlgeom
*Static
0.1, 1., 1e-05, 0.1
**
** LOADS
**
** Name: GravityLoad Type: Gravity
*Dload
PickedSet875, GRAV, 9.81, 0., 0., -1.
** Name: Formwork Type: Pressure
*Dload
PickedSurf903, P, 5000.
** Name: Wind Type: Pressure
*Dload
PickedSurf905, P, 1500.
**
** OUTPUT REQUESTS
**
*Restart, write, frequency=1
**
** FIELD OUTPUT: F-Output-1
**
*Output, field, variable=PRESELECT
**
** HISTORY OUTPUT: H-Output-1
**
*Output, history, variable=PRESELECT

```

```

*El Print, freq=999999
*Node Print, freq=999999
*End Step
** -----
**
*****
** STEP 2 - CAST CONCRETE
*****
** STEP: Casting
**
*Step, name=Casting, nlgeom
*Static, riks
0.2, 1., 1e-05, 0.2, 3,
**
** LOADS
**
** Name: Casting Type: Pressure
*Dload
PickedSurf904, P, 45000.
**
** OUTPUT REQUESTS
**
*Restart, write, frequency=1
**
** FIELD OUTPUT: F-Output-1
**
*Output, field, variable=PRESELECT
**
** HISTORY OUTPUT: H-Output-1
**
*Output, history, variable=PRESELECT
*End Step

```

B.2.2 Box Girder with Closed Cross-Section

Prebuckling Input File

The same file is used for the prebuckling analysis as in the analysis with the open cross-section

Postbuckling Input File

```

*Heading
TORSIONAL STABILITY OF BOX GIRDER WITH CLOSED CROSS-SECTION
Units: Length - m, Force - N, Stress - N/m2

```

```

** Job name:  BIG-TP-pb2 Model name:  Model-1
**
**-----DEFINING THE PARTS-----
**
*Part, name="TP,inner"
*End Part
*Part, name="TP,ytter"
*End Part
*Part, name=Y288
*End Part
**
**-----ASSEMBLY OF THE PARTS-----
**
The assembly is left out.
*End Assembly
**
**-----MATERIAL DATA-----
**
*Material, name=Sheet
*Density
7850.,
*Elastic
2.1e+11, 0.3
*Material, name=Y288-Steel
*Density
7850.,
*Elastic
2.1e+11, 0.3
**
*Imperfection, file=BIG-TP-Buckle, Step=1
1, 1e-3
2, 1e-3
3, 1e-3
9, 0.05
**
**-----BOUNDARY CONDITIONS-----
**
** Name:  Support,Fix Type:  Symmetry/Antisymmetry/Encastre
*Boundary
PickedSet1243, PINNED
** Name:  Support,Moveable Type:  Symmetry/Antisymmetry/Encastre
*Boundary
PickedSet1244, XASYMM
** -----
**
*****

```

```

** STEP 1 - APPLYING GRAVITY, FORMWORK AND WIND
*****
** STEP: General
**
*Step, name=General, nlgeom
*Static
0.1, 1., 1e-08, 0.1
**
** LOADS
**
** Name: Formwork Type: Pressure
*Dload
PickedSurf1469, P, 5000.
** Name: Gravity Type: Gravity
*Dload
PickedSet1480, GRAV, 9.81, 0., 0., -1.
** Name: Wind Load Type: Pressure
*Dload
PickedSurf1470, P, 1500.
**
** OUTPUT REQUESTS
**
*Restart, write, frequency=1
**
** FIELD OUTPUT: F-Output-1
**
*Output, field, variable=PRESELECT
**
** HISTORY OUTPUT: H-Output-1
**
*Output, history, variable=PRESELECT
*El Print, freq=999999
*Node Print, freq=999999
*End Step
** -----
**
*****
** STEP 2 - CAST CONCRETE
*****
** STEP: Casting
**
*Step, name=Casting, nlgeom
*Static, riks
0.1, 1., 1e-08, 0.1, 1.,
**
** LOADS

```

```

**
** Name: Casting Type: Pressure
*Dload
PickedSurf1471, P, 45000.
**
** OUTPUT REQUESTS
**
*Restart, write, frequency=1
**
** FIELD OUTPUT: F-Output-1
**
*Output, field, variable=PRESELECT
**
** HISTORY OUTPUT: H-Output-1
**
*Output, history, variable=PRESELECT
*End Step

```

B.2.3 Box Girder with Partly Closed Cross-Section

Prebuckling Input File

The same file is used for the prebuckling analysis as in the analysis with the open cross-section

Postbuckling Input File

```

*Heading
** Job name: BIG-TP-Missing-pb4 Model name: Model-1
**
** PARTS
**
*Part, name="TP,inner"
*End Part
*Part, name="TP,ytter"
*End Part
*Part, name=Y288
*End Part
**
** ASSEMBLY
**
The assembly is left out.
*End Assembly
**
** MATERIALS

```

```

**
*Material, name=Sheet
*Density
7850.,
*Elastic
2.1e+11, 0.3
*Material, name=Y288-Steel
*Density
7850.,
*Elastic
2.1e+11, 0.3
**
*Imperfection, file=BIG-TP-Buckle-3, Step=1
1, 1e-3
2, 1e-3
3, 1e-3
9, 0.05
**
** BOUNDARY CONDITIONS
**
** Name: Support,Fix Type: Symmetry/Antisymmetry/Encastre
*Boundary
PickedSet1243, PINNED
** Name: Support,Moveable Type: Symmetry/Antisymmetry/Encastre
*Boundary
PickedSet1244, XASYMM
** -----
**
*****
** STEP 1 - APPLYING GRAVITY, FORMWORK AND WIND
*****
** STEP: General
**
*Step, name=General, nlgeom
*Static
0.1, 1., 1e-08, 0.1
**
** LOADS
**
** Name: Formwork Type: Pressure
*Dload
PickedSurf1469, P, 5000.
** Name: Gravity Type: Gravity
*Dload
PickedSet1480, GRAV, 9.81, 0., 0., -1.
** Name: Wind Load Type: Pressure
*Dload

```

```

PickedSurf1470, P, 1500.
**
** OUTPUT REQUESTS
**
*Restart, write, frequency=1
**
** FIELD OUTPUT: F-Output-1
**
*Output, field, variable=PRESELECT
**
** HISTORY OUTPUT: H-Output-1
**
*Output, history, variable=PRESELECT
*El Print, freq=999999
*Node Print, freq=999999
*End Step
** -----
**
*****
** STEP 2 - CAST CONCRETE
*****
** STEP: Casting
**
*Step, name=Casting, nlgeom
*Static, riks
0.1, 1., 1e-08, 0.1, 1.,
**
** LOADS
**
** Name: Casting Type: Pressure
*Dload
PickedSurf1471, P, 45000.
**
** OUTPUT REQUESTS
**
*Restart, write, frequency=1
**
** FIELD OUTPUT: F-Output-1
**
*Output, field, variable=PRESELECT
**
** HISTORY OUTPUT: H-Output-1
**
*Output, history, variable=PRESELECT
*End Step

```

B.2.4 Example of Assembly

The following is a shortened version of the assembly for the postbuckling analysis of the model with the partly closed cross-section.

```

*Heading
** Job name:  BIG-TP-Missing-pb4 Model name:  Model-1
**
** PARTS
**
*Part, name="TP,inner"
*End Part
*Part, name="TP,ytter"
*End Part
*Part, name=Y288
*End Part
**
** ASSEMBLY
**
*Assembly, name=Assembly
**
*Instance, name=Y288-1, part=Y288
*Node
1, -14.25, 1.368, 2.015
2, -14.25, 1.418, 2.015
3, -14.25, 1.818, 2.015
...
10075, -27.9713, -1.683858, 0.
10076, -27.95896, -1.714647, 0.
*Element, type=S4R
1, 1, 2, 3138, 384
2, 2, 3, 363, 3138
...
10001, 10063, 10062, 3132, 3133
10002, 10062, 3131, 362, 3132
** Region:  (Överfläns0,038:Picked)
*Elset, elset=I1, internal
1, 2, 3,..., 1117, 1118
** Section:  Överfläns0,038
*Shell Section, elset=I1, material=Y288-Steel
0.038, 5
** Region:  (Överflänsplåt0,025:Picked)
*Elset, elset=I2, internal
217, 218, 219,...,1357, 1358
** Section:  Överflänsplåt0,025
*Shell Section, elset=I2, material=Y288-Steel
0.025, 5

```

```
** Region: (Överfläns0,025:Picked)
*Elset, elset=I3, internal
247, 248, 249,..., 1505, 1506
** Section: Överfläns0,025
*Shell Section, elset=I3, material=Y288-Steel
0.025, 5
** Region: (Livplåt0,019:Picked)
*Elset, elset=I4, internal
1507, 1508, 1509,..., 9855, 9856
** Section: Livplåt0,019
*Shell Section, elset=I4, material=Y288-Steel
0.019, 5
** Region: (Y288-BoxGirder:Picked)
*Elset, elset=I5, internal
1859, 1860, 1861,..., 9911, 9912
** Section: Y288-BoxGirder
*Shell Section, elset=I5, material=Y288-Steel
0.03, 5
** Region: (Livplåt0,016:Picked)
*Elset, elset=I6, internal
1864, 1865, 1866,..., 7020, 7021
** Section: Livplåt0,016
*Shell Section, elset=I6, material=Y288-Steel
0.016, 5
** Region: (Underfläns0,02:Picked)
*Elset, elset=I7, internal
2435, 2436, 2437,..., 8299, 8300
** Section: Underfläns0,02
*Shell Section, elset=I7, material=Y288-Steel
0.02, 5
** Region: (Underfläns0,032:Picked)
*Elset, elset=I8, internal
2599, 2600, 2601,..., 9025, 9026
** Section: Underfläns0,032
*Shell Section, elset=I8, material=Y288-Steel
0.032, 5
** Region: (Avstyvning0,025:Picked)
*Elset, elset=I9, internal
3112, 3113, 3114,..., 10001, 10002
** Section: Avstyvning0,025
*Shell Section, elset=I9, material=Y288-Steel
0.025, 5
** Region: (Underfläns0,02:Picked)
*Elset, elset=I10, internal
3402, 3403, 3448,..., 9883, 9884
** Section: Underfläns0,02
```

```

*Shell Section, elset=I10, material=Y288-Steel
0.02, 5
** Region: (Ändplåt0,02:Picked)
*Elset, elset=I11, internal
3404, 3405, 3406,..., 9452, 9453
** Section: Ändplåt0,02
*Shell Section, elset=I11, material=Y288-Steel
0.02, 5
** Region: (Tvärskott0,02:Picked)
*Elset, elset=I12, internal
3540, 3541, 3542,..., 7244, 7245
** Section: Överflänsplåt0,015
*Shell Section, elset=I14, material=Y288-Steel
0.015, 5
** Region: (Tvärskott0,01:Picked)
*Elset, elset=I15, internal
4883, 4884, 4885,..., 7658, 7659
** Section: Tvärskott0,01
*Shell Section, elset=I15, material=Y288-Steel
0.01, 5
*End Instance
**
*Instance, name="TP,ytter-2", part="TP,ytter"
27.1125, 1.70031441048035, 2.015
27.1125, 1.70031441048035, 2.015
28.1125, 1.70031441048035, 2.015, 90.
*Node
1, -0.495, 0.02125, 0.03495415
2, -0.4775, 0., 0.0349083
3, -0.4775, 0., 3.368
...
689, 0.4925, 0., 3.034437
690, 0.4925, 0., 3.201218
*Element, type=S4R
1, 1, 2, 117, 116
2, 116, 117, 118, 115
3, 115, 118, 119, 114
...
637, 2, 1, 576, 112
638, 1, 15, 113, 576
** Region: (y288-TP:Picked)
*Elset, elset=I1, internal, generate
1, 638, 1
** Section: y288-TP
*Shell Section, elset=I1, material=Sheet
0.00086, 5

```

```
*End Instance
**
*Instance, name="TP,ytter-3", part="TP,ytter"
26.1625, 1.70031441048035, 2.015
26.1625, 1.70031441048035, 2.015
27.1625, 1.70031441048035, 2.015, 90.
*Node
1, -0.495, 0.02125, 0.03495415
2, -0.4775, 0., 0.0349083
3, -0.4775, 0., 3.368
...
689, 0.4925, 0., 3.034437
690, 0.4925, 0., 3.201218
*Element, type=S4R
1, 1, 2, 117, 116
2, 116, 117, 118, 115
3, 115, 118, 119, 114
...
637, 2, 1, 576, 112
638, 1, 15, 113, 576
** Region: (y288-TP:Picked)
*Elset, elset=I1, internal, generate
1, 638, 1
** Section: y288-TP
*Shell Section, elset=I1, material=Sheet
0.00086, 5
*End Instance
**
*Instance, name="TP,ytter-11", part="TP,ytter"
18.5625, 1.70031441048035, 2.015
18.5625, 1.70031441048035, 2.015
19.5625, 1.70031441048035, 2.015, 90.
*Node
1, -0.495, 0.02125, 0.03495415
2, -0.4775, 0., 0.0349083
3, -0.4775, 0., 3.368
...
689, 0.4925, 0., 3.034437
690, 0.4925, 0., 3.201218
*Element, type=S4R
1, 1, 2, 117, 116
2, 116, 117, 118, 115
3, 115, 118, 119, 114
...
637, 2, 1, 576, 112
638, 1, 15, 113, 576
```

```
** Region: (y288-TP:Picked)
*Elset, elset=I1, internal, generate
1, 638, 1
** Section: y288-TP
*Shell Section, elset=I1, material=Sheet
0.00086, 5
*End Instance
**
*Instance, name="TP,inner-1", part="TP,inner"
17.6125, 1.40040611353712, 2.015
17.6125, 1.40040611353712, 2.015
18.6125, 1.40040611353712, 2.015, 90.
*Node
1, -0.495, 0.02125, 0.025
2, -0.4775, 0., 0.025
3, -0.4775, 0., 2.775
...
569, -0.4575, 0., 2.43125
570, -0.4575, 0., 2.603125
*Element, type=S4R
1, 1, 2, 115, 114
2, 114, 115, 116, 4
3, 4, 116, 117, 136
...
521, 10, 130, 466, 467
522, 130, 11, 72, 466
** Region: (y288-TP:Picked)
*Elset, elset=I1, internal, generate
1, 522, 1
** Section: y288-TP
*Shell Section, elset=I1, material=Sheet
0.00086, 5
*End Instance
**
*Instance, name="TP,inner-2", part="TP,inner"
16.6625, 1.40040611353712, 2.015
16.6625, 1.40040611353712, 2.015
17.6625, 1.40040611353712, 2.015, 90.
*Node
1, -0.495, 0.02125, 0.025
2, -0.4775, 0., 0.025
3, -0.4775, 0., 2.775
...
569, -0.4575, 0., 2.43125
570, -0.4575, 0., 2.603125
*Element, type=S4R
```

```

1, 1, 2, 115, 114
2, 114, 115, 116, 4
3, 4, 116, 117, 136
...
521, 10, 130, 466, 467
522, 130, 11, 72, 466
** Region: (y288-TP:Picked)
*Elset, elset=I1, internal, generate
1, 522, 1
** Section: y288-TP
*Shell Section, elset=I1, material=Sheet
0.00086, 5
*End Instance
**
*Instance, name="TP,inner-38", part="TP,inner"
-17.5375, 1.40040611353712, 2.015
-17.5375, 1.40040611353712, 2.015
-16.5375, 1.40040611353712, 2.015, 90.
*Node
1, -0.495, 0.02125, 0.025
2, -0.4775, 0., 0.025
3, -0.4775, 0., 2.775
...
569, -0.4575, 0., 2.43125
570, -0.4575, 0., 2.603125
*Element, type=S4R
1, 1, 2, 115, 114
2, 114, 115, 116, 4
3, 4, 116, 117, 136
...
521, 10, 130, 466, 467
522, 130, 11, 72, 466
** Region: (y288-TP:Picked)
*Elset, elset=I1, internal, generate
1, 522, 1
** Section: y288-TP
*Shell Section, elset=I1, material=Sheet
0.00086, 5
*End Instance
**
*Instance, name="TP,ytter-12", part="TP,ytter"
-18.4875, 1.69782532751092, 2.015
-18.4875, 1.69782532751092, 2.015
-17.4875, 1.69782532751092, 2.015, 90.
*Node
1, -0.495, 0.02125, 0.03495415

```

```
2, -0.4775, 0., 0.0349083
3, -0.4775, 0., 3.368
...
689, 0.4925, 0., 3.034437
690, 0.4925, 0., 3.201218
*Element, type=S4R
1, 1, 2, 117, 116
2, 116, 117, 118, 115
3, 115, 118, 119, 114
...
637, 2, 1, 576, 112
638, 1, 15, 113, 576
** Region: (y288-TP:Picked)
*Elset, elset=I1, internal, generate
1, 638, 1
** Section: y288-TP
*Shell Section, elset=I1, material=Sheet
0.00086, 5
*End Instance
**
*Instance, name="TP,ytter-13", part="TP,ytter"
-19.4375, 1.69782532751092, 2.015
-19.4375, 1.69782532751092, 2.015
-18.4375, 1.69782532751092, 2.015, 90.
*Node
1, -0.495, 0.02125, 0.03495415
2, -0.4775, 0., 0.0349083
3, -0.4775, 0., 3.368
...
689, 0.4925, 0., 3.034437
690, 0.4925, 0., 3.201218
*Element, type=S4R
1, 1, 2, 117, 116
2, 116, 117, 118, 115
3, 115, 118, 119, 114
...
637, 2, 1, 576, 112
638, 1, 15, 113, 576
** Region: (y288-TP:Picked)
*Elset, elset=I1, internal, generate
1, 638, 1
** Section: y288-TP
*Shell Section, elset=I1, material=Sheet
0.00086, 5
*End Instance
**
```

```
*Instance, name="TP,ytter-21", part="TP,ytter"
-27.0375, 1.69782532751092, 2.015
-27.0375, 1.69782532751092, 2.015
-26.0375, 1.69782532751092, 2.015, 90.
*Node
1, -0.495, 0.02125, 0.03495415
2, -0.4775, 0., 0.0349083
3, -0.4775, 0., 3.368
...
689, 0.4925, 0., 3.034437
690, 0.4925, 0., 3.201218
*Element, type=S4R
1, 1, 2, 117, 116
2, 116, 117, 118, 115
3, 115, 118, 119, 114
...
637, 2, 1, 576, 112
638, 1, 15, 113, 576
** Region: (y288-TP:Picked)
*Elset, elset=I1, internal, generate
1, 638, 1
** Section: y288-TP
*Shell Section, elset=I1, material=Sheet
0.00086, 5
*End Instance
*Nset, nset=PickedSet1241, internal, instance=Y288-1
68, 69, 78
*Nset, nset=PickedSet1243, internal, instance=Y288-1
305, 309
*Nset, nset=PickedSet1244, internal, instance=Y288-1
220, 226
*Nset, nset=PickedSet1336, internal, instance="TP,ytter-2"
4, 10, 1
*Nset, nset=PickedSet1338, internal, instance="TP,ytter-3"
4, 10, 1
*Nset, nset=PickedSet1354, internal, instance="TP,ytter-11"
4, 10, 1
*Nset, nset=PickedSet1356, internal, instance="TP,inner-1"
4, 10, 1
*Nset, nset=PickedSet1358, internal, instance="TP,inner-2"
4, 10, 1
*Nset, nset=PickedSet1430, internal, instance="TP,inner-38"
4, 10, 1
*Nset, nset=PickedSet1432, internal, instance="TP,ytter-12"
4, 10, 1
*Nset, nset=PickedSet1434, internal, instance="TP,ytter-13"
```

```

4, 10, 1
*Nset, nset=PickedSet1480, internal, instance="TP,ytter-21"
1, 690, 1
*Elset, elset=PickedSet1480, internal, instance=Y288-1
1, 10002, 1
*Elset, elset=PickedSet1480, internal, instance="TP,ytter-2"
1, 638, 1
*Elset, elset=PickedSet1480, internal, instance="TP,ytter-3"
1, 638, 1
*Elset, elset=PickedSet1480, internal, instance="TP,inner-1"
1, 522, 1
*Elset, elset=PickedSet1480, internal, instance="TP,ytter-13"
1, 638, 1
*Elset, elset=PickedSet1480, internal, instance="TP,inner-2"
1, 522, 1
*Elset, elset=PickedSet1480, internal, instance="TP,inner-38"
1, 522, 1
*Elset, elset=PickedSet1480, internal, instance="TP,ytter-11"
1, 638, 1
** Constraint: LS1-inner
*Tie, name=LS1-inner, adjust=no, position tolerance=10., no rotation
PickedSurf1487, PickedSurf1312
** Constraint: LS1-ytter1
*Tie, name=LS1-ytter1, adjust=no, position tolerance=10., no rotation
PickedSurf1489, PickedSurf1320
** Constraint: LS1-ytter2
*Tie, name=LS1-ytter2, adjust=no, position tolerance=10., no rotation
PickedSurf1490, PickedSurf1322
** Constraint: LS2-inner
*Tie, name=LS2-inner, adjust=no, position tolerance=10., no rotation
PickedSurf1488, PickedSurf1316
** Constraint: LS2-ytter1
*Tie, name=LS2-ytter1, adjust=no, position tolerance=10., no rotation
PickedSurf1491, PickedSurf1324
** Constraint: LS2-ytter2
*Tie, name=LS2-ytter2, adjust=no, position tolerance=10., no rotation
PickedSurf1492, PickedSurf1326
** Constraint: tpi1-tpi2
*Tie, name=tpi1-tpi2, adjust=yes, no rotation
PickedSet1356-CNS, PickedSurf1355
** Constraint: tpi10-tpi11
*Tie, name=tpi10-tpi11, adjust=yes, no rotation
PickedSet1374-CNS, PickedSurf1373
** Constraint: tpi11-tpi12
*Tie, name=tpi11-tpi12, adjust=yes, no rotation
PickedSet1376-CNS, PickedSurf1375

```

```
** Constraint: tpi12-tpi13
*Tie, name=tpi12-tpi13, adjust=yes, no rotation
PickedSet1378-CNS, PickedSurf1377
** Constraint: tpi13-tpi14
*Tie, name=tpi13-tpi14, adjust=yes, no rotation
PickedSet1380-CNS, PickedSurf1379
** Constraint: tpi14-tpi15
*Tie, name=tpi14-tpi15, adjust=yes, no rotation
PickedSet1382-CNS, PickedSurf1381
** Constraint: tpi15-tpi16
*Tie, name=tpi15-tpi16, adjust=yes, no rotation
PickedSet1384-CNS, PickedSurf1383
** Constraint: tpi16-tpi17
*Tie, name=tpi16-tpi17, adjust=yes, no rotation
PickedSet1386-CNS, PickedSurf1385
** Constraint: tpi17-tpi18
*Tie, name=tpi17-tpi18, adjust=yes, no rotation
PickedSet1388-CNS, PickedSurf1387
** Constraint: tpi18-tpi19
*Tie, name=tpi18-tpi19, adjust=yes, no rotation
PickedSet1390-CNS, PickedSurf1389
** Constraint: tpi19-tpi20
*Tie, name=tpi19-tpi20, adjust=yes, no rotation
PickedSet1392-CNS, PickedSurf1391
** Constraint: tpi2-tpi3
*Tie, name=tpi2-tpi3, adjust=yes, no rotation
PickedSet1358-CNS, PickedSurf1357
** Constraint: tpi20-tpi21
*Tie, name=tpi20-tpi21, adjust=yes, no rotation
PickedSet1394-CNS, PickedSurf1393
** Constraint: tpi21-tpi22
*Tie, name=tpi21-tpi22, adjust=yes, no rotation
PickedSet1396-CNS, PickedSurf1395
** Constraint: tpi22-tpi23
*Tie, name=tpi22-tpi23, adjust=yes, no rotation
PickedSet1398-CNS, PickedSurf1397
** Constraint: tpi23-tpi24
*Tie, name=tpi23-tpi24, adjust=yes, no rotation
PickedSet1400-CNS, PickedSurf1399
** Constraint: tpi24-tpi25
*Tie, name=tpi24-tpi25, adjust=yes, no rotation
PickedSet1402-CNS, PickedSurf1401
** Constraint: tpi25-tpi26
*Tie, name=tpi25-tpi26, adjust=yes, no rotation
PickedSet1404-CNS, PickedSurf1403
** Constraint: tpi26-tpi27
```

*Tie, name=tpi26-tpi27, adjust=yes, no rotation
PickedSet1406-CNS, PickedSurf1405
** Constraint: tpi27-tpi28
*Tie, name=tpi27-tpi28, adjust=yes, no rotation
PickedSet1408-CNS, PickedSurf1407
** Constraint: tpi28-tpi29
*Tie, name=tpi28-tpi29, adjust=yes, no rotation
PickedSet1410-CNS, PickedSurf1409
** Constraint: tpi29-tpi30
*Tie, name=tpi29-tpi30, adjust=yes, no rotation
PickedSet1412-CNS, PickedSurf1411
** Constraint: tpi3-tpi4
*Tie, name=tpi3-tpi4, adjust=yes, no rotation
PickedSet1360-CNS, PickedSurf1359
** Constraint: tpi30-tpi31
*Tie, name=tpi30-tpi31, adjust=yes, no rotation
PickedSet1414-CNS, PickedSurf1413
** Constraint: tpi31-tpi32
*Tie, name=tpi31-tpi32, adjust=yes, no rotation
PickedSet1416-CNS, PickedSurf1415
** Constraint: tpi32-tpi33
*Tie, name=tpi32-tpi33, adjust=yes, no rotation
PickedSet1418-CNS, PickedSurf1417
** Constraint: tpi33-tpi34
*Tie, name=tpi33-tpi34, adjust=yes, no rotation
PickedSet1420-CNS, PickedSurf1419
** Constraint: tpi34-tpi35
*Tie, name=tpi34-tpi35, adjust=yes, no rotation
PickedSet1422-CNS, PickedSurf1421
** Constraint: tpi35-tpi36
*Tie, name=tpi35-tpi36, adjust=yes, no rotation
PickedSet1424-CNS, PickedSurf1423
** Constraint: tpi36-tpi37
*Tie, name=tpi36-tpi37, adjust=yes, no rotation
PickedSet1426-CNS, PickedSurf1425
** Constraint: tpi37-tpi38
*Tie, name=tpi37-tpi38, adjust=yes, no rotation
PickedSet1428-CNS, PickedSurf1427
** Constraint: tpi38-tpy12
*Tie, name=tpi38-tpy12, adjust=yes, no rotation
PickedSet1430-CNS, PickedSurf1429
** Constraint: tpi4-tpi5
*Tie, name=tpi4-tpi5, adjust=yes, no rotation
PickedSet1362-CNS, PickedSurf1361
** Constraint: tpi5-tpi6
*Tie, name=tpi5-tpi6, adjust=yes, no rotation

```

PickedSet1364-CNS, PickedSurf1363
** Constraint: tpi6-tpi7
*Tie, name=tpi6-tpi7, adjust=yes, no rotation
PickedSet1366-CNS, PickedSurf1365
** Constraint: tpi7-tpi8
*Tie, name=tpi7-tpi8, adjust=yes, no rotation
PickedSet1368-CNS, PickedSurf1367
** Constraint: tpi8-tpi9
*Tie, name=tpi8-tpi9, adjust=yes, no rotation
PickedSet1370-CNS, PickedSurf1369
** Constraint: tpi9-tpi10
*Tie, name=tpi9-tpi10, adjust=yes, no rotation
PickedSet1372-CNS, PickedSurf1371
** Constraint: tpy10-tpy11
*Tie, name=tpy10-tpy11, adjust=yes, no rotation
PickedSet1352-CNS, PickedSurf1351
** Constraint: tpy11-tpi1
*Tie, name=tpy11-tpi1, adjust=yes, no rotation
PickedSet1354-CNS, PickedSurf1353
** Constraint: tpy12-tpy13
*Tie, name=tpy12-tpy13, adjust=yes, no rotation
PickedSet1432-CNS, PickedSurf1431
** Constraint: tpy13-tpy14
*Tie, name=tpy13-tpy14, adjust=yes, no rotation
PickedSet1434-CNS, PickedSurf1433
** Constraint: tpy14-tpy15
*Tie, name=tpy14-tpy15, adjust=yes, no rotation
PickedSet1436-CNS, PickedSurf1435
** Constraint: tpy15-tpy16
*Tie, name=tpy15-tpy16, adjust=yes, no rotation
PickedSet1438-CNS, PickedSurf1437
** Constraint: tpy16-tpy17
*Tie, name=tpy16-tpy17, adjust=yes, no rotation
PickedSet1440-CNS, PickedSurf1439
** Constraint: tpy17-tpy18
*Tie, name=tpy17-tpy18, adjust=yes, no rotation
PickedSet1442-CNS, PickedSurf1441
** Constraint: tpy18-tpy19
*Tie, name=tpy18-tpy19, adjust=yes, no rotation
PickedSet1444-CNS, PickedSurf1443
** Constraint: tpy19-tpy20
*Tie, name=tpy19-tpy20, adjust=yes, no rotation
PickedSet1446-CNS, PickedSurf1445
** Constraint: tpy2-tpy3
*Tie, name=tpy2-tpy3, adjust=yes, no rotation
PickedSet1336-CNS, PickedSurf1335

```

```
** Constraint: tpy20-tpy21
*Tie, name=tpy20-tpy21, adjust=yes, no rotation
PickedSet1448-CNS, PickedSurf1447
** Constraint: tpy3-tpy4
*Tie, name=tpy3-tpy4, adjust=yes, no rotation
PickedSet1338-CNS, PickedSurf1337
** Constraint: tpy4-tpy5
*Tie, name=tpy4-tpy5, adjust=yes, no rotation
PickedSet1340-CNS, PickedSurf1339
** Constraint: tpy5-tpy6
*Tie, name=tpy5-tpy6, adjust=yes, no rotation
PickedSet1342-CNS, PickedSurf1341
** Constraint: tpy6-tpy7
*Tie, name=tpy6-tpy7, adjust=yes, no rotation
PickedSet1344-CNS, PickedSurf1343
** Constraint: tpy7-tpy8
*Tie, name=tpy7-tpy8, adjust=yes, no rotation
PickedSet1346-CNS, PickedSurf1345
** Constraint: tpy8-tpy9
*Tie, name=tpy8-tpy9, adjust=yes, no rotation
PickedSet1348-CNS, PickedSurf1347
** Constraint: tpy9-tpy10
*Tie, name=tpy9-tpy10, adjust=yes, no rotation
PickedSet1350-CNS, PickedSurf1349
*End Assembly
```